

# The Long-run Effect of Air Pollution on Survival\*

Tatyana Deryugina and Julian Reif

University of Illinois and NBER

June 2025

## Abstract

Many environmental hazards have long-run health effects, but quasi-experimental studies typically measure outcomes and treatment over short time periods. We develop a new framework for quantifying the effect of air pollution exposure on life expectancy. Using daily changes in wind direction as an instrument for air pollution, we first characterize the dynamic mortality effects of short-run exposure. We then incorporate these estimates into a demographic model to quantify the lifelong effects of a permanent reduction in air pollution exposure. Ninety percent of the survival benefits accrue after the first fifty years of life.

**JEL Classification:** I18, Q52, Q53

**Keywords:** Air pollution, chronic exposure, mortality, survival

---

\*Deryugina: deryugin@illinois.edu. Reif: jreif@illinois.edu. Lexi Chen, Prakrati Thakur, Zimao Xiao, and Xinhui Sun provided excellent research assistance. We are grateful to the editor, three anonymous reviewers, Josh Gottlieb, Peter Hull, Adriana Lleras-Muney, Nolan Miller, David Molitor, Nick Muller, Nicole Riemer, Wolfram Schlenker, Hannes Schwandt, Matthew West, Nikos Ziropiannis, and seminar participants at Arizona State University, Baltic Economic Association, Cornell University, DePaul University, Exeter University, GSSI School of Advanced Studies, Iowa State University, ITAM, IZA Workshop on Environment and Labor Markets, Jinan University, Johns Hopkins University, London School of Economics, MHEC, Nova SBE, Oxford University, Santa Clara University, Southern Economic Association meetings, Southern Illinois University, Stanford University, Tinbergen Institute, Toulouse School of Economics, University of Birmingham, UC Berkeley, University of Chicago, University of Duisburg-Essen, University of Geneva, UIC, University of Indiana, University of Mannheim, University of Navarra, University of Pennsylvania, and Wake Forest University for helpful feedback. This research was supported by the National Institutes of Health under Award Numbers R01AG053350 and R01AG073365.

# 1 Introduction

Environmental hazards such as air pollution, extreme temperatures, and water pollution are major contributors to human morbidity and mortality. For example, The Lancet Commission on Pollution and Health estimates that air pollution caused 6.5 million premature deaths in 2015, amounting to 12 percent of all deaths worldwide (Landrigan et al., 2018). Such assessments typically rely on observational studies, which are susceptible to omitted variable bias (Dominici, Greenstone and Sunstein, 2014). Quasi-experimental studies can address this bias but typically measure health outcomes and treatment exposure over short time periods, often less than one year. As a result, they may miss long-run effects that develop over decades, as well as the distinct effects of chronic (prolonged) exposure—neither of which is likely to be a simple extrapolation of short-run effects.

Overcoming these limitations is challenging because few datasets track individuals over long time periods, quasi-experimental variation in chronic exposure is rare, and endogenous responses such as relocation complicate the interpretation of estimates. However, understanding the lifelong health consequences of sustained changes in exposure is essential for designing effective health and environmental policy.

This paper proposes a new approach for estimating long-run mortality effects. Our method combines well-identified short-run estimates with an individual-level model of health production that fits human survival curves well and accommodates a wide range of mortality patterns (Lleras-Muney and Moreau, 2022). We calibrate the model using short-run empirical mortality estimates and use it to quantify counterfactual survival outcomes under acute and chronic changes in exposure. The model demonstrates strong out-of-sample performance: its predictions align closely with our empirical estimates across different age groups and follow-up periods, and are consistent with three-year quasi-experimental estimates from Anderson (2020).

We use our approach to estimate the short- and long-run mortality effects of air pollution exposure in the United States. Our study focuses on sulfur dioxide (SO<sub>2</sub>), a major precursor

of fine particulate matter ( $\text{PM}_{2.5}$ ) and the predominant pollutant measured in the decades following the 1970 Clean Air Act. We assemble a new dataset that combines the universe of publicly available death records from 1972 to 1988 with daily data on air pollution and weather. We then investigate the causal effect of acute (1-day) air pollution exposure on county-level mortality by instrumenting for observed changes in  $\text{SO}_2$  with changes in wind direction. We estimate that a 1-unit ( $\approx 10$  percent) increase in  $\text{SO}_2$  raises 1-day mortality by 0.08 deaths per million (0.33 percent). Secondary analyses indicate that this effect reflects exposure to both  $\text{SO}_2$  as well as  $\text{PM}_{2.5}$ . When we extend the outcome window to one month (28 days), the cumulative mortality effect more than triples, demonstrating that air pollution continues to affect mortality well beyond the day of exposure.

We document striking differences in mortality dynamics by cause of death. Our 1-day mortality estimate is driven roughly equally by deaths related to three groups of causes: cardiovascular disease, cancer, and “other diseases,” a residual category that includes chronic lower respiratory illness and diabetes. When the outcome window is extended to one month, cumulative mortality from cardiovascular and other diseases increases more than fourfold. This finding aligns with evidence from the medical literature suggesting that air pollution causes “accelerated aging” by, for example, hardening arteries and increasing the risk of heart disease ([Rajagopalan and Landrigan, 2021](#)). By contrast, the estimated mortality from cancer declines and becomes statistically insignificant over the longer window. Given the implausibility of developing and dying from cancer in under a month, this pattern suggests that these cancer deaths largely reflect “mortality displacement”—that is, they occurred among frail individuals with pre-existing cancer and short counterfactual life expectancies.

Altogether, our empirical estimates indicate that acute exposure to air pollution produces two distinct mortality patterns: a short-term, transient effect due to mortality displacement among frail individuals, and a longer-term, growing effect due to accelerated aging among healthier individuals. On net, the accelerated aging effect dominates.

Medical and epidemiological research suggests that long-run exposure to air pollution

also triggers adverse health processes, such as artery hardening, that gradually impair health over many years. To translate our acute estimates into lifetime projections, we adapt the health production model of [Lleras-Muney and Moreau \(2022\)](#) to our daily mortality setting. While there are many ways to model survival, this model is particularly well-suited to our needs because it can capture both the accelerated aging and mortality displacement patterns observed in our setting.

Our approach maps our short-run empirical estimates to the model’s parameters, allowing us to form long-run projections that align with well-documented age patterns of human mortality. Specifically, we use age-specific estimates of 1-day cancer mortality to calibrate the effect of pollution exposure on the model parameter governing mortality displacement, and use the corresponding non-cancer estimates to calibrate the effect of exposure on the model’s biological aging parameter. We then use this calibrated model to quantify the short- and long-run effects of both acute and chronic exposure.

We validate the model internally in several ways. Because it is calibrated using only 1-day mortality estimates, we can measure the model’s accuracy by comparing its mortality predictions in the months following acute exposure to our corresponding empirical estimates. We also assess the plausibility of a key modeling assumption—that the effect of a given exposure on model parameters is constant—by checking whether parameters calibrated using one age group predict mortality effects in other age groups. For example, we calibrate a model using IV mortality estimates for ages 70 and over and then assess how well it predicts mortality effects for 65–69-year-olds, a younger age group with a different exposure history. Finally, we benchmark the model against IV mortality estimates of short-term (up to 90-day) chronic pollution exposure.

The model performs well: the vast majority of predictions lie inside the 95% confidence intervals of the corresponding IV estimates. These predictions depend meaningfully on our estimated share of deaths due to mortality displacement. When we assume either 0% or 100% mortality displacement, the resulting predictions fall far outside the 95% confidence intervals.

These results demonstrate that while all-cause mortality estimates alone are insufficient for forming reliable long-run predictions, incorporating cause-of-death information into a structural model can overcome this challenge.

Finally, we use our model to quantify the effect of a permanent, 1-unit decrease in  $\text{SO}_2$ —and, by implication, associated reductions in  $\text{PM}_{2.5}$ —on life expectancy. The model predicts that, holding behavior fixed, this reduction would extend life expectancy at birth by 1.1 years (90% bootstrap CI: 0.4–2.0). Alternative model specifications yield similar projections, spanning 0.77–1.24 years. All of these projections substantially exceed the 0.15-year gain implied by a simple extrapolation of our one-month IV estimates. Although the modeled decrease in chronic exposure begins at birth, ninety percent of the improvements in life expectancy occur after age 50, and over three-quarters occur after age 65. This result suggests that most of the survival benefits from the dramatic reductions in US air pollution since the 1970 Clean Air Act have yet to materialize for cohorts born in subsequent years.

The main contribution of our study is the development and application of a new framework for estimating the long-run mortality effects of chronic exposure to environmental hazards. The conventional approach estimates the short-run mortality effects of acute exposure and then quantifies long-run mortality effects using population life tables (e.g., [Deschênes and Greenstone, 2011](#)), with more recent work improving accuracy by incorporating individual-level predictions of counterfactual life expectancy ([Deryugina et al., 2019](#)). However, these methods remain prone to bias from unobserved characteristics that are correlated with both life expectancy and the probability of dying from exposure, and they cannot quantify the effects of chronic exposure. Our approach, by contrast, uses a health production model to infer long-run mortality effects from short-run quasi-experimental estimates, providing a novel example of a “best of both worlds” approach that combines structural and experimental methods ([Allcott, Gentzkow and Song, 2022](#); [Todd and Wolpin, 2023](#); [Obradovi, 2024](#)). By incorporating established features of human life-cycle mortality, the model is better equipped to produce reliable projections than approaches that ignore this information.

Our approach complements ongoing efforts to directly estimate the long-run mortality effects of pollution—an important but difficult task. Direct estimation requires identifying quasi-experimental variation in exposure that lasts for many years and carefully accounting for long-run avoidance behaviors (Graff Zivin and Neidell, 2012; Currie et al., 2014). Because such settings are rare, only a handful of studies have produced credible multi-year mortality estimates (Chen et al., 2013; Ebenstein et al., 2017; Anderson, 2020; Barreca, Neidell and Sanders, 2021; Andersen et al., 2023), and even these struggle to rule out selective migration.<sup>1</sup> By leveraging quasi-experimental variation in daily exposure, our approach avoids many of the potential confounders that complicate long-run designs. In addition, our findings suggest that pollution’s health effects build up gradually over decades, implying that even well-designed multi-year studies are likely to understate its full lifetime mortality burden.

Our short-run analysis also advances the literature on the health effects of acute exposure to air pollution. To our knowledge, this paper is the largest quasi-experimental study of acute pollution exposure and mortality to date, encompassing 18 million deaths and enabling precise age-specific mortality estimates. Our results underscore the importance of distinguishing mortality displacement among frail individuals, where the cumulative mortality effect dissipates, from accelerated aging among healthier individuals, where effects accumulate. Recognizing this distinction is essential for accurately inferring long-run mortality effects from short-run estimates. Although lengthening the outcome window helps address this challenge, the vast majority of quasi-experimental studies of air pollution rely on short outcome windows of one year or less.<sup>2</sup>

---

<sup>1</sup>For example, Barreca, Neidell and Sanders (2021) use repeated cross-sectional data to rule out large changes in total county-level population following pollution reductions, but differential migration remains a potential concern. Experimental animal studies also offer limited guidance, as most focus on simple organisms such as *C. elegans* or *Drosophila*. To our knowledge, no laboratory experiment has estimated the survival effects of chronic pollution exposure in more complex species such as mice or primates.

<sup>2</sup>See, for example, Currie and Neidell (2005); Knittel, Miller and Sanders (2016); Schlenker and Walker (2016); Deschênes, Greenstone and Shapiro (2017); Deryugina et al. (2019); Hollingsworth, Konisky and Ziogiannis (2021); Hollingsworth and Rudik (2021); and Heo, Ito and Kotamarthi (2023). A smaller literature studies early-life exposure and later-life outcomes (e.g., Isen, Rossin-Slater and Walker, 2017; Voorheis, 2017; Colmer and Voorheis, 2020), including one study on mortality before age 55 (Arenberg and Neller, 2023), but none focus on chronic exposure.

The rest of the paper is organized as follows. Section 2 provides background on air pollution and describes our data. Section 3 describes our instrumental variables design. Section 4 presents estimates of the short-run mortality effects of acute exposure. Section 5 introduces the health production model, calibrates it, and quantifies the long-run survival effects of chronic exposure. Section 6 concludes.

## 2 Background and data

### 2.1 Air pollution

Sulfur dioxide ( $\text{SO}_2$ ) is a major air pollutant produced primarily by the combustion of coal and oil. Historically, coal-burning power plants were the main source of  $\text{SO}_2$  emissions in the US. Ambient concentrations of  $\text{SO}_2$  declined significantly during our sample period and have continued to fall in more recent years (Figure A.1a), driven by a shift to low-sulfur coal, increased use of pollution control equipment, and greater reliance on alternative energy sources such as natural gas.

$\text{SO}_2$  harms human health through two main channels. First, clinical trials have shown that direct exposure to  $\text{SO}_2$  impairs respiratory function, especially among people with asthma (Agency for Toxic Substances and Disease Registry, 1998). Animal experiments have also demonstrated that  $\text{SO}_2$  inhalation can cause brain damage (Sang et al., 2010; Yao et al., 2015) and contribute to cardiac and mitochondrial dysfunction (Qin et al., 2016). Second,  $\text{SO}_2$  transforms naturally into sulfate ( $\text{SO}_4^{2-}$ ) at a rate of several percent per hour (Luria et al., 2001). Sulfates are a major component of fine particulate matter ( $\text{PM}_{2.5}$ ), a catch-all term for particles whose diameter is 2.5 micrometers ( $\mu\text{m}$ ) or less.  $\text{PM}_{2.5}$  is thought to be particularly harmful to health because of its ability to cross the blood-alveolar and blood-brain barriers. Prior quasi-experimental research has found causal links between short-run exposure to  $\text{PM}_{2.5}$  and a number of health-related outcomes, such as short-run healthcare spending, hospitalizations, and mortality (e.g., Barwick et al., 2018; Deryugina

et al., 2019; Heo, Ito and Kotamarthi, 2023).

While research on the exact pathophysiological mechanisms underlying these health effects continues, medical studies have documented significant associations between air pollution and hypertension, diabetes, coronary artery calcification, and the progression of chronic kidney disease, all of which are risk factors for cardiovascular disease (Rajagopalan and Landerigan, 2021). Air pollution exposure has also been linked to the initiation, promotion, and progression phases of lung cancer (Turner et al., 2020; Hill et al., 2023). Once initiated, lung cancer typically grows for over 10 years before it is diagnosed (Nadler and Zurbenko, 2014). Thus, the short-run health effects of air pollution exposure—including mortality—cannot be easily extrapolated to capture its long-run effects.

We measure air pollution using the EPA’s Air Quality System database, which provides hourly data at the pollution-monitor level for criteria pollutants regulated by the EPA. The extent of spatial and temporal coverage varies by pollutant (see Section A.1 for additional detail). Although our analysis focuses on SO<sub>2</sub>, we also examine four other air pollutants that have been monitored since the 1970s or the 1980s: nitrogen dioxide (NO<sub>2</sub>), total suspended particulates (TSP), ozone (O<sub>3</sub>), and carbon monoxide (CO). TSP includes all particulates with diameters less than 100  $\mu m$ , encompassing the finer PM<sub>2.5</sub>, which was not consistently monitored until the late 1990s—well after our sample period. Because SO<sub>2</sub> is a precursor to PM<sub>2.5</sub>, ambient SO<sub>2</sub> levels are likely correlated with unobserved fine particulate matter. We discuss the implications of this relationship for interpreting our estimates in Section 4.2.

Panel A of Table 1 shows county-level summary statistics for daily ambient pollution concentrations during our 1972–1988 sample period. The average SO<sub>2</sub> concentration is 9.1 parts per billion (ppb), with a standard deviation of 12.7. Thus, a one-ppb change in SO<sub>2</sub> represents slightly more than 10 percent of the mean and slightly less than 10 percent of a standard deviation. During this sample period, SO<sub>2</sub> is observed more than twice as frequently as any of the other four pollutants.

## 2.2 Mortality

We obtain daily death counts from the National Vital Statistics. These data are based on death certificate records and include information on both the cause of death and the county in which the death occurred. Our analysis focuses on the years 1972–1988, the only period for which the exact date of death is publicly available.<sup>3</sup> To calculate death rates, we divide death counts by annual county-level population estimates from the Surveillance, Epidemiology, and End Results (SEER) Program.

Panel B of Table 1 summarizes daily mortality rates during our 1972–1988 time period. The overall death rate is about 24 per million. Mortality is higher among infants (33 deaths per million), and much higher among those over age 85 (437 deaths per million).<sup>4</sup> We classify causes of death into four main categories: cardiovascular, cancer, external, and other. Cardiovascular disease is the leading cause of death in our sample, accounting for nearly half of all deaths (12 deaths per million). Cancer accounts for just over twenty percent (5 deaths per million), while external causes—which include car accidents, poisonings, suicides, and other causes not originating in the body—represent about eight percent. The remaining twenty percent, which includes deaths from respiratory illness, are grouped into an “other” category. We report estimates for subcategories of cardiovascular and other disease deaths in secondary analyses.

## 2.3 Wind and weather

Our empirical strategy builds on the well-established fact that wind currents carry air pollution over long distances. For example, regional contributions to sulfate pollution substantially exceed local contributions in many US cities ([Environmental Protection Agency, 2004](#)). Following the approach of [Deryugina et al. \(2019\)](#), we instrument for changes in SO<sub>2</sub> using

---

<sup>3</sup>The exact date of death is unavailable prior to 1972, and is only accessible after 1988 through the Research Data Center of the National Center of Health Statistics.

<sup>4</sup>Figure A.2 reports annual death rates by age group and cause of death during our sample period.

changes in wind direction.<sup>5</sup>

To construct our wind measures, we use hourly data on wind speed and wind direction from the ERA5 reanalysis dataset, published by the European Centre for Medium-Range Weather Forecasts. The data provide wind vectors measured at 10 meters above the Earth’s surface, with separate variables for east-west (u-component) and north-south (v-component), measured on a 0.25-by-0.25 degree grid (approximately 17-by-17 miles).<sup>6</sup> We interpolate these hourly wind vector components to the centroid of each county and compute daily averages to match the frequency of our mortality data. Finally, we convert the averaged u- and v-components into daily measures of wind direction and wind speed using trigonometry.

Our key identifying assumption is that, conditional on weather controls and a rich set of fixed effects, wind direction affects mortality only through its effects on air pollution. Our main specification controls for daily temperature and precipitation using data from [Schlenker and Roberts \(2009\)](#), who combine monthly data from the PRISM Climate Group with daily weather station observations to produce a gridded daily dataset. The data include daily total precipitation and daily maximum and minimum temperatures at a 2.5-by-2.5 mile resolution across the contiguous US for 1972–1988. We aggregate to the county-day level by calculating a population-weighted daily average across grid points within each county.<sup>7</sup>

We also incorporate relative humidity measures from the NCEP-NCAR Reanalysis 1 data provided by the NOAA PSL ([Kalnay et al., 1996](#)). This dataset combines historical weather observations with a global atmospheric model to produce daily estimates dating back to 1948. We use daily mean relative humidity reported at standard pressure levels, averaged from four sub-daily observations. These data are gridded at a 2.5-by-2.5 degree resolution.

---

<sup>5</sup>[Deryugina et al. \(2019\)](#) estimate the effects of PM<sub>2.5</sub> on 3-day mortality and medical spending among the elderly Medicare population. Our empirical analysis, which includes all ages and a longer sample period, focuses on mortality dynamics by age and cause of death. These dynamics help characterize the incidence of short-run pollution exposure and are crucial to forming the long-run projections presented in Section 5.

<sup>6</sup>These data are available from <https://cds.climate.copernicus.eu/datasets/reanalysis-era5-single-levels?tab=overview>.

<sup>7</sup>See <http://www.prism.oregonstate.edu/> for the original PRISM dataset and <https://zenodo.org/records/10625288> for the daily data. Because the 1970 and 1980 Census tract boundary data are incomplete, we assign population weights using 1990 Census tract boundaries.

We interpolate to each county’s geographic centroid to obtain county-level measures.

### 3 Empirical strategy

#### 3.1 Estimating equations

Our first objective is to estimate the causal effect of acute (1-day) air pollution exposure on short-run mortality. We model this relationship using the following regression:

$$Y_{cd}^k = \beta^k \text{SO2}_{cd} + X_{cd}^{k'} \delta + \alpha_{cm} + \alpha_{my} + \varepsilon_{cd} \tag{1}$$

where  $Y_{cd}^k$  denotes the cumulative mortality rate in county  $c$  in the  $k$  days following exposure on day  $d$  (including same-day mortality). The parameter of interest,  $\beta^k$ , captures the effect of acute  $\text{SO}_2$  exposure on  $k$ -day mortality. To isolate this effect, the controls  $X_{cd}^k$  include contemporaneous weather conditions and their  $k - 1$  leads, as well as two leads and two lags of our wind direction instrument (described below). These controls help ensure that our estimate of  $\beta^k$  is not confounded by weather conditions during the mortality outcome window or by  $\text{SO}_2$  exposure occurring before or after the focal day.

Equation (1) includes fixed effects for county-by-calendar-month ( $\alpha_{cm}$ ) and calendar-month-by-year ( $\alpha_{my}$ ), hereafter referred to as “county-by-month” and “month-by-year”. The county-by-month fixed effects allow geographic differences in mortality, air pollution, and wind patterns to vary by month. The month-by-year fixed effects control for common time-varying shocks, such as those induced by environmental policy changes during our study period. We cluster standard errors at the county level and weight observations by the relevant county-year population.

Our main specification controls for daily maximum temperature, relative humidity, precipitation, and wind speed. Maximum temperature is modeled using indicators for 3-degree Celsius bins. The interior bins range from  $-15^\circ\text{C}$  to  $-12^\circ\text{C}$  up to  $27^\circ\text{C}$  to  $30^\circ\text{C}$ , with

two additional bins capturing temperatures below  $-15^\circ\text{C}$  and above  $30^\circ\text{C}$ . Relative humidity (measured in percent) is binned into five intervals:  $[0,10)$ ,  $[10,30)$ ,  $[30,60)$ ,  $[60,90)$ , and  $[90,100]$ . Precipitation (measured in millimeters) is binned into seven intervals:  $[0,0.1]$ ,  $(0.1,1]$ ,  $(1,10]$ ,  $(10,20]$ ,  $(20,50]$ ,  $(50,100]$ , and  $(100, \infty)$ . Wind speed (measured in miles per hour) is binned into eight intervals based on the Beaufort scale:  $[0,1)$ ,  $[1,4)$ ,  $[4,8)$ ,  $[8,13)$ ,  $[13,19)$ ,  $[19,25)$ ,  $[25,32)$ , and  $[32, \infty)$ .<sup>8</sup> To account for potentially important interactions between weather conditions, we include indicators for all observed combinations of maximum temperature, precipitation, wind speed, and relative humidity bins, yielding 2,373 distinct weather condition indicators. To assess robustness, we also report results from specifications that use different sets of weather controls.

OLS estimates of Equation (1) may be biased because  $\text{SO}_2$  exposure is both non-random and measured with error, as monitor-level pollution readings are an imperfect measure of population exposure. To address these concerns, we instrument for daily  $\text{SO}_2$  using contemporaneous wind direction in the county, allowing the effect of wind direction on  $\text{SO}_2$  to vary by geographic group  $g$ :

$$\text{SO2}_{cd} = \sum_{g=1}^{50} f^g(\theta_{cd}) + X_{cd}^k \delta + \alpha_{cm} + \alpha_{my} + \varepsilon_{cd} \quad (2)$$

where:

$$f^g(\theta_{cd}) = \gamma_g^1 1[G_c = g] \times \sin(\theta_{cd}) + \gamma_g^2 1[G_c = g] \times \sin(\theta_{cd}/2)$$

The indicator function  $1[G_c = g]$  is equal to 1 if county  $c$  is a member of group  $g$  and 0 otherwise. The variable  $\theta_{cd}$  is the local wind direction, measured in radians. The excluded instruments consist of 100 regressors formed by the interaction of group indicators,  $1[G_c = g]$ , with measures of contemporaneous wind direction,  $\sin(\theta_{cd})$  and  $\sin(\theta_{cd}/2)$ . Section A.2 shows that our results are robust to alternative ways of parameterizing  $f^g(\theta_{cd})$ .

---

<sup>8</sup>These choices aim to strike a balance between computational considerations and capturing weather conditions that could both affect mortality and be correlated with wind direction. See <https://www.weather.gov/mfl/beaufort> for additional detail on the Beaufort scale.

The wind direction instruments vary at the county level. We allow their effects on pollution exposure to differ across geographic groups—as captured by the parameters  $\gamma_g^1$  and  $\gamma_g^2$ —because the relationship between wind direction and pollution transport is location-specific. For example, a westerly wind may reduce pollution levels in coastal California while increasing it in areas located to the east of industrial sources near Chicago. To capture this heterogeneity, we construct 50 geographic groups using a  $k$ -means clustering algorithm that assigns all SO<sub>2</sub> pollution monitors to spatial groups based on their latitude and longitude.<sup>9</sup>

To address autocorrelation in wind direction—which could bias our estimate of  $\beta^k$ , the effect of a one-day, one-unit change in SO<sub>2</sub> exposure—we include two leads and two lags of wind direction, each interacted with geographic indicators, as part of our controls,  $X_{cd}^k$ . Thus, contemporaneous wind direction serves as our excluded instrument, while past and future wind directions serve as controls. Section A.2 demonstrates that including these leads and lags successfully addresses autocorrelation in wind-driven SO<sub>2</sub> exposure.

### 3.2 Identifying variation

Ambient air pollution comes from both local and distant sources. For example, a city’s pollution levels reflect not only nearby vehicle exhaust but also smoke from distant wildfires and emissions transported from power plants hundreds of miles away. The location of the source matters: while distant emissions tend to disperse relatively evenly over large areas, local emissions can create sharp spatial gradients in exposure that depend on wind patterns and proximity to the source. These local gradients can introduce serious measurement error when estimating county-level effects.<sup>10</sup> To address this concern, our first-stage Equation (2)

---

<sup>9</sup>The  $k$ -means clustering algorithm uses monitor coordinates and the desired number of groups (50) as inputs. If multiple monitors from the same county are assigned to different groups, we assign the county to the larger integer group number, which is effectively random assignment. Figure A.3 displays the locations of in-sample SO<sub>2</sub> monitors and their assigned geographic groups. On average, each geographic group includes 95 SO<sub>2</sub> monitors and 21 counties.

<sup>10</sup>Consider a county with one air pollution monitor located west of a centrally positioned power plant—the only pollution source in the area. When the wind blows from the east, the monitor detects high pollution; when it blows from the west, it detects low levels. Yet in this example, average county exposure does not change; variation in monitor readings reflects measurement error rather than true variation in countywide

allows the effect of (county-level) wind direction on pollution to vary across geographic groups but constrains it to be constant within each group. This approach emphasizes wind-driven variation from distant sources, which are more likely to affect entire counties uniformly, thereby reducing measurement error in our estimation.

Figure 1 illustrates our first-stage variation, using the Greater Philadelphia and Southern California geographic groups as examples. In the maps on the left, black dots indicate the locations of the SO<sub>2</sub> monitors within each region. The plots on the right show the group-specific relationships between daily average wind direction and SO<sub>2</sub> concentrations.<sup>11</sup> Each regression includes our standard controls: county-by-month and month-by-year fixed effects, along with indicators for all observed combinations of maximum temperature, relative humidity, precipitation, and wind speed bins. To flexibly capture the relationship between wind and SO<sub>2</sub>, we discretize wind direction into 36 10-degree bins and estimate the first-stage equation separately by geographic group. For comparison, we also overlay the fit implied by our sine-function parameterization.

Figure 1 reveals a strong first-stage relationship between wind direction and SO<sub>2</sub> levels. In the Greater Philadelphia area, pollution levels are highest when the wind blows from the west-southwest direction, and lowest when the wind blows from the east-southeast direction, where the Atlantic Ocean lies. By contrast, in the Southern California area, the highest pollution levels occur when the wind blows from the east, a densely populated area, while the cleanest air comes from the south-southwest direction, where the Pacific Ocean lies. A change in wind direction in these areas can alter SO<sub>2</sub> levels by 3–4 ppb, equal to 30–40 percent of the national mean during this time period (Table 1).

We estimate our second stage using two-stage least squares (2SLS) and interpret the resulting IV estimate as a weighted average of treatment effects among compliers, where weights are larger for compliers with larger first stages (Angrist, Graddy and Imbens, 2000).

Figure A.5 shows the geographic distribution of the strength of the first stage, as measured

---

exposure.

<sup>11</sup>Figure A.4 shows corresponding plots for all 50 geographic groups.

by the difference in predicted SO<sub>2</sub> levels between the most and least polluting wind directions.<sup>12</sup> The strongest compliers—regions with over 4 ppb of predicted SO<sub>2</sub> variation—are concentrated in the Midwest and the Northeast. Moderate (1–4 ppb) and weak (<1 ppb) compliers are more geographically dispersed. Appendix Section A.2 presents an analysis of complier characteristics and discusses the monotonicity assumption.

Our empirical approach permits us to instrument for multiple pollutants simultaneously because they originate from different sets of sources and are carried differently by the wind.<sup>13</sup> In a later analysis, we investigate the sensitivity of our main estimate to controlling for the four other pollutants measured during our study period: NO<sub>2</sub>, CO, O<sub>3</sub>, and TSP. However, because these pollutants are monitored far less frequently than SO<sub>2</sub>, including them reduces our sample size by over 90 percent. We therefore focus on SO<sub>2</sub> in our main analysis and treat the multi-pollutant estimates as a robustness check.

## 4 Short-run empirical results

### 4.1 Mortality by age and cause

We begin by estimating the effect of daily air pollution exposure on same-day mortality. Table 2 presents OLS and IV estimates of Equation (1). Column (1) reports that a 1-day, 1-ppb increase in SO<sub>2</sub> is associated with a same-day mortality increase of 0.008 deaths per million, nearly ten times smaller than the corresponding IV estimate of 0.07 deaths per million reported in Column (2). This downward bias in the OLS estimate is consistent with findings from other quasi-experimental studies of air pollution and is commonly attributed, at least in part, to measurement error in pollution exposure (Deryugina et al., 2019; Alexander and

---

<sup>12</sup>For each geographic group  $g$ , we calculate  $\widehat{\gamma}_g^1 \sin(\theta) + \widehat{\gamma}_g^2 \sin(\theta/2)$  for  $\theta \in [0, 2\pi)$  and take the difference between the maximum and minimum values.

<sup>13</sup>For example, manufacturing plants emit significant amounts of particulate matter, but not SO<sub>2</sub>, while coal power plants emit both.

Schwandt, 2022). Our first-stage  $F$ -statistic exceeds 600, indicating a strong instrument.<sup>14</sup>

Our key identifying assumption is that changes in wind direction affect mortality only through their effects on pollution levels. This assumption would be violated if wind direction were correlated with unobserved weather patterns that independently influence mortality. While impossible to test directly, we assess the plausibility of the assumption by examining the sensitivity of our estimates to alternative ways of controlling for weather conditions, as shown in Columns (3)–(6) of Table 2. Column (3) presents results from a specification that omits all weather controls. Column (4) adds controls for minimum temperature—defined using the same bins as those for maximum temperature—along with all of its possible interactions with other weather controls. In Column (5), we coarsen the interior temperature bins to span 6°C instead of 3°C, and redefine extreme bins to include temperatures below –9°C and above 27°C. Finally, Column (6) replaces temperature and precipitation bins based on county-day averages with bins based on the underlying 2.5-by-2.5-mile grid cells.<sup>15</sup> Our estimate remains stable across all specifications, supporting the validity of the identifying assumption.

Figure 2 presents IV estimates of the effects of a 1-day, 1-ppb increase in SO<sub>2</sub> levels on cumulative mortality up to one month following exposure. The blue point at day 0 corresponds to the estimate of 0.07 deaths per million from Column (2) of Table 2. If short-term mortality displacement were the predominant driver of this 1-day mortality effect, the cumulative effect would decline over time, potentially all the way to zero. Instead, the estimated effect increases steadily, reaching 0.17 deaths per million after one week and 0.25 deaths per million after one month, implying that acute air pollution exposure continues to

---

<sup>14</sup>The  $F$ -statistic is computed assuming errors are homoskedastic, which means it can be compared to the well-known critical values published in Stock and Yogo (2005). Heteroskedasticity-robust  $F$ -statistics also lie well above conventional thresholds. The weak-instrument test of Olea and Pflueger (2013) is not computationally feasible in our setting.

<sup>15</sup>To construct this alternative set of weather variables, we first assign each grid cell to a temperature and precipitation bin, then aggregate to the county level by taking the the maximum and minimum bin values observed across the county’s grid cells. We avoid averaging bin indicators across grid cells, as this would produce too many distinct values and make it computationally infeasible to include fixed effects for all observed weather conditions.

have lethal effects even after exposure has ended. Figure A.6 extends the analysis to 90 days following exposure. The estimated effect continues to rise slightly, eventually exceeding 0.3 deaths per million. However, as the outcome window lengthens, the standard errors increase substantially, limiting statistical precision.

As a falsification test, Figure 2 also reports estimates for the effect of exposure on cumulative mortality during the two weeks *prior* to exposure. These pre-period estimates are small and largely statistically insignificant, supporting the validity of our empirical strategy.

Figure 3 disaggregates the mortality effects by cause of death. As in the aggregate results, the pre-period estimates are small and centered around zero. The sharp increase in 1-day total mortality is driven by roughly equal contributions from cardiovascular disease, cancer, and other diseases. Over longer time horizons, however, the cancer estimate declines, consistent with short-run mortality displacement. Indeed, we cannot reject the null hypothesis that these deaths would have occurred within one month even in the absence of exposure. By contrast, mortality from cardiovascular and other diseases continues to rise with the length of the outcome window, more than quadrupling over the month. Estimated effects for external causes remain consistently small and largely insignificant across all time windows.

Figure 4 shows how the 1-day mortality effect varies by age group.<sup>16</sup> Panel (a) presents the absolute effect (in deaths per million), while Panel (b) expresses the effect as a percentage of the age group's average 1-day mortality. We fail to detect significant mortality increases for the two youngest age groups (covering ages 0–19). For older age groups, effects range from 0.0087 deaths per million for ages 20–44 to 1.9 deaths per million for those over age 85 (Figure 4a). However, these differences are much smaller when expressed in relative terms: the effect represents 0.2 percent of daily mortality for ages 20–44, compared to 0.44 percent for those over age 85. For most age groups, we cannot reject the null of equal relative effects.

Our estimates for older age groups are similar in magnitude to those reported in Deryug-

---

<sup>16</sup>See Appendix Section A.2 for age-specific estimates up to 28 days following exposure.

ina et al. (2019), who investigate the effect of acute exposure to  $\text{PM}_{2.5}$  on 3-day elderly mortality. To our knowledge, no prior quasi-experimental estimates exist for the effect of air pollution on short-run mortality for ages 1–64. For infants, the most comparable studies are Currie and Neidell (2005) and Knittel, Miller and Sanders (2016), both of which estimate the effect of  $\text{PM}_{10}$  (particulate matter with diameter less than  $10 \mu\text{m}$ ) on weekly infant mortality. Currie and Neidell (2005) report null effects, while Knittel, Miller and Sanders (2016) estimate significant positive effects. Our results are broadly consistent with this mixed evidence: we find statistically insignificant but imprecise effects on 1-day and monthly infant mortality, but detect a significant effect on 3-day infant mortality (Table A.6).

Finally, Section A.2 presents an analysis that rules out composition bias as an explanation for the dynamic patterns in Figure 3—specifically, the possibility that cancer-related deaths occurring weeks after exposure are misattributed to other causes. The appendix also reports estimates by more detailed causes of death and includes a series of robustness checks following Deryugina et al. (2019). These include using different sets of fixed effects, varying the number of instrument leads and lags, clustering standard errors at different levels, estimating LIML rather than 2SLS, and using placebo instruments.

## 4.2 Other air pollutants

Our main estimating equation focuses on the relationship between  $\text{SO}_2$  exposure and mortality. However,  $\text{SO}_2$  may be co-transported with other harmful air pollutants or converted into a secondary pollutant that also contributes to observed mortality effects. In particular,  $\text{SO}_2$  transforms into sulfate ( $\text{SO}_4^{2-}$ ), a major component of  $\text{PM}_{2.5}$ , at a rate of several percent per hour. Our estimates may thus reflect the mortality effects of both  $\text{SO}_2$  and its secondary products.

We investigate these possibilities using two complementary approaches. The first controls directly for other air pollutants, instrumenting for each one separately. The second models the atmospheric transport of  $\text{SO}_2$ ,  $\text{NO}_2$ , and  $\text{PM}_{2.5}$ , as well as the chemical conversion of  $\text{SO}_2$

and  $\text{NO}_2$  into  $\text{PM}_{2.5}$ , to assess the extent to which our estimates may reflect these additional pollutants.

The air pollutants available in our dataset come from a variety of sources located in different areas, are carried differently by the wind, and exhibit different chemical behaviors in the atmosphere. Our instruments can capture this variation, but most pollutants aside from  $\text{SO}_2$  are sparsely measured during our sample period, causing sharp drops in sample size when they are included. We therefore limit our multi-pollutant analysis to two subsamples: a small one that includes  $\text{SO}_2$  and four additional pollutants— $\text{NO}_2$ ,  $\text{O}_3$ ,  $\text{CO}$ , and TSP—and a larger one that includes only  $\text{SO}_2$  and TSP, our best proxy for  $\text{PM}_{2.5}$ .

Panels A and B of Table 3 summarize the results. For reference, Column (1) in Panel A reports that a 1-ppb increase in  $\text{SO}_2$  raises 1-day mortality by 0.089 deaths per million in the smallest subsample. This effect decreases by about 40 percent when TSP is added (Column 2), and by about 20 percent when  $\text{NO}_2$ ,  $\text{CO}$ , and  $\text{O}_3$  are added (Column 3). Controlling for all four pollutants simultaneously again shows a similar 40 percent decline (Column 4), suggesting that part of our baseline estimate reflects the influence of particulate matter. In a complementary analysis excluding TSP but including other pollutants (Table A.8), the  $\text{SO}_2$  coefficient remains stable, reinforcing the conclusion that only TSP meaningfully influences the estimated effect of  $\text{SO}_2$ .

Panel B presents results from the larger subsample that includes all observations with non-missing values for  $\text{SO}_2$  and TSP. In this sample, the  $\text{SO}_2$  coefficient falls by 50 percent after controlling for TSP, and the TSP coefficient falls by 30 percent after controlling for  $\text{SO}_2$ .<sup>17</sup> These findings suggest that roughly half of the observed mortality effect attributed to  $\text{SO}_2$  may reflect the influence of particulate matter that is either co-transported with or formed from  $\text{SO}_2$ .

Further interpretation of the estimates in Table 3 is complicated by our inability to observe  $\text{PM}_{2.5}$  or to distinguish “primary” particulate matter that is directly emitted and

---

<sup>17</sup>A similar pattern holds for longer outcome windows: the  $\text{SO}_2$  and TSP coefficients decline in size when jointly included but generally remain statistically significant.

co-transported with SO<sub>2</sub> from “secondary” particulate matter that is formed from SO<sub>2</sub>. To address this limitation, we turn to simulations from the Intervention Model for Air Pollution (InMAP), which models the atmospheric transport and chemical transformations of SO<sub>2</sub>, PM<sub>2.5</sub> (a component of TSP), and NO<sub>2</sub> across the US.<sup>18</sup> InMAP allows us to separately measure primary and secondary PM<sub>2.5</sub> and to quantify the share of secondary PM<sub>2.5</sub> formed specifically from SO<sub>2</sub>. For this analysis, we use data from the 1990 National Emissions Inventory (NEI), the earliest year with suitable emissions information.<sup>19</sup> We simulate two scenarios. The first includes emissions solely from coal-fired power plants, the largest source of SO<sub>2</sub> emissions in the NEI. The second includes all emissions from counties with at least one coal-fired power plant, thus capturing additional co-transported pollutants.

InMAP simulations yield the equilibrium ratio of ambient PM<sub>2.5</sub> to ambient SO<sub>2</sub>, expressed in  $\mu\text{g}/\text{m}^3$  per ppb.<sup>20</sup> In the first scenario—restricting emissions to those from coal-fired power plants—that ratio is 2.3, indicating that each transported ppb of SO<sub>2</sub> is accompanied by 2.3  $\mu\text{g}/\text{m}^3$  of PM<sub>2.5</sub>. Notably, over 90 percent of this PM<sub>2.5</sub> is sulfate, a secondary pollutant derived from SO<sub>2</sub>. The second scenario, which includes emissions from all sources located in counties with coal-fired power plants, yields a similar ratio of 2.5, with over 70 percent of PM<sub>2.5</sub> consisting of sulfate. These findings suggest that most PM<sub>2.5</sub> associated with SO<sub>2</sub> is not independently emitted but chemically derived from SO<sub>2</sub> and would therefore fall if SO<sub>2</sub> emissions declined.

We can use these results to construct an upper bound for the mortality effect of PM<sub>2.5</sub>: if all mortality is due to PM<sub>2.5</sub> rather than SO<sub>2</sub> itself, dividing our estimates by 2.5 would yield the implied effect of one additional  $\mu\text{g}/\text{m}^3$  of PM<sub>2.5</sub>. While we remain agnostic about the precise decomposition, we recognize that our estimates likely reflect a combination of both SO<sub>2</sub> and PM<sub>2.5</sub>. For brevity, we continue to refer to the combined effect simply as the

---

<sup>18</sup>The InMAP model is available for download from <https://github.com/spatialmodel/inmap/releases/tag/v1.9.6>. The evaluation data used in our simulations are from Tessum et al. (2019).

<sup>19</sup>These data are available from [https://gaftp.epa.gov/air/nei/nei\\_criteria\\_summaries/1990criteriasummaryfiles/](https://gaftp.epa.gov/air/nei/nei_criteria_summaries/1990criteriasummaryfiles/).

<sup>20</sup>InMAP reports all pollutants in units of  $\mu\text{g}/\text{m}^3$ . At standard temperature (15 degrees Celsius), 1 ppb of SO<sub>2</sub> corresponds to about 2.62  $\mu\text{g}/\text{m}^3$ .

effect of SO<sub>2</sub>.

## 5 Long-run survival

### 5.1 Framework

Our framework for quantifying the long-run survival effects of chronic exposure to air pollution builds on the dynamic production model of health developed by [Lleras-Muney and Moreau \(2022\)](#). This model offers several advantages. First, it matches the predictive accuracy of leading demographic models across a wide range of population survival curves. Second, it can separately capture both mortality displacement and accelerated aging, two distinct patterns that emerge in our empirical analysis and that have different implications for long-run survival. Finally, the model requires only mortality data for calibration, unlike other models such as [Grossman \(1972\)](#), which depend on additional inputs such as income, prices, healthcare utilization, as well as how these respond to pollution exposure.

Let  $H_{it}$  denote the health capital of individual  $i \in \{1, \dots, N\}$  at age  $t \in \{0, \dots, T\}$ . At birth, each individual is endowed with an initial stock of health,  $H_{i0}^*$ , drawn from a normal distribution. This health stock evolves over the individual's lifetime according to the following equation:

$$H_{it} = H_{i,t-1} - d(t) + I + \varepsilon_{it} \quad (3)$$

where:

$$H_{i0} = H_{i0}^* \sim N(\mu_H, \sigma_H),$$

$$d(t) = \delta t^\alpha,$$

$$\varepsilon_{it} \sim N(0, \sigma_\varepsilon)$$

The health stock depreciates at a rate,  $d(t)$ , which increases with the age of the individual.

It is replenished at a constant rate,  $I$ , which captures time-invariant factors such as early-life parental investment or lifetime health habits, and varies with an i.i.d. health shock,  $\varepsilon_{it}$ . Death occurs when the individual's health stock falls below a critical threshold,  $\underline{H}$ , and is denoted by the indicator variable  $D_{it}$ , where:

$$D_{i0} = 1 [H_{i0} < \underline{H}],$$

$$D_{it} = 1 [H_{it} < \underline{H} | D_{i,t-1} = 0], \quad t > 0$$

The model is fully characterized by seven parameters:  $\{\alpha, \delta, I, \mu_H, \sigma_H, \sigma_e, \underline{H}\}$ .<sup>21</sup>

We compute cohort mortality by simulating Equation (3) for a large population. The mortality rate at age  $t$ ,  $M_t$ , is defined as the number of individuals who die at age  $t$  divided by the number who survive through age  $t - 1$ . Survival at age  $t$ ,  $S_t$ , is calculated recursively:

$$S_1 = 1 - M_0,$$

$$S_t = S_{t-1} (1 - M_{t-1}), \quad t > 1$$

Pollution exposure affects mortality by altering the parameters of the model. While it is plausible that exposure could affect the investment parameter,  $I$ , this channel would imply large and persistent mortality increases across all ages, which is inconsistent with our empirical estimates (Table A.6). Similarly, modifying the variance of the i.i.d. health shock,  $\varepsilon_{it}$ , would imply that pollution improves health for half the population on average, which is implausible. We therefore focus on two key channels: (1) changes to the death threshold,  $\underline{H}$ , which produces mortality displacement, and (2) changes to the depreciation parameter,  $\delta$ , which governs the aging process.<sup>22</sup> These two channels have distinct implications for

<sup>21</sup>The model can be extended to incorporate external causes of death such as car accidents by including two additional parameters specifying the age of onset and the severity of these external causes (Lleras-Muney and Moreau, 2022). However, this extension is unnecessary for our analysis, which focuses on deaths from biological (internal) causes.

<sup>22</sup>Deryugina and Reif (2023) show that estimates are very similar whether changes in depreciation are modeled via  $\delta$  or  $\alpha$ . For simplicity, we focus on  $\delta$ .

long-run mortality. A temporary increase in the death threshold raises mortality among frail individuals close to death but leaves the health of survivors unchanged. Once the threshold reverts to its original level, mortality rates decline temporarily due to the reduced number of individuals close to death. This dynamic produces short-run mortality displacement without affecting long-term survival.

By contrast, a temporary increase in the depreciation rate,  $d(t)$ , reduces the health capital of all individuals—both healthy and frail—leading to persistently higher mortality. As with a higher death threshold, mortality rises among frail individuals, but in this case, the decline in the health stock also extends to the rest of the population. Because future health depends on past health, mortality rates remain elevated even after  $d(t)$  reverts to its original trajectory.

To incorporate our empirical estimates into the model, we assume that the effect of pollution exposure on model parameters depends only on current exposure. Under this assumption, a given exposure shifts the death threshold and the depreciation parameter,  $\delta$ , by the same fixed amounts across all ages. However, because depreciation increases with age ( $d(t) = \delta t^\alpha$ ), older individuals experience larger health declines from the same exposure shock. In addition, because they have lower baseline health capital, the same exposure will increase mortality more at older ages. This prediction aligns with the age-specific mortality patterns observed in our empirical analysis (Figure 4).

Our assumption that the effect of a given exposure on model parameters is constant is supported by medical research showing that pollution triggers similar biological mechanisms across different populations. For example, ambient air pollution exposure increases oxidative stress and inflammation in both healthy and unhealthy individuals (Brook et al., 2010). Likewise, randomized trials find that higher PM<sub>2.5</sub> exposure raises stress hormone levels, insulin resistance, inflammatory markers, and blood pressure even among healthy young adults (Li et al., 2017).

We provide two empirical validations of our modeling framework. First, our assumption that air pollution affects model parameters only through current exposure implies a testable

prediction: parameter values calibrated using one age group should yield accurate mortality predictions for other age groups. We confirm this prediction in the “leave-one-out” exercise presented in Section 5.3. Second, we show that the model’s chronic exposure projections align with both a three-month IV estimate from our empirical model and a three-year estimate from Anderson (2020).

Our analysis proceeds in three steps. First, we calibrate the model’s baseline parameters using a period life table. Second, we downscale the model from annual to daily frequency and identify the change in parameter values required to match our IV estimates of the one-day effect of pollution exposure. We assess model performance by comparing its short-run predictions to internal and external estimates. Finally, we use the model to project the long-run effect of chronic pollution exposure on survival. We explain these steps in more detail below.

## 5.2 Calibration

### 5.2.1 Baseline parameters

The health production model described by Equation (3) depends on seven parameters:  $\{\alpha, \delta, I, \sigma_e, \mu_H, \sigma_H, \underline{H}\}$ . To achieve identification—that is, to ensure a unique solution—we follow Lleras-Muney and Moreau (2022) and normalize two parameters:  $\underline{H} = 0$  and  $\sigma_H = 1$ . We calibrate the five remaining parameters using simulated method of moments. Specifically, we use the Nelder-Mead method to minimize the squared distance between the model’s predicted age-specific survival and observed US population survival in 1972, the first year of our sample.

Whereas Lleras-Muney and Moreau (2022) model mortality at the annual level, our analysis requires a daily resolution to match the granularity of our IV estimates. These estimates imply that a 1-unit increase in  $\text{SO}_2$  raises same-day mortality by less than 0.1 deaths per million (Table 2). Accurately capturing such small effects requires simulating a population of several million individuals. However, calibrating the model’s baseline parameters involves

solving a high-dimensional optimization problem over the entire life cycle, which becomes computationally infeasible at the daily level with such a large population.<sup>23</sup> We therefore proceed in three steps.

First, we calibrate the baseline model at the annual level using  $N = 1,000,000$  individuals. Second, we refine this calibration using daily survival data and  $N = 100,000$  individuals, employing appropriately rescaled estimates from the annual model as starting values.<sup>24</sup> Finally, we use the fully calibrated daily model to simulate  $N = 20,000,000$  individuals. This high-resolution version is used to calibrate the effect of pollution exposure on model parameters, as described in the next section. Because that calibration involves evaluating parameter changes at a single point in time—rather than solving an optimization problem over the full life cycle—it remains computationally tractable at this scale.

Figure A.10 illustrates the results of our baseline calibration. The solid blue line shows the survival curve from the US 1972 life table, while the dashed red line reports the survival curve produced by our model. Apart from a small discrepancy in infancy, the two curves align closely and produce life expectancy estimates that differ by only 0.1 years, indicating a strong model fit. The calibrated parameter values are reported in Table A.15.

### 5.2.2 Pollution exposure parameters

Our IV estimates from Section 4 identify the effect of a 1-day, 1-unit increase in air pollution exposure on mortality over the following month. To incorporate these estimates into our model, we allow exposure to affect two parameters: the death threshold,  $\underline{H}$ , which governs mortality displacement, and  $\delta$ , which governs the aging process. A 1-day increase in the death threshold raises mortality rates temporarily among frail individuals, followed by

---

<sup>23</sup>Assuming a maximum lifespan of 110 years, a daily model requires  $T = 110 \times 365 = 40,150$  daily periods. Simulating  $N = 10,000,000$  individuals produces 401.5 billion health capital values—3.2 terabytes if each value is stored as an 8-byte number. A single simulation of this size takes several hours on a large server, and the optimization routine requires hundreds of such simulations.

<sup>24</sup>We obtain the starting values by dividing the annual estimates of  $I$  and  $\delta$  by 365, and  $\sigma_e$  by  $\sqrt{365}$ . We leave  $\mu_H$  or  $\alpha$  unchanged. While these starting values provide a close approximation, recalibration remains necessary due to the model’s nonlinear dependence on  $t$ .

a compensating drop. In contrast, an increase in  $\delta$  reduces health capital for the entire population, raising both current and future mortality.

Consistent with Figure 3, we assume that cancer-related deaths reflect mortality displacement, while all other deaths reflect accelerated aging. Let  $\hat{\beta}_{a,c}^1$  denote the same-day IV mortality estimate for age group  $a$  and cause of death  $c$ . Consider a specific daily age,  $t$ , within age group  $a$ . Using the high-resolution model described above, we solve numerically for a new death threshold,  $\tilde{H}$ , that raises mortality by  $\hat{\beta}_{a,cancer}^1$  when applied for one day at age  $t$ . We then solve for  $\tilde{\delta}$  such that the combination of  $\tilde{H}$  and  $\tilde{\delta}$  reproduces  $\hat{\beta}_{a,all}^1$ , the total same-day mortality effect.

Because we assume that pollution affects model parameters uniformly across ages, the model can, in principle, be calibrated using any age group. To increase precision, we calibrate the model separately using several older age groups and then average the resulting parameter values when projecting long-run survival. We do not use age groups younger than 65 because their mortality rates are too small to produce stable calibrations. The specific IV estimates used for these calibrations are reported in Table A.16.

To reduce noise from daily variation in the i.i.d. health shocks, we average the calibration across 50 different days near the midpoint of each age bin. For example, for the 65–69 age group, we solve for the parameter changes using ages 68y1d, 68y2d, ..., 68y50d, and take the mean.<sup>25</sup> Section A.3 provides additional details. The final result is a set of parameters for each age group, denoted as  $\{\tilde{H}_a, \tilde{\delta}_a\}$ , that capture the effect of a 1-unit increase in exposure.

To account for econometric uncertainty in the IV estimates, we use a resampling-based methodology. For each age group, we draw a value from a normal distribution centered at the point estimate  $\hat{\beta}_{a,all}^1$ , using the estimated standard error as the standard deviation. We then recalibrate the model based on this draw, holding fixed the proportion of cancer-related deaths. We repeat the process 100 times and report the 5th and 95th percentiles of the resulting distribution of parameter estimates.

---

<sup>25</sup>The optimal strategy would employ all  $365 \times 5 = 1825$  days in each 5-year age bin, giving more weight to ages near the midpoint. However, this level of precision is computationally burdensome.

Figure A.11 presents the resulting age-specific changes in the mortality threshold and the depreciation rate parameters. The estimates are broadly similar across age groups, with most values falling within the 90% confidence intervals of one another. This consistency supports our modeling assumption that the effect of exposure on model parameters does not vary systematically with age. Nonetheless, our long-run projections also explore alternative scenarios in which these parameters are allowed to vary by age.

## 5.3 Validation

We perform two sets of validation exercises. The first compares out-of-sample mortality projections from our model to our IV estimates. The second compares three-year projections to quasi-experimental estimates from Anderson (2020).<sup>26</sup>

### 5.3.1 Internal validation

Because the model is calibrated only to 1-day IV estimates, we begin by assessing its ability to predict mortality effects up to 90 days following exposure. Figure 5 shows results for the 65–69 age group. The solid blue line plots IV estimates of cumulative mortality, and the green dot-dashed line reports “own-age” predictions—model projections based on calibration using  $\hat{\beta}_{65,cancer}^1$  and  $\hat{\beta}_{65,all}^1$ . By construction, the own-age prediction exactly matches the one-day IV estimate; more importantly, it remains within the 95% confidence intervals of the IV estimates over the full 90-day horizon, indicating strong out-of-sample performance.

Next, we conduct a leave-one-out validation exercise. For each age group, we generate predictions using the average of the calibrated parameters from the other four age groups. For example, mortality in the 65–69 age group is predicted using  $\{\frac{1}{4} \sum_{a>65} \tilde{H}_a, \frac{1}{4} \sum_{a>65} \tilde{\delta}_a\}$  rather than the group’s own values. The resulting predictions, shown by the thick red dashed line in Figure 5, also lie inside the 95% confidence intervals of the IV estimates—including the

---

<sup>26</sup>When comparing model projections to external estimates, it is important to recognize that projected survival gains depend on baseline life expectancy. Simulations with alternative life tables suggest that each one-year decrease in baseline life expectancy reduces the estimated survival gain from a fixed decrease in exposure by 0.02 years. Lower baseline life expectancy also causes survival gains to occur earlier in life.

1-day effect, which was not used for calibration. This result is especially notable given that these predictions rely entirely on older age groups whose mortality effects are nearly an order of magnitude larger (Figure 4a). As explained in Section 5.1, this pattern is consistent with the model’s power-function specification for aging, where a fixed increase in  $\delta$  produces larger mortality effects at older ages. The accuracy of the leave-one-out predictions supports both this functional form and our assumption that pollution affects health parameters uniformly across ages.

To demonstrate that the model’s fit is not merely due to wide confidence intervals, we compare it to two extreme alternatives: one in which none of the 1-day mortality effect is due to displacement (“no displacement”) and another in which all of it is (“all displacement”). In the no-displacement scenario, depicted by the orange dashed line at the top of Figure 5, the mortality predictions rise sharply and overshoot the IV estimates. In the all-displacement scenario, depicted by the black dashed line at the bottom of the figure, cumulative mortality falls rapidly to zero, implying no lasting effect. Both scenarios lie well outside the 95% confidence intervals, demonstrating that our IV estimates are sufficiently precise to rule out a meaningful range of counterfactual model predictions. The wide gap between these two extremes also highlights the importance of accurately distinguishing between mortality displacement and accelerated aging.

Figure A.12 extends the leave-one-out validation to all five age groups 65 and over. In general, the model’s predictions remain within the 95% confidence intervals across all five age groups. The main exception is the 85+ age group, where the model’s predictions modestly undershoot the IV estimates for the first half of the 90-day window. Overall, the close agreement between model predictions and empirical estimates provides strong evidence that the model accurately captures mortality dynamics following short-term exposure.

We further validate the model using IV estimates from longer exposure windows. Although our wind-based instrument lacks the persistence to estimate chronic exposure effects directly, it can still identify the effects of prolonged exposure lasting up to several months. To

that end, we construct predicted SO<sub>2</sub> concentrations,  $\widehat{\text{SO}}_2_{cd}$ , using the first-stage estimates from Equation (2):

$$\widehat{\text{SO}}_2_{cd} = \sum_{g=1}^{50} \hat{f}^g(\theta_{cd}) \quad (4)$$

We then aggregate these predicted quantities into multi-day periods  $\bar{d}$  ranging from 2 to 90 days and calculate both observed and predicted SO<sub>2</sub> averages for each period, denoted as  $\text{SO}_2_{c\bar{d}}$  and  $\widehat{\text{SO}}_2_{c\bar{d}}$ . Finally, we regress  $Y_{c\bar{d}}$ , the mortality rate in time period  $\bar{d}$ , on  $\text{SO}_2_{c\bar{d}}$ , instrumenting with  $\widehat{\text{SO}}_2_{c\bar{d}}$ , and controlling for county-by-month, month-by-year, and time period ( $\bar{d}$ ) fixed effects.<sup>27</sup> We then compare the resulting estimates to model predictions over the same horizons.

Figure 6 reports results for the 65–69 age group. Cumulative mortality rises with exposure duration, reaching about 10 deaths per million after one month and 30 after three months—roughly fifteen times larger than the corresponding acute effects (Figure 5). Notably, the model’s predictions track the empirical estimates closely and remain within the 95% confidence intervals throughout, lending further credibility to its ability to predict the mortality effects of pollution exposure. However, the strength of our first stage declines substantially with longer exposure windows, and many estimates for older age groups become highly imprecise. We therefore interpret these longer-exposure results as suggestive rather than conclusive.

### 5.3.2 External validation

Validating the model’s long-run accuracy is challenging because wind direction provides little quasi-experimental variation beyond a few months and mortality estimates become imprecise at longer horizons. Instead, we draw on quasi-experimental evidence from Anderson (2020), who studies the impact of living downwind of Los Angeles highways on three-year mortality among individuals aged 75 and older.

---

<sup>27</sup>Because some time periods  $\bar{d}$  cross calendar month boundaries, the month-by-year fixed effects are not perfectly collinear with the time-period fixed effects. In those cases, we assign the month-by-year fixed effect based on the earliest calendar month covered by the period.

To compare our model’s predictions to his estimates, we construct a counterfactual for our 1972 cohort where we increase SO<sub>2</sub> levels by 1 unit ( $\approx$  10 percent) beginning at age 72 and continuing for 10 years—the approximate exposure duration faced by individuals in Anderson’s sample.<sup>28</sup> We then calculate the ensuing three-year mortality increase for ages 82–84 and express the result as a change in life expectancy at birth to enable a direct comparison. Under this counterfactual, our model predicts a life expectancy reduction of 0.06 years (90% bootstrap CI: 0.02–0.13 years), which aligns with Anderson’s estimates that a 10 percent increase in NO<sub>2</sub> levels reduces life expectancy by 0.05–0.064 years.<sup>29</sup>

Because the model spans the full life cycle, it can also project effects beyond Anderson’s three-year horizon. Extending the analysis to the end of life, we find that these 10 years of increased exposure reduce life expectancy at birth by 0.12 years (90% bootstrap CI: 0.03 to 0.22)—roughly twice the effect observed over three years. This result implies that even a three-year outcome window may substantially understate the total mortality burden of chronic pollution exposure.

## 5.4 Long-run projections

Finally, we use our calibrated model to quantify the effects of a permanent, 1-ppb ( $\approx$  10%) decrease in SO<sub>2</sub> exposure on life expectancy. To simulate this counterfactual, we compute survival for the 1972 cohort using the average of the age-specific calibrated parameter values:

$$\{\tilde{\mathbf{H}}, \tilde{\delta}\} = \left\{ \frac{1}{5} \sum_{a \geq 65} \tilde{\mathbf{H}}_a, \frac{1}{5} \sum_{a \geq 65} \tilde{\delta}_a \right\}$$

We assume this reduction in exposure begins at birth, affecting model parameters for all  $t \geq 0$ . For comparison, we also estimate survival gains by extrapolating our age-specific

---

<sup>28</sup>Anderson (2020) estimates that 78 percent of the sample had lived in the same location for at least 10 years. The average age of the US population over 75 in the year 2000—the midpoint of the study—was 82.

<sup>29</sup>Like SO<sub>2</sub>, NO<sub>2</sub> contributes to the formation of secondary particulate matter (e.g., nitrates). Anderson (2020) attributes his estimated mortality effect to a mix of near-roadway air pollutants, which include ultrafine particles, NO<sub>2</sub>, and CO.

28-day IV estimates over the full life cycle.<sup>30</sup>

Figure 7 presents the results. Absent any change in exposure, the model predicts a life expectancy of 71.32 years for the 1972 cohort. Under our preferred (“baseline”) specification, depicted by the solid blue line, a permanent, 1-ppb decrease in SO<sub>2</sub> exposure would improve life expectancy by 1.13 years (1.58%). By contrast, the simple IV extrapolation implies a gain of only 0.15 years (0.21%), about one-seventh as large and well below the model’s 90 percent confidence interval (0.40–1.99 years).<sup>31</sup> This downward bias reflects a key limitation of naive extrapolation: it fails to capture the gradual accumulation of health deficits that may take decades to surface as increased mortality.

To test the sensitivity of the results to our assumption that pollution exposure has a constant effect on model parameters, we consider two alternative specifications that allow these effects to vary with age (Figure A.14). Model 2 (“age bins”) uses separate parameter values for each older age group (65–69, 70–74, 75–79, 80–84, and 85+) and assigns the 65–69 values to younger ages. This approach, depicted by the red dashed line in Figure 7, produces slightly larger survival improvements than the baseline specification. Model 3 (“linear fit”) imposes a linear age trend on parameter values, subject to the constraint that pollution cannot improve health and has no effect on health at birth. This more conservative approach implies minimal latent health effects of pollution at young ages (Figure A.14) and thus predicts smaller survival gains than the baseline specification. Even so, the predicted gains remain much larger than those implied by extrapolating short-run IV estimates (Table A.17).

Although the exposure reduction begins at birth, the resulting survival gains are concentrated in older ages. In our baseline specification, over 90 percent of improvement occurs after age 50, and over 75 percent after age 65. This pattern reflects two distinct mechanisms.

---

<sup>30</sup>We use the 28-day IV estimates reported in the last row of Table A.6. We assign each estimate to the midpoint of its age bin, set negative values to 0, and interpolate between points to construct a complete age profile.

<sup>31</sup>Table A.17 reports survival gains and confidence intervals for exposure changes of up to 3 ppb. The dose-response relationship is roughly linear, although we caution that this result relies on the assumed linear relationship between air pollution and mortality in Equation (1).

First, because health capital depreciates as a power function of age, the effect of reducing the depreciation rate is larger later in life. Second, while early-life reductions in exposure do boost health capital, their short-run effects on mortality are muted because most younger individuals remain well above the death threshold. As individuals age and their health capital declines, these earlier gains begin to translate into higher survival.

#### 5.4.1 Discussion

Because our model does not account for behavioral responses, its survival projections should be interpreted as holding long-run behavior fixed. In the context of air pollution, economists typically distinguish between two types of responses: avoidance and mitigation. Avoidance refers to *ex ante* actions that reduce exposure, such as moving to a less polluted neighborhood. While avoidance behavior complicates the measurement of actual exposure, it does not undermine the model’s predictive ability provided that the timing and extent of exposure are correctly specified. For example, the model can predict survival gains from relocation if the age at which the move occurs and the resulting change in exposure are known.

Mitigation, by contrast, refers to *ex post* actions that reduce the harmful effects of exposure, such as increased medical care. Because mitigation can alter the mapping from exposure to model parameters, it poses a more serious challenge for long-run mortality projections. Nonetheless, our validation exercises suggest that mitigation has limited influence on survival projections over short and medium time horizons: our model accurately extrapolates 1-day estimates to 90-day outcomes, and its three-year projections are consistent with estimates from [Anderson \(2020\)](#). However, we cannot rule out the possibility that mitigation becomes more important over longer horizons. While prior studies have found that air pollution exposure increases healthcare utilization over periods of up to three to five months (e.g., [Deschênes, Greenstone and Shapiro, 2017](#); [Barwick et al., 2024](#)), we are not aware of quasi-experimental research on mitigation behavior over longer time periods. It also remains unclear whether real-world mitigation meaningfully weakens the relationship between

pollution and health. More direct evidence on these questions would be valuable.

If long-run mitigation does reduce the health impacts of air pollution, our model’s projections may alternatively be interpreted as capturing the *total cost* (or benefit) of a change in pollution exposure, rather than its direct survival effect, provided certain assumptions hold. In the context of temperature, [Carleton et al. \(2022\)](#) argue that a fully optimizing agent will invest in mitigation until marginal benefit equals marginal cost. Applied to pollution, this logic implies that the marginal mortality effect predicted by our model—when expressed in monetary terms—could be interpreted as the sum of two components: the realized (post-mitigation) marginal mortality costs and the marginal costs of mitigation itself. In this sense, the predicted mortality effect approximates the full cost of pollution exposure.

## 6 Conclusion

Accurate estimates of the long-run health effects of chronic air pollution exposure are vital for making informed policy decisions. We develop a novel two-step approach that combines short-run causal mortality estimates with a structural model that produces reliable long-run survival projections. Although we focus on air pollution, the framework is general and can be applied to other health risks, provided that short-run mortality effects are available and can be credibly mapped to relevant structural parameters.

To obtain causal estimates, we assemble a new dataset that combines daily data on weather, air pollution, and mortality. We then instrument for changes in  $\text{SO}_2$  levels using changes in wind direction. We find that acute air pollution exposure affects mortality through two distinct channels: mortality displacement, where exposure hastens death among frail individuals, and accelerated aging, where exposure produces lasting health damage that raises future mortality risk.

We then incorporate these short-run IV estimates into our structural model to project the long-run consequences of pollution exposure. We find that a permanent, ten percent decrease

in air pollution exposure would improve life expectancy by 1.13 years, holding behavior fixed. This gain is about seven times larger than what a naive extrapolation of short-run IV estimates would suggest, demonstrating the importance of accounting for latent health changes that unfold over time. While we do not assess the costs of reducing air pollution emissions—a necessary ingredient for a full cost-benefit analysis—our results suggest that the benefits of reducing chronic pollution exposure may be substantially underestimated.

Our analysis offers several lessons for applying this modeling approach in other contexts. First, distinguishing between short-run mortality displacement and persistent damage to latent health is crucial, as these two pathways have sharply different implications for long-run survival. Second, age-specific mortality estimates can help identify which model parameters are affected by exposure. Finally, in the absence of direct long-run empirical estimates, pathophysiological evidence can inform model design. In the case of air pollution, medical evidence points to accelerated aging as a key mechanism, with consistent biological responses—like oxidative stress and inflammation—observed at different ages.

## References

- Agency for Toxic Substances and Disease Registry (1998). Public health statement for sulfur dioxide. Technical report, U.S. Department of Health and Human Services.
- Alexander, D. and H. Schwandt (2022). The impact of car pollution on infant and child health: Evidence from emissions cheating. *The Review of Economic Studies* 89(6), 2872–2910.
- Allcott, H., M. Gentzkow, and L. Song (2022). Digital addiction. *American Economic Review* 112(7), 2424–2463.
- Andersen, S., L. Guiso, F. Marciano, P. Sapienza, and L. Zingales (2023). Measuring the Long-Term Impact of Environmental Externalities. Working Paper.
- Anderson, M. L. (2020). As the Wind Blows: The Effects of Long-Term Exposure to Air Pollution on Mortality. *Journal of the European Economic Association* 18(4), 1886–1927.
- Angrist, J. D., K. Graddy, and G. W. Imbens (2000). The interpretation of instrumental variables estimators in simultaneous equations models with an application to the demand for fish. *The Review of Economic Studies* 67(3), 499–527.
- Arenberg, S. and S. Neller (2023). Ashes to ashes: The lifelong consequences of early-life wildfire exposure. Working Paper.
- Barreca, A. I., M. Neidell, and N. J. Sanders (2021). Long-run pollution exposure and adult mortality: Evidence from the acid rain program. *Journal of Public Economics* 200, 104440.
- Barwick, P. J., S. Li, D. Rao, and N. B. Zahur (2018). The healthcare cost of air pollution: Evidence from the worlds largest payment network. Technical report, National Bureau of Economic Research.
- Barwick, P. J., S. Li, D. Rao, and N. B. Zahur (2024). The healthcare cost of air pollution: Evidence from the world’s largest payment network. *Review of Economics and Statistics*, 1–52.
- Brook, R. D., S. Rajagopalan, C. A. Pope III, J. R. Brook, A. Bhatnagar, A. V. Diez-Roux, F. Holguin, Y. Hong, R. V. Luepker, M. A. Mittleman, et al. (2010). Particulate matter air pollution and cardiovascular disease: an update to the scientific statement from the american heart association. *Circulation* 121(21), 2331–2378.
- Carleton, T., A. Jina, M. Delgado, M. Greenstone, T. Houser, S. Hsiang, A. Hultgren, R. E. Kopp, K. E. McCusker, I. Nath, J. Rising, A. Rode, H. K. Seo, A. Viaene, J. Yuan, and A. T. Zhang (2022). Valuing the global mortality consequences of climate change accounting for adaptation costs and benefits. *The Quarterly Journal of Economics* 137(4), 2037–2105.

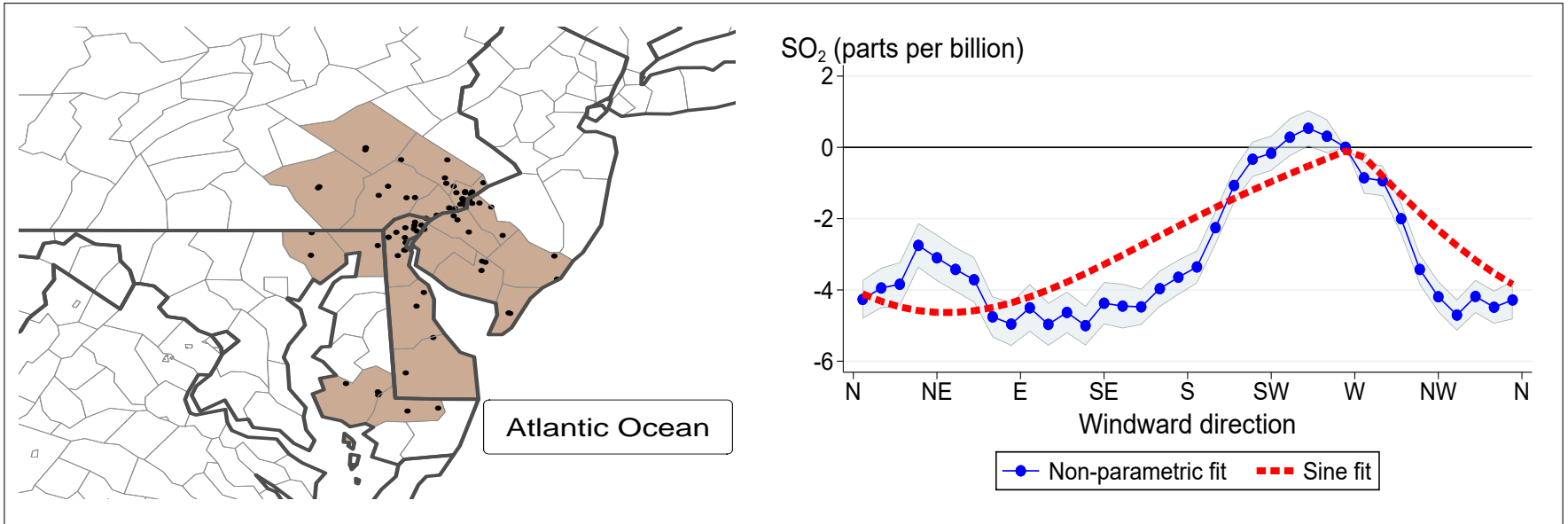
- Chen, Y., A. Ebenstein, M. Greenstone, and H. Li (2013). Evidence on the impact of sustained exposure to air pollution on life expectancy from chinas huai river policy. *Proceedings of the National Academy of Sciences* 110(32), 12936–12941.
- Colmer, J. and J. Voorheis (2020). The grandkids aren't alright: the intergenerational effects of prenatal pollution exposure. Working Paper.
- Currie, J. and M. Neidell (2005). Air pollution and infant health: What can we learn from california's recent experience? *Quarterly Journal of Economics* 120(3), 1003–1030.
- Currie, J., J. G. Zivin, J. Mullins, and M. Neidell (2014). What do we know about short- and long-term effects of early-life exposure to pollution? *Annual Review of Resource Economics* 6(1), 217–247.
- Deryugina, T., G. Heutel, N. Miller, D. Molitor, and J. Reif (2019). The mortality and medical costs of air pollution: Evidence from changes in wind direction. *American Economic Review* 109(12), 4178–4219.
- Deryugina, T. and J. Reif (2023). The long-run effect of air pollution on survival. NBER Working Paper 31858, National Bureau of Economic Research.
- Deschênes, O. and M. Greenstone (2011). Climate change, mortality, and adaptation: Evidence from annual fluctuations in weather in the us. *American Economic Journal: Applied Economics* 3(4), 152–185.
- Deschênes, O., M. Greenstone, and J. S. Shapiro (2017). Defensive investments and the demand for air quality: Evidence from the nox budget program. *American Economic Review* 107(10), 2958–89.
- Dominici, F., M. Greenstone, and C. R. Sunstein (2014). Particulate matter matters. *Science* 344(6181), 257–259.
- Ebenstein, A., M. Fan, M. Greenstone, G. He, and M. Zhou (2017). New evidence on the impact of sustained exposure to air pollution on life expectancy from chinas huai river policy. *Proceedings of the National Academy of Sciences* 114(39), 10384–10389.
- Environmental Protection Agency (2004). The particle pollution report: Current understanding of air quality and emissions through 2003. Technical report, U.S. Environmental Protection Agency.
- Graff Zivin, J. and M. Neidell (2012). The impact of pollution on worker productivity. *American Economic Review* 102(7), 3652–3673.
- Grossman, M. (1972). On the concept of health capital and the demand for health. *Journal of Political Economy* 80(2), 223–255.
- Heo, S. W., K. Ito, and R. Kotamarthi (2023). International spillover effects of air pollution: Evidence from mortality and health data. Technical report, National Bureau of Economic Research.

- Hill, W., E. L. Lim, C. E. Weeden, C. Lee, M. Augustine, K. Chen, F.-C. Kuan, F. Marongiu, E. J. Evans Jr, D. A. Moore, et al. (2023). Lung adenocarcinoma promotion by air pollutants. *Nature* 616(7955), 159–167.
- Hollingsworth, A. and I. Rudik (2021). The effect of leaded gasoline on elderly mortality: Evidence from regulatory exemptions. *American Economic Journal: Economic Policy* 13(3), 345–73.
- Hollingsworth, A. J., D. M. Konisky, and N. Zirogiannis (2021). The health consequences of excess emissions: Evidence from texas. *Journal of Environmental Economics and Management* 108, 102449.
- Isen, A., M. Rossin-Slater, and R. Walker (2017). Every breath you take - every dollar you'll make: The long-term consequences of the clean air act of 1970. *Journal of Political Economy* 125(3), 848–902.
- Kalnay, E., M. Kanamitsu, R. Kistler, W. Collins, D. Deaven, L. Gandin, M. Iredell, S. Saha, G. White, J. Woollen, Y. Zhu, M. Chelliah, W. Ebisuzaki, W. Higgins, J. Janowiak, K. C. Mo, C. Ropelewski, J. Wang, A. Leetmaa, R. Reynolds, R. Jenne, and D. Joseph (1996). The ncep/ncar 40-year reanalysis project. *Bulletin of the American Meteorological Society* 77(3), 437–471.
- Knittel, C. R., D. L. Miller, and N. J. Sanders (2016). Caution, drivers! children present: Traffic, pollution, and infant health. *Review of Economics and Statistics* 98(2), 350–366.
- Landrigan, P. J., R. Fuller, N. J. Acosta, O. Adeyi, R. Arnold, A. B. Baldé, R. Bertollini, S. Bose-O'Reilly, J. I. Boufford, P. N. Breyse, et al. (2018). The lancet commission on pollution and health. *The Lancet* 391(10119), 462–512.
- Li, H., J. Cai, R. Chen, Z. Zhao, Z. Ying, L. Wang, J. Chen, K. Hao, P. L. Kinney, H. Chen, et al. (2017). Particulate matter exposure and stress hormone levels: a randomized, double-blind, crossover trial of air purification. *Circulation* 136(7), 618–627.
- Lleras-Muney, A. and F. Moreau (2022). A unified model of cohort mortality. *Demography* 59(6), 2109–2134.
- Luria, M., R. E. Imhoff, R. J. Valente, W. J. Parkhurst, and R. L. Tanner (2001). Rates of conversion of sulfur dioxide to sulfate in a scrubbed power plant plume. *Journal of the Air & Waste Management Association* 51(10), 1408–1413.
- Nadler, D. L. and I. G. Zurbenko (2014). Estimating cancer latency times using a weibull model. *Advances in Epidemiology 2014*, Article ID 746769, 8 pages.
- Obradovi, F. (2024). Identification of long-term treatment effects via temporal links, observational, and experimental data. arXiv preprint arXiv:2411.04380.
- Olea, J. L. M. and C. Pflueger (2013). A robust test for weak instruments. *Journal of Business & Economic Statistics* 31(3), 358–369.

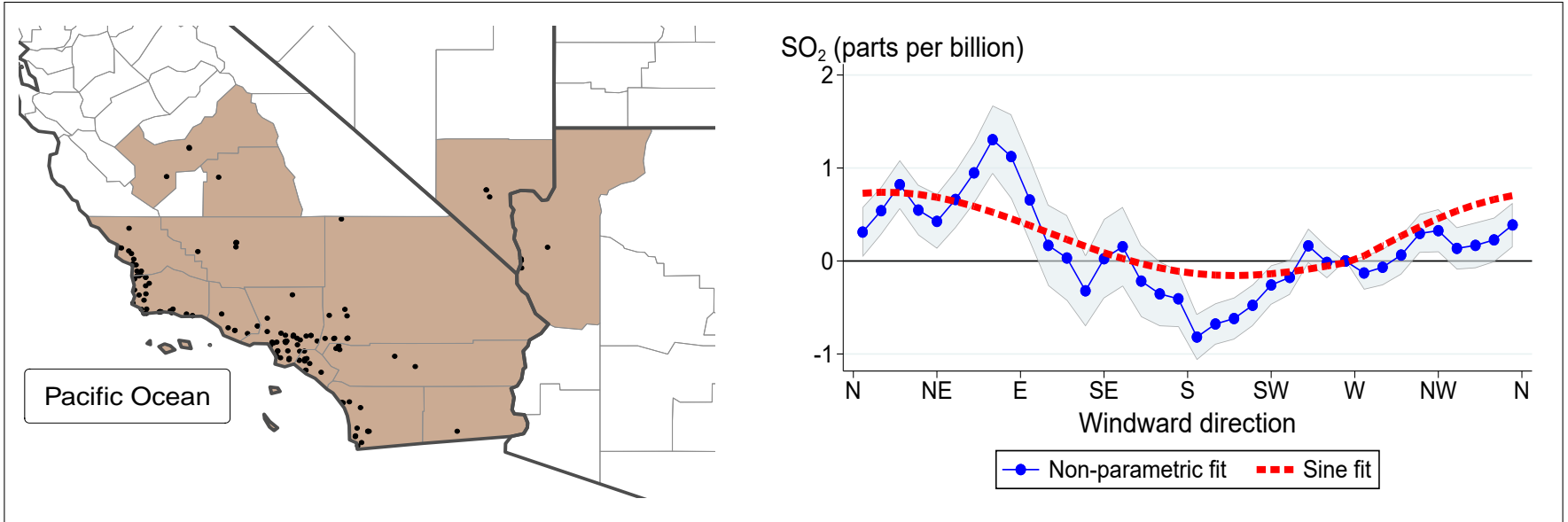
- Qin, G., M. Wu, J. Wang, Z. Xu, J. Xia, and N. Sang (2016). Sulfur dioxide contributes to the cardiac and mitochondrial dysfunction in rats. *Toxicological Sciences* 151(2), 334–346.
- Rajagopalan, S. and P. J. Landrigan (2021). Pollution and the heart. *New England Journal of Medicine* 385(20), 1881–1892.
- Sang, N., Y. Yun, H. Li, L. Hou, M. Han, and G. Li (2010). So<sub>2</sub> inhalation contributes to the development and progression of ischemic stroke in the brain. *Toxicological Sciences* 114(2), 226–236.
- Schlenker, W. and M. J. Roberts (2009). Nonlinear temperature effects indicate severe damages to u.s. crop yields under climate change. *Proceedings of the National Academy of Sciences* 106(37), 15594–15598.
- Schlenker, W. and W. R. Walker (2016). Airports, air pollution, and contemporaneous health. *Review of Economic Studies* 83(2), 768–809.
- Stock, J. and M. Yogo (2005). Testing for weak instruments in linear iv regression. In *Identification and Inference for Econometric Models: Essays in Honor of Thomas Rothenberg*, Chapter 5, pp. 80–108. Cambridge University Press.
- Tessum, C., J. Hill, J. Marshall, and D. Paoletta (2019, September). Evaluation data for the Intervention Model for Air Pollution (InMAP) version 1.6.1.
- Todd, P. E. and K. I. Wolpin (2023). The best of both worlds: combining randomized controlled trials with structural modeling. *Journal of Economic Literature* 61(1), 41–85.
- Turner, M. C., Z. J. Andersen, A. Baccarelli, W. R. Diver, S. M. Gapstur, C. A. Pope III, D. Prada, J. Samet, G. Thurston, and A. Cohen (2020). Outdoor air pollution and cancer: An overview of the current evidence and public health recommendations. *CA: a Cancer Journal for Clinicians* 70(6), 460–479.
- Voorheis, J. (2017). Air quality, human capital formation and the long-term effects of environmental inequality at birth. US Census Center for Economic Studies, CARRA Working Paper Series.
- Yao, G., H. Yue, Y. Yun, and N. Sang (2015). Chronic so<sub>2</sub> inhalation above environmental standard impairs neuronal behavior and represses glutamate receptor gene expression and memory-related kinase activation via neuroinflammation in rats. *Environmental Research* 137, 85–93.

**Figure 1:** The relationship between wind direction and SO<sub>2</sub> concentration, Greater Philadelphia and Southern California areas

**Greater Philadelphia area**

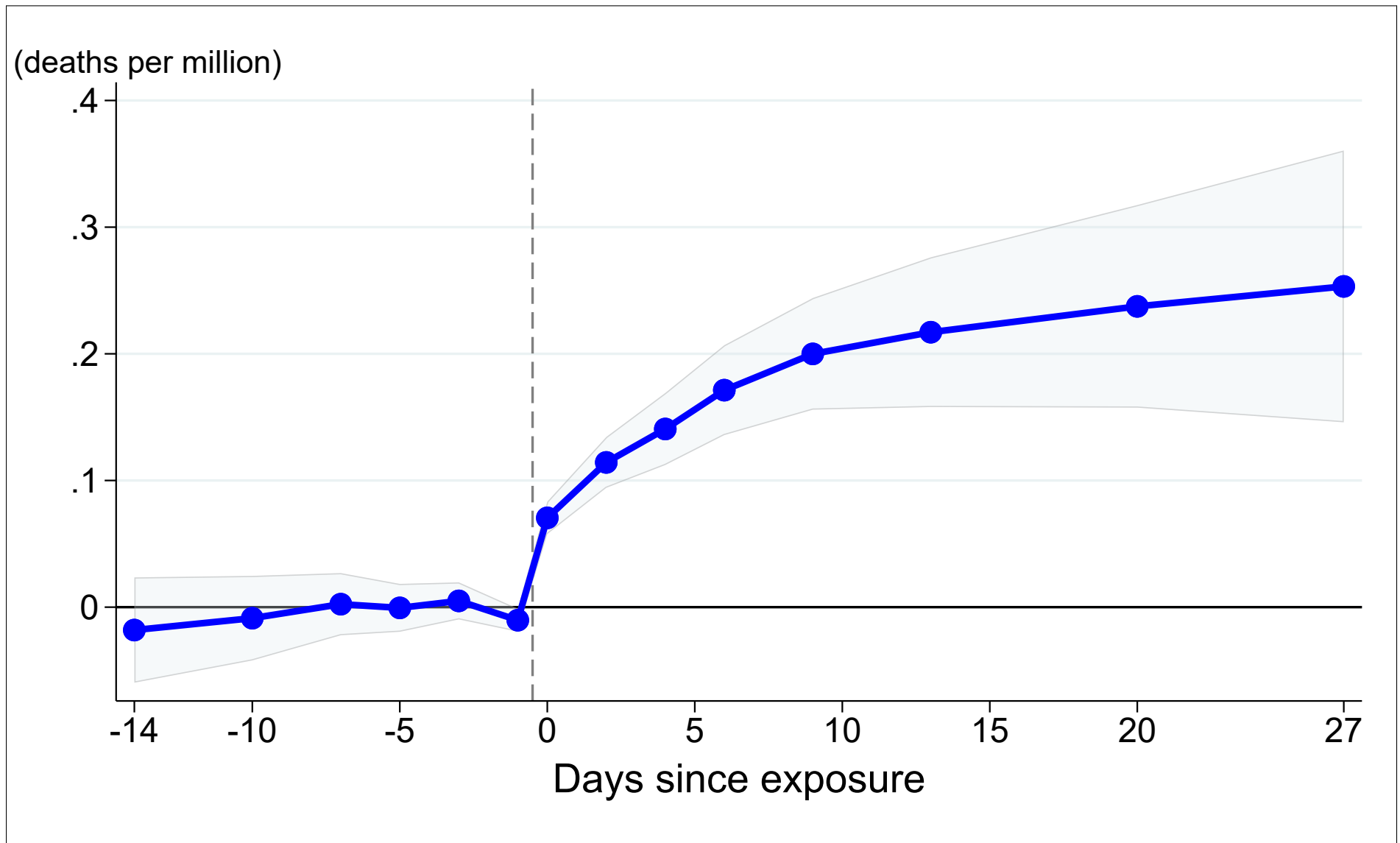


**Southern California area**



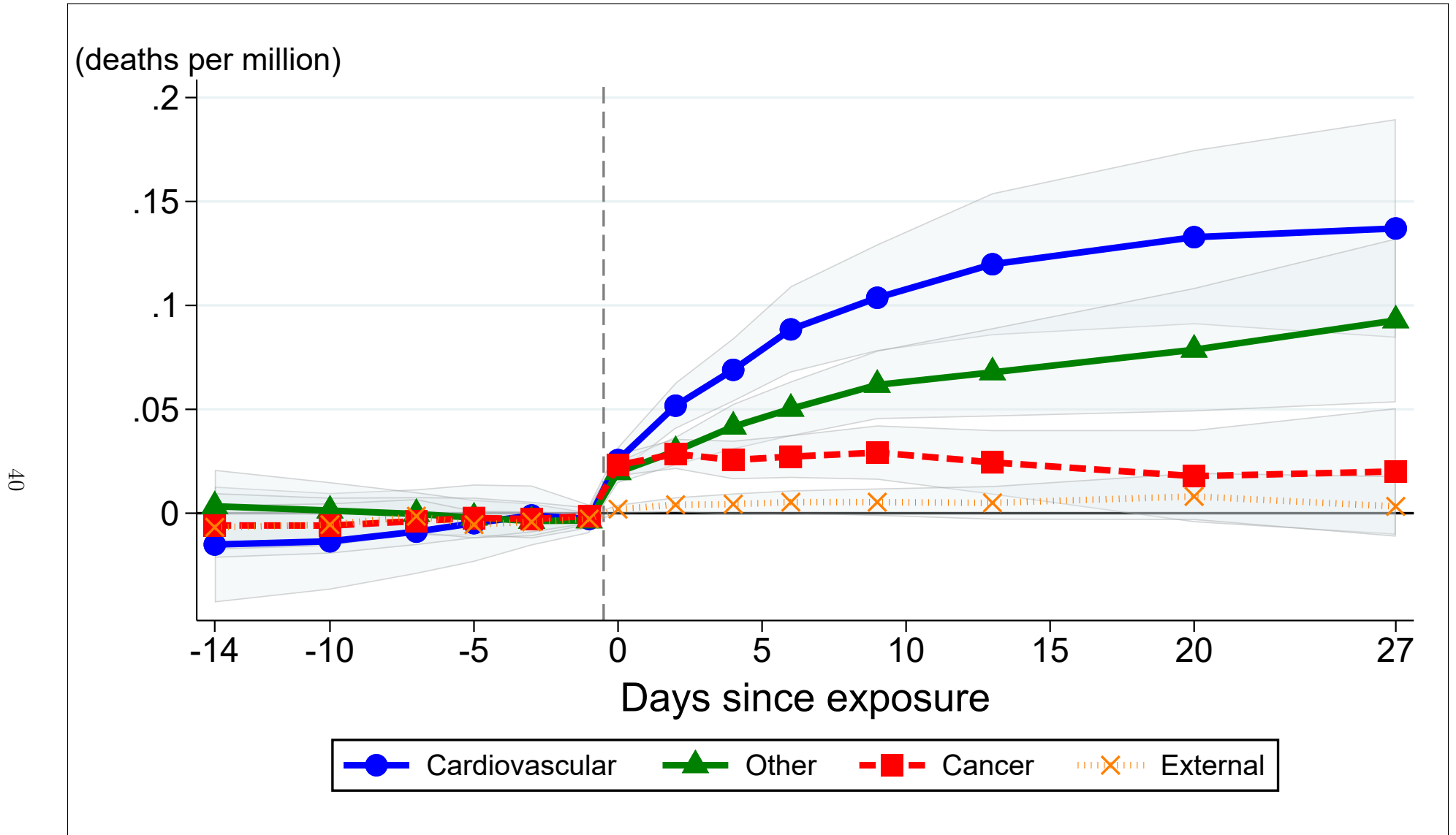
Notes: Black dots on the maps indicate the locations of sulfur dioxide (SO<sub>2</sub>) pollution monitors. The graphs on the right plot the relationship between SO<sub>2</sub> levels and windward direction in each area. Windward direction refers to the direction the wind is coming from (e.g., “N” for wind blowing from the North and “NE” for wind blowing from the Northeast). The 36 blue points report coefficient estimates from a non-parametric regression of SO<sub>2</sub> levels on wind direction, grouped into 10-degree angle bins. The shaded areas denote 95% confidence intervals. Red dashed lines report fitted values from the parametric sine-based specification given by  $f^q(\theta)$  in Equation (2). All regressions include county-by-month and month-by-year fixed effects, as well as flexible controls for maximum temperature, precipitation, humidity, and wind speed; and two leads and two lags of the instruments. Standard errors are robust to heteroskedasticity.

**Figure 2:** IV estimates for the effect of acute (1-day) air pollution exposure on cumulative mortality



Notes: Each point reports an IV estimate from Equation (1) for the effect of a 1-day, 1 ppb increase in sulfur dioxide ( $\text{SO}_2$ ) exposure on mortality, measured as cumulative deaths per million over time windows ranging from 14 days before to 27 days after exposure (with 0 indicating the day of exposure). The shaded area denotes 95% confidence intervals. Post-exposure point estimates are reported in Column (2) of Table A.4. All regressions include county-by-month and month-by-year fixed effects, as well as flexible controls for maximum temperature, precipitation, humidity, and wind speed; leads of these weather controls; and two leads and two lags of the instruments. Estimates are weighted by county population. Standard errors are clustered by county.

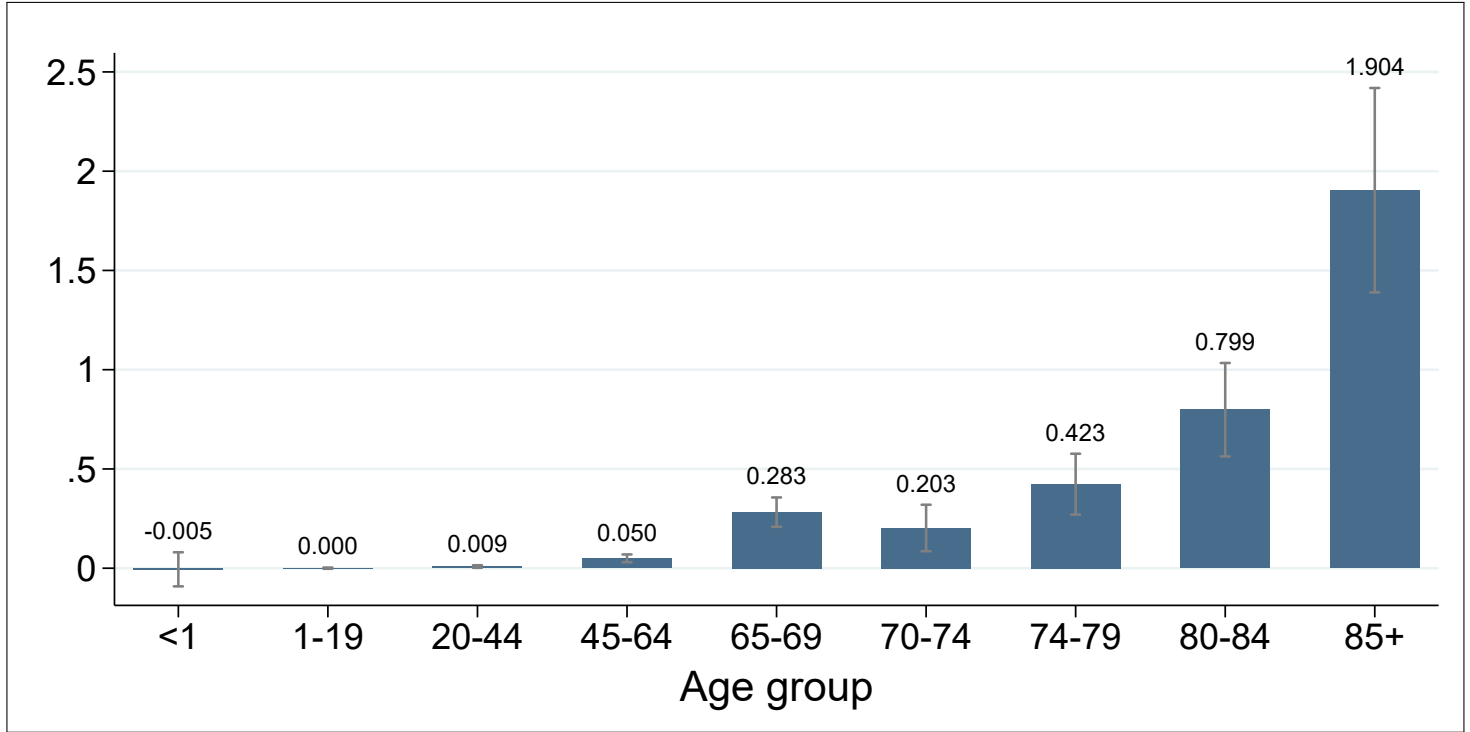
**Figure 3:** IV estimates for the effect of acute (1-day) air pollution exposure on cumulative mortality, by cause of death



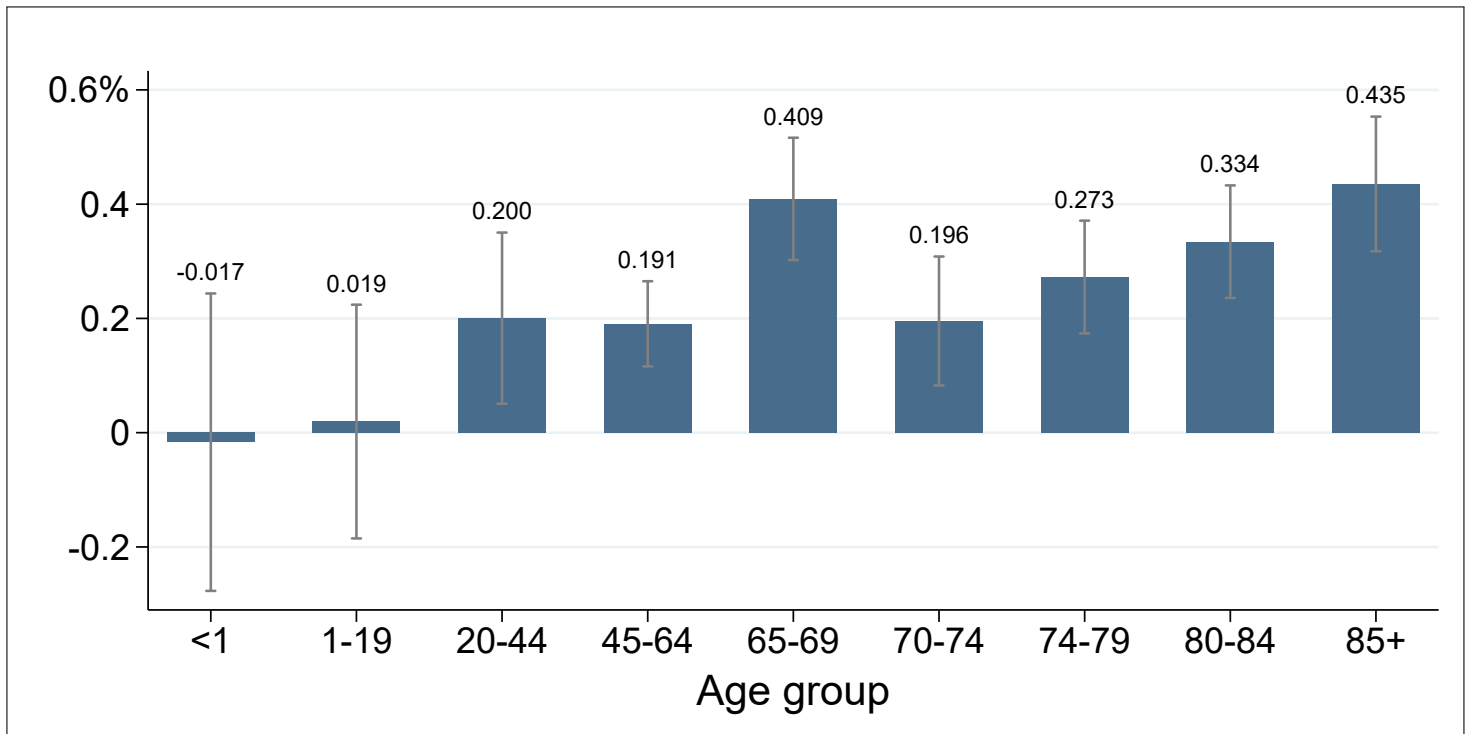
Notes: Each point reports an IV estimate from Equation (1) for the effect of a 1-day, 1 ppb increase in sulfur dioxide (SO<sub>2</sub>) exposure on mortality from four causes of death: cardiovascular disease, other diseases, cancer, and external causes. Mortality is measured as cumulative deaths per million over time windows ranging from 14 days before to 27 days after exposure (with 0 indicating the day of exposure). The shaded areas denote 95% confidence intervals. Post-exposure point estimates are reported in Table A.7. All regressions include county-by-month and month-by-year fixed effects, as well as flexible controls for maximum temperature, precipitation, humidity, and wind speed; leads of these weather controls; and two leads and two lags of the instruments. Estimates are weighted by county population. Standard errors are clustered by county.

**Figure 4:** IV estimates for the effect of acute (1-day) air pollution exposure on 1-day mortality, by age group

(a) Absolute increase (deaths per million)

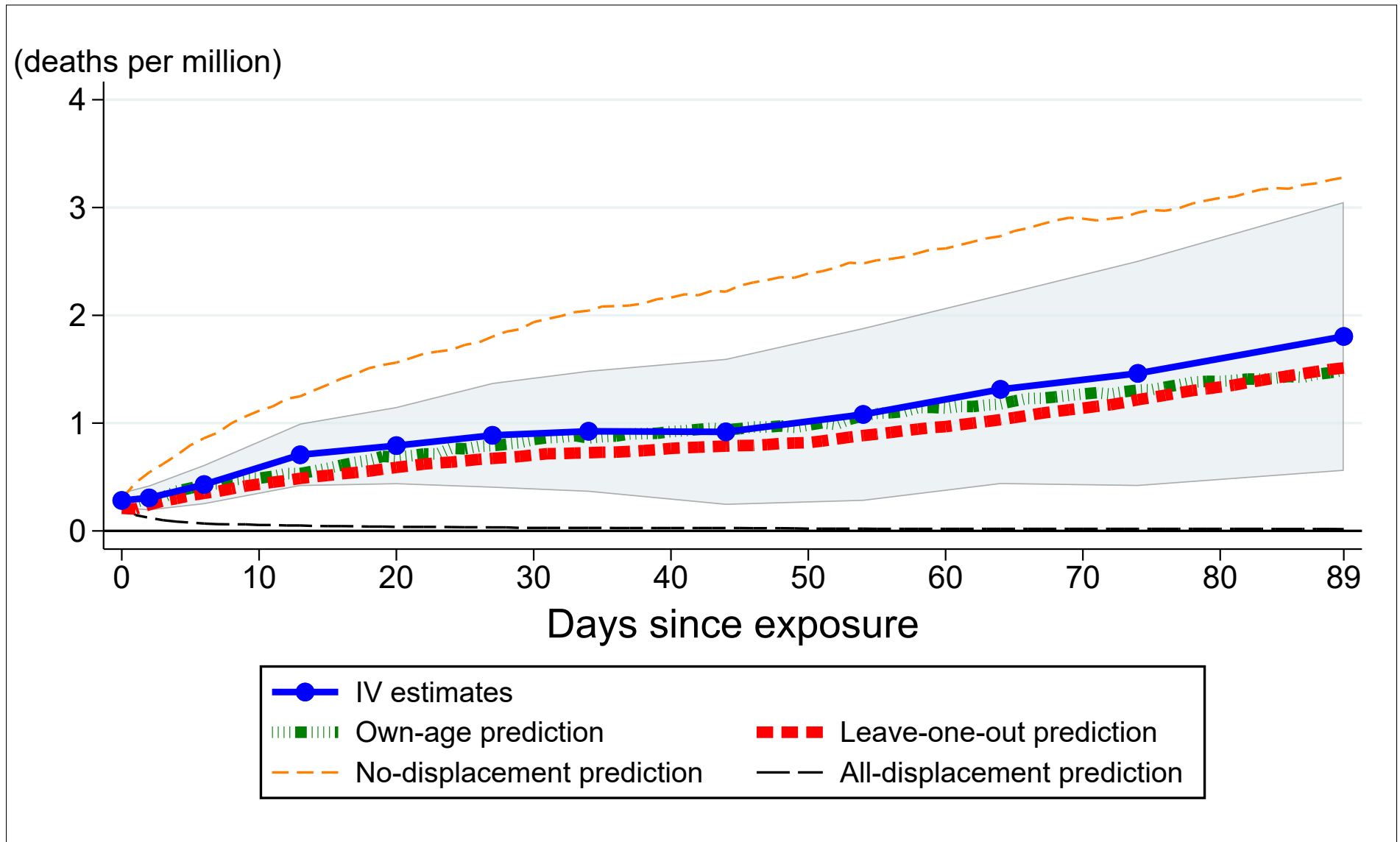


(b) Relative increase (percent of 1-day mortality)



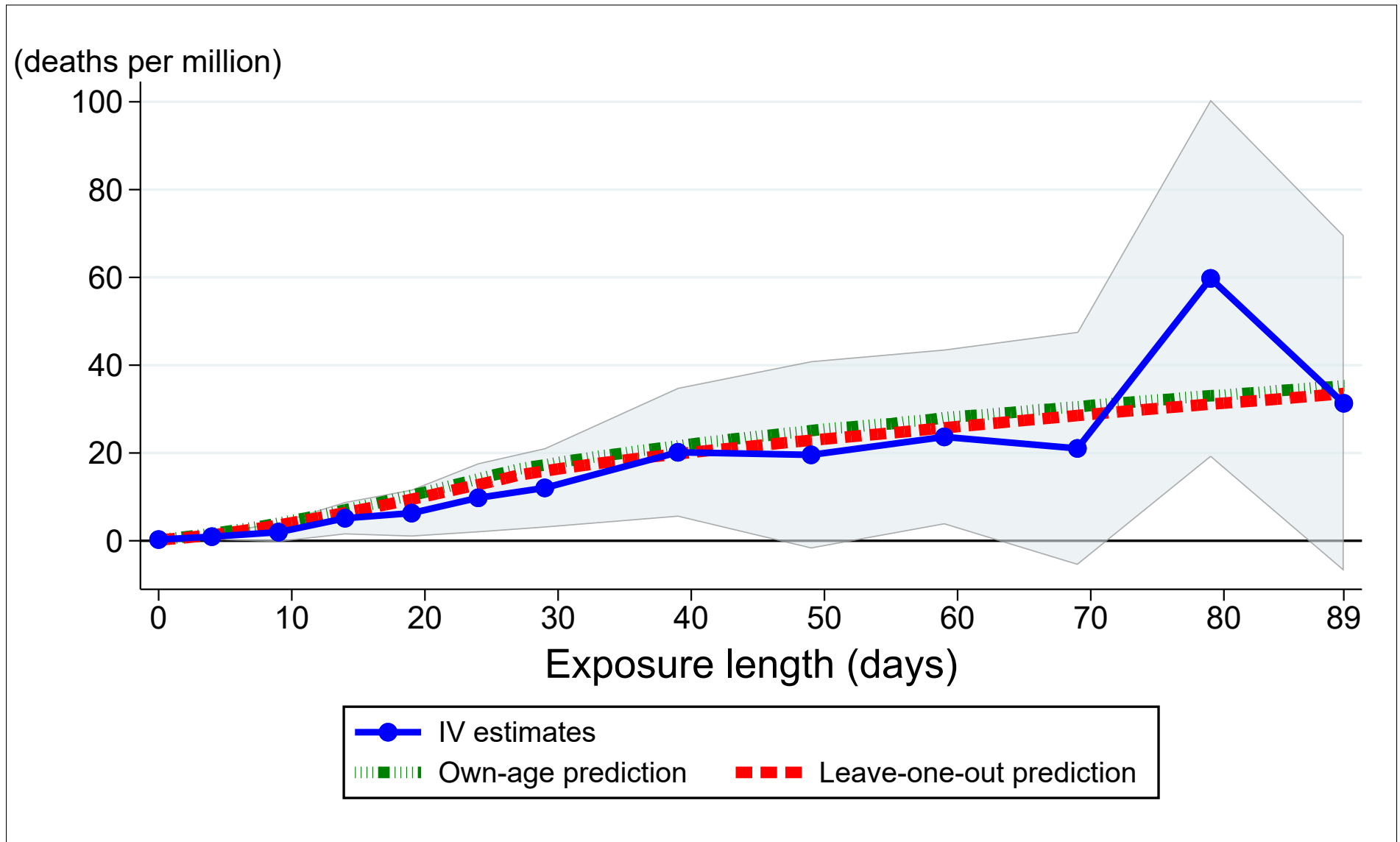
Notes: Each bar represents an IV estimate from Equation (1) for the effect of a 1-day, 1 ppb increase in sulfur dioxide ( $\text{SO}_2$ ) exposure on same-day mortality for a particular age group. Error bars represent 95% confidence intervals. Corresponding estimates are reported in Table A.5. All regressions include county-by-month and month-by-year fixed effects, as well as flexible controls for maximum temperature, precipitation, humidity, and wind speed; leads of these weather controls; and two leads and two lags of the instruments. Estimates are weighted by county population in each age group. Standard errors are clustered by county. IV estimates for 28-day cumulative mortality by age group are shown in Figure A.9.

**Figure 5:** Model-predicted effect of acute (1-day) air pollution exposure on survival, ages 65–69



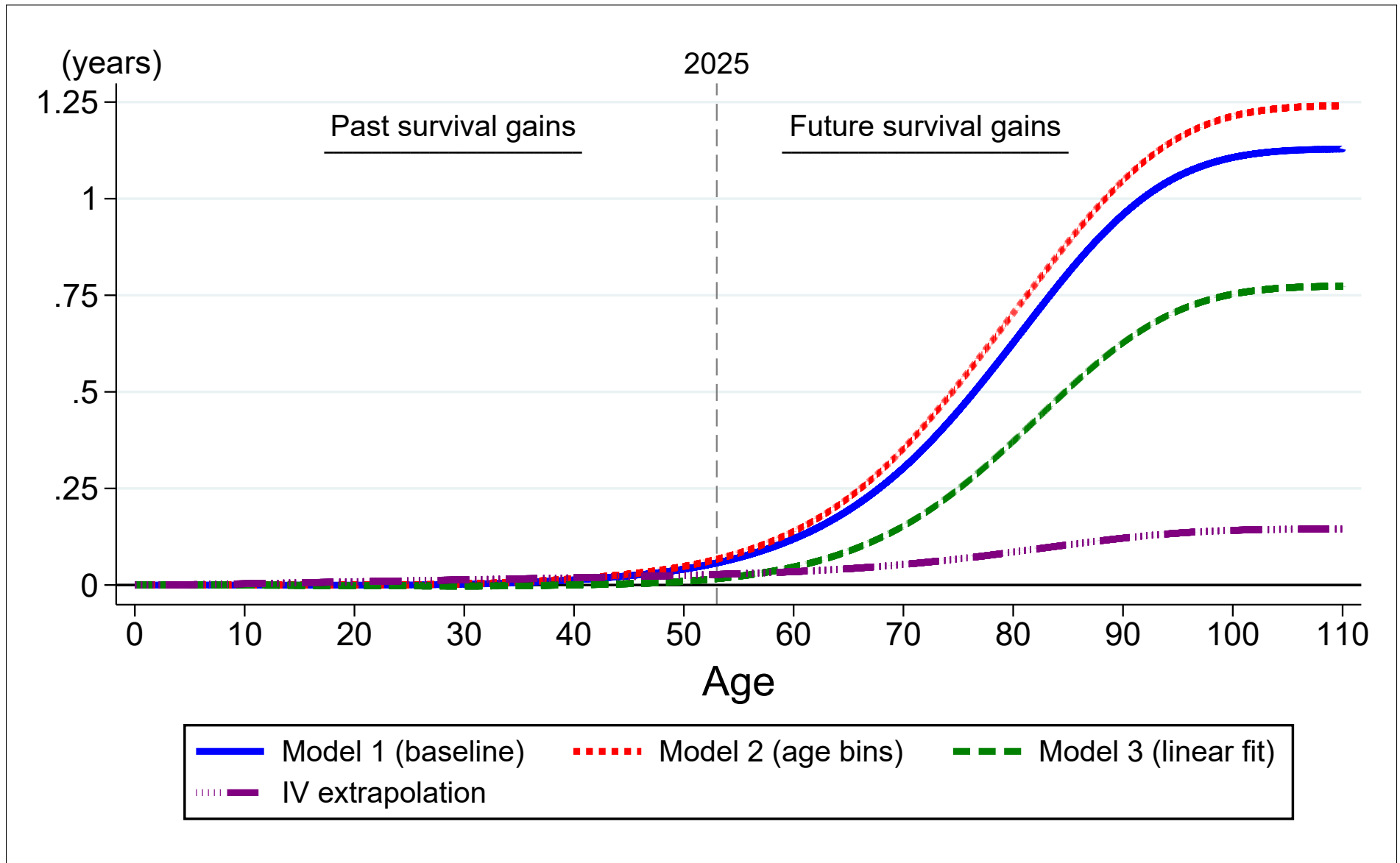
Notes: The solid blue line reports IV estimates from Equation (1) for the effect of a 1-day, 1 ppb increase in sulfur dioxide (SO<sub>2</sub>) exposure on cumulative mortality for individuals ages 65–69. The shaded area denotes 95% confidence intervals. The thick green dashed line reports the “own-age” prediction from the dynamic production model of health described by Equation (3), calibrated to match the 1-day IV estimate (first blue point) and to attribute the cancer-related portion of that estimate to mortality displacement. The thick red dashed line (“leave-one-out”) reports model predictions using the average of the calibrated values from other, older age groups (70–74, 75–79, 80–84, and 85+). The orange dashed line (“no-displacement”) at the top of the plot reports model predictions under the assumption that none of the 1-day mortality effect reflects mortality displacement, while the black dashed line (“all-displacement”) at the bottom of the plot assumes that the entire 1-day effect reflects mortality displacement. Figure A.12 shows analogous plots for all age groups 65 and older.

**Figure 6:** Model-predicted effect of prolonged air pollution exposure on survival, ages 65–69



Notes: The solid blue line reports IV estimates for the effect of a prolonged, 1 ppb increase in sulfur dioxide (SO<sub>2</sub>) exposure on cumulative mortality for individuals ages 65–69. The shaded area denotes 95% confidence intervals. Estimates are obtained by constructing predicted SO<sub>2</sub> fluctuations (Equation 4), aggregating the data into multi-day periods, and then regressing mortality on average SO<sub>2</sub> levels, instrumenting with the predicted SO<sub>2</sub> fluctuations and controlling for county-by-month, month-by-year, and multi-day period fixed effects. Estimates are weighted by county population in the 65–69 age group. The thick green dashed line reports the “own-age” prediction from the dynamic production model of health described by Equation (3), calibrated to match the 1-day IV estimate (first blue point) and to attribute the cancer-related portion of that estimate to mortality displacement. The thick red dashed line (“leave-one-out”) reports model predictions using the average of the calibrated values from other, older age groups (70–74, 75–79, 80–84, and 85+).

**Figure 7:** Projected effect of a permanent 1-unit decrease in air pollution exposure on survival gains for cohort born in 1972



Notes: This figure shows the cumulative effect of a permanent, 1 ppb decrease in sulfur dioxide ( $\text{SO}_2$ ) exposure on survival for the cohort of US individuals born in 1972. Projections are produced by the dynamic production model of health in Equation (3), calibrated using our 1-day IV estimates from Equation (1). Model 1 (“baseline”) assumes that the effect of pollution exposure on model parameters is constant across ages. Model 2 (“age bins”) uses separate parameter values for each older age group (65–69, 70–74, 75–79, 80–84, and 85+) and assigns the 65–69 values to younger ages. Model 3 (“linear fit”) imposes a linear age trend on parameter values. “IV extrapolation” projects changes in life expectancy by extrapolating our age-specific 28-day IV estimates over the full life cycle. The cumulative gains at age 110 equal the values reported in the first row of Table A.17. In the absence of any change in  $\text{SO}_2$  exposure, the model predicts a life expectancy of 71.32 years.

**Table 1:** Summary statistics, 1972–1988

	(1)	(2)	(3)
	Mean	Std. Dev.	Observations
<b>A. Pollution outcomes</b>			
SO <sub>2</sub> , ppb	9.07	12.68	2,042,258
NO <sub>2</sub> , ppb	21.45	15.74	796,539
CO, ppm	1.67	1.40	855,824
O <sub>3</sub> , ppb	25.54	13.73	674,340
TSP, $\mu\text{g}/\text{m}^3$	63.23	40.10	634,095
<b>B. One-day mortality rate outcomes</b>			
All-cause mortality, deaths per million	24.33	22.88	2,042,258
Cardiovascular	12.03	15.47	2,042,258
Cancer	5.08	8.97	2,042,258
Other	5.36	9.78	2,042,258
External	1.86	7.94	2,042,258
All-cause mortality by age group, deaths per million			
Age 1 and under	32.98	165.37	2,042,258
Age 1–19	1.50	11.47	2,042,258
Age 20–44	4.33	18.22	2,042,258
Age 45–64	26.17	47.88	2,042,258
Age 65–69	69.05	168.34	2,042,258
Age 70–74	103.74	238.58	2,042,258
Age 75–79	155.36	355.93	2,042,258
Age 80–84	238.87	568.83	2,042,258
Age 85+	437.05	913.59	2,042,258

Notes: Unit of observation is a county-day. Statistics are unweighted. Sample is restricted to observations where both mortality and sulfur dioxide (SO<sub>2</sub>) are non-missing. Mortality is calculated as the number of daily deaths per million individuals. Pollution data are from the Environmental Protection Agency, mortality counts are from the National Vital Statistics, and population estimates are from the Surveillance, Epidemiology, and End Results (SEER) Program.

**Table 2:** OLS and IV estimates for the effect of acute SO<sub>2</sub> exposure on 1-day mortality

	OLS		IV			
	(1)	(2)	(3)	(4)	(5)	(6)
SO <sub>2</sub> , ppb	0.0083** (0.0028)	0.070** (0.0065)	0.074** (0.0063)	0.067** (0.0065)	0.068** (0.0065)	0.069** (0.0063)
First-stage <i>F</i> -statistic		636	669	626	635	637
Mean outcome	24	24	24	24	24	24
Sample size	2,042,258	2,042,258	2,042,258	2,040,691	2,041,828	2,037,216
Number of weather controls	2,373	2,373	0	10,150	3,954	16,152
Weather controls						
Baseline weather variables	X	X		X	X	X
Min. temperature variables				X	X	
Less granular bins					X	
Grid-level bins						X

Notes: The dependent variable is number of deaths per million people on the day of exposure. All regressions include county-by-month and month-by-year fixed effects, as well as two leads and two lags of the instruments. Column (2) presents our baseline specification, which includes controls for all observed combinations of bins of maximum temperature, precipitation, humidity, and wind speed. Column (3) omits all weather controls. Column (4) adds bins of minimum temperature and controls for all observed weather bin combinations. Column (5) uses 6-degree Celsius temperature bins instead of 3-degree bins. Column (6) replaces temperature and precipitation bins based on county-day averages with bins based on the underlying 2.5-by-2.5-mile grid cells. All regressions are weighted by county population. Standard errors, clustered by county, are reported in parentheses. A \*/\*\* indicates significance at the 5%/1% level.

**Table 3:** IV estimates for the effect of acute SO<sub>2</sub> exposure on 1-day mortality, controlling for other pollutants

	(1)	(2)	(3)	(4)
<b>A. All-pollutant sample</b>				
SO <sub>2</sub> , ppb	0.089** (0.014)	0.053** (0.017)	0.068** (0.017)	0.053** (0.018)
TSP, $\mu\text{g}/\text{m}^3$		0.021** (0.0056)		0.021** (0.0047)
NO <sub>2</sub> , ppb			0.046* (0.018)	0.015 (0.018)
O <sub>3</sub> , ppb			-0.045 (0.029)	-0.057** (0.021)
CO, ppm			-0.084 (0.25)	-0.059 (0.19)
First-stage $F$ -statistic	91	20	12	10
Mean outcome	27	27	27	27
Sample size	79,049	79,049	79,049	79,049
<b>B. SO<sub>2</sub>/TSP sample</b>				
SO <sub>2</sub> , ppb	0.063** (0.0077)		0.030* (0.012)	
TSP, $\mu\text{g}/\text{m}^3$		0.027** (0.0040)	0.017** (0.0059)	
First-stage $F$ -statistic	243	117	46	
Mean outcome	25	25	25	
Sample size	633,878	633,878	633,878	

Notes: The dependent variable is number of deaths per million people on the day of exposure. Regressions are estimated using two-stage least squares where each pollutant is treated as an endogenous regressor. All regressions include county-by-month and month-by-year fixed effects, along with flexible controls for maximum temperature, precipitation, humidity, and wind speed; leads of these weather controls; and two leads and two lags of the instruments. All regressions are weighted by county population. Standard errors, clustered by county, are reported in parentheses. A \*/\*\* indicates significance at the 5%/1% level. National means for all air pollutants appear in Table 1. Table A.8 presents estimates using a third sample that does not condition on observing TSP.

# Online Appendix

“The Long-run Effect of Air Pollution on Survival”

Tatyana Deryugina, University of Illinois and NBER

Julian Reif, University of Illinois and NBER

## A Supplementary information and analysis

### A.1 Data

Monitor-level data for sulfur dioxide (SO<sub>2</sub>), total suspended particulates (TSP), nitrogen dioxide (NO<sub>2</sub>), O<sub>3</sub>, and carbon monoxide (CO) for the years 1972–1988 were obtained by email request from the US Environmental Protection Agency (EPA). Each SO<sub>2</sub> observation provides a sample measurement, usually recorded over a period of one hour. We dropped SO<sub>2</sub> observations with durations longer than 24 hours or values above 1000 parts per billion (ppb) or below  $-2$  ppb.<sup>1</sup> We dropped CO, NO<sub>2</sub>, and O<sub>3</sub> observations with negative values. All TSP observations had non-negative values. We then aggregated pollutant data to the monitor-day level, weighting by the time duration of each measurement. Finally, data were aggregated to the county-day level by averaging across all monitors within each county.

Figure A.1 displays the population-weighted concentrations and the number of counties with at least one operational monitor, by year for each pollutant. With the exception of O<sub>3</sub>, the population-weighted means for all pollutants decline substantially during our sample period. CO data are readily available from the mid-1970s onward, covering about 225 counties annually, while O<sub>3</sub> data are unavailable prior to 1980. NO<sub>2</sub> coverage is high for most of the 1970s but drops sharply by the late 1980s. SO<sub>2</sub> data offer broader spatial coverage than most other pollutants, with over 400 counties monitoring SO<sub>2</sub> each year and about half the US population living in a county with at least one SO<sub>2</sub> monitor. While TSP monitors cover more counties than SO<sub>2</sub> monitors, they collect data less frequently and are more often located in sparsely populated areas. At the county-day level, we have 62 percent fewer population-weighted TSP observations than SO<sub>2</sub> observations.

Figure A.3 shows the locations of the 4,740 active SO<sub>2</sub> pollution monitors during our 1972–1988 sample period. The monitors are present in 1,041 counties.

### A.2 Short-run empirical results: additional analyses and robustness checks

#### Complier analysis

Table A.1 describes complier characteristics by regressing county-level measures obtained from the Regional Economic Information System dataset on the strength of the first stage. The unit of observation is a county-year. Regressions include year fixed effects and are weighted by the county population in each

---

<sup>1</sup>According to the AQS Data Coding Manual version 2.38 (February 2, 2010), the maximum allowable sample value for SO<sub>2</sub> is 1000 ppb. The EPA informed us by email that small negative values can arise due to noise and should be included in sample averages to avoid bias. We chose  $-2$  as the bottom cutoff because it appeared to be the minimum allowable sample value.

year. The strength of the first stage is not significantly associated with population size, the percent of Black residents, per-capita income, or the employment rate. Counties with stronger first stages have higher per-capita government transfers, but the magnitude of the coefficient is small: a \$55 difference for each 1 ppb difference in the first stage, relative to a mean of \$1,290. The largest difference is for mean SO<sub>2</sub> concentrations: 1.5 ppb higher for each 1 ppb difference in the first stage relative to a mean of 9.5 ppb.

### **Controlling for autocorrelation in air pollution**

Because wind direction is autocorrelated, our IV estimates for the effect of 1-day exposure may inadvertently capture the effects of multi-day exposure. Table A.2 addresses this concern by regressing tomorrow's SO<sub>2</sub> levels on today's (instrumented) SO<sub>2</sub> levels and baseline controls, while varying the number of leads and lags of the wind instrument. Without any leads and lags of the instrument, the correlation between predicted SO<sub>2</sub> today and SO<sub>2</sub> one day from now is 0.26, which is large and statistically significant. However, including just one lead reduces this correlation to near zero and renders it statistically insignificant. This finding suggests that our preferred specification with two leads and two lags is conservative, and that similar results could be obtained with fewer leads and lags. Table A.3 further shows that our main estimates are insensitive to the numbers of leads and lags included in the regression.

### **Ruling out composition bias**

The observed differences in mortality trends by cause of death (Figure 3) could potentially be driven by composition bias. For example, if cancer-related deaths occurring weeks after exposure are misattributed to cardiovascular causes, we might incorrectly observe a rising trend in cardiovascular mortality in place of a true increase in cancer deaths. This type of misclassification is especially plausible among people with multiple chronic conditions. To investigate this possibility, we estimate the effect of acute exposure on deaths where cancer was listed as either the underlying *or* secondary (contributing) cause of death. Those estimates, shown in Figure A.7, are very similar to our main estimates, indicating that misclassification in the underlying cause of death does not explain the cancer pattern in Figure 3.

### **Estimates by detailed causes of death**

Figure A.8 shows cause-specific estimates for the mortality effect of SO<sub>2</sub> over time, disaggregating cardiovascular and other diseases into 5 and 21 subcategories, respectively. Three cardiovascular subcategories—heart disease, cerebrovascular disease, and atherosclerosis—show significant same-day and monthly mortality increases. We also find strong and growing effects for deaths from chronic obstructive pulmonary disease (COPD), pneumonia and influenza, and other respiratory diseases, which collectively account for over 99 percent of all deaths from respiratory illness (Table A.14). By contrast, we find no significant monthly effects for conditions not previously linked to air pollution exposure, such as stomach ulcers and appendicitis.

## Longer mortality window by age

Figure A.9 and Table A.6 report age-specific mortality estimates for outcome windows up to one month (28 days) following exposure. Among individuals aged 65 and over, the monthly estimates are at least three times larger than the 1-day estimates, indicating that any short-run mortality displacement is more than offset by delayed effects of acute exposure. Among individuals aged 20–64, however, the monthly estimates are smaller than the 1-day estimates and statistically insignificant. This pattern suggests that acute pollution exposure increases mortality among young adults primarily by accelerating death among those who would have died within a month regardless. By contrast, older adults who die following acute air pollution exposure would have survived at least one month.

## Alternative control variables and clustering levels

Table A.9 investigates the sensitivity of our estimates to including alternative sets of fixed effects. Column (1) reproduces our baseline estimate, while Columns (2)–(6) present five reasonable alternatives, including variants that control for state-by-calendar-month-by-year (Column 3) or county-by-year (Column 4) fixed effects. These changes have little effect on the size of our estimate, indicating that our estimates are robust to seasonal variation in the climate-mortality relationship and unobserved variables that vary across locations.

Table A.10 shows that clustering standard errors at broader geographic levels, such as state or geographic group, also has little effect on the size of our standard errors.

## Assessing potential violations of monotonicity

We interpret our IV estimate as a weighted average treatment effect where the weights are non-negative, which requires monotonicity of air pollution in the instruments (Angrist, Graddy and Imbens, 2000). In other words, if the instruments increase SO<sub>2</sub> levels in one county, then SO<sub>2</sub> levels in other counties assigned to the same geographic group cannot fall. This assumption could be violated if the relationship between wind direction and SO<sub>2</sub> varies substantially across counties located within the same group. We investigate this possibility with two alternative specifications that allow the effect of wind direction on SO<sub>2</sub> to vary over either a larger or smaller geographic area. Columns (2)–(3) of Table A.11 show that these alternatives produce estimates similar to our main estimate (Column 1), suggesting that violations of the monotonicity assumption are unlikely to drive our findings.

Columns (4)–(6) of Table A.11 show that our estimates change little if we employ the following non-parametric specification for  $f^g(\theta_{cd})$ :

$$f^g(\theta_{cd}) = \sum_{i=1}^b \gamma_g^i 1[G_c = g] \times 1 \left[ \frac{360}{b}(i-1) \leq \theta_{cd} < \frac{360}{b}i \right]$$

where the first indicator function,  $1[G_c = g]$ , is equal to 1 if county  $c$  is a member of group  $g$  and 0 otherwise. The second indicator function is equal to 1 if the local wind direction,  $\theta_{cd}$ , now expressed in degrees rather than radians, lies between  $\frac{360}{b}(i-1)$  and  $\frac{360}{b}i$  for some fixed value  $b$ . For example, when

$b = 4$  and  $i = 1$ , the indicator function will equal 1 if the wind direction lies between 0 and 90 degrees. Columns (4)–(6) report estimates when we set  $b$  equal to 9, 6, and 4, respectively.

### Assessing potential weak instrument bias

Our reported  $F$ -statistics in Table 2 exceed 600 and our 2SLS estimates differ significantly from OLS estimates, indicating that weak instrument bias is unlikely. As an additional check, Table A.12 shows that our 2SLS estimates are similar to those from LIML, which is approximately median unbiased even in the presence of many weak instruments. We also conduct a placebo exercise using randomly generated wind directions in place of the actual wind direction (Table A.13). The resulting first-stage  $F$ -statistics never exceed 4, confirming that actual wind direction captures meaningful variation in  $\text{SO}_2$  levels rather than spurious correlations.

### A.3 Model calibration

The dynamic production model of health given by Equation (3) depends on seven parameters:

$\{\alpha, \delta, I, \sigma_e, \mu_H, \sigma_H, \underline{H}\}$ . To achieve identification, we normalize two parameters:  $\underline{H}^* = 0$  and  $\sigma_H^* = 1$ . The five remaining parameters are calibrated using a 1972 period life table, as described in Section 5.2. We assume that pollution exposure only affects the parameters  $\delta$  and  $\underline{H}$ , and denote their post-exposure-change values as  $\{\tilde{\delta}, \tilde{\underline{H}}\}$ .

Let  $\Theta^* = \{\alpha^*, I^*, \mu_H^*, \sigma_H^*, \sigma_e^*\}$  denote the calibrated baseline parameters before any changes in exposure. Consider a population of  $N$  individuals whose health capital evolves according to Equation (3). Let  $S$  be a random-number seed that fixes the initial stock of health capital,  $H_{i0}$ , and the evolution of the i.i.d. shock,  $\varepsilon_{it}$ , for all individuals. Define  $M_t(\delta^*, \underline{H}^* | \Theta^*, N, S)$  as the deterministic mortality rate at time  $t \geq 0$  in the absence of changes in pollution exposure.

We use age-specific IV estimates for the mortality effect of air pollution exposure to recover  $\{\tilde{\delta}, \tilde{\underline{H}}\}$ . Let  $\hat{\beta}_{a,c}^1$  denote the IV estimate for the effect of acute exposure on 1-day mortality for age group  $a$  from cause of death  $c$ , and let  $[t_a^0, t_a^1]$  define the age range (in days) spanned by age group  $a$ . For any age,  $t \in [t_a^0, t_a^1]$ , we can solve for  $\tilde{\underline{H}}_{at}$  as the implicit solution to:

$$\hat{\beta}_{a,cancer}^1 = M_t(\delta^*, \tilde{\underline{H}}_{at} | \Theta^*, N, S) - M_t(\delta^*, \underline{H}^* | \Theta^*, N, S) \quad (\text{A.1})$$

We then solve for  $\tilde{\delta}$ , which is defined implicitly by:

$$\hat{\beta}_{a,all}^1 = M_t(\tilde{\delta}_{at}, \tilde{\underline{H}}_{at} | \Theta^*, N, S) - M_t(\delta^*, \tilde{\underline{H}}_{at} | \Theta^*, N, S) \quad (\text{A.2})$$

Because health capital is strictly decreasing in  $\delta$  and death occurs when health falls below  $\underline{H}$ , the mortality rate,  $M_t(\cdot)$ , is monotonically increasing in both  $\delta$  and  $\underline{H}$ . Consequently, the solutions  $\{\tilde{\delta}_{at}, \tilde{\underline{H}}_{at}\}$  to Equations (A.1) and (A.2) are unique and can be found using standard root-finding algorithms.<sup>2</sup>

We can solve for  $\{\tilde{\delta}_{at}, \tilde{\underline{H}}_{at}\}$  for any  $t \in [t_a^0, t_a^1]$ . We use the approximate integer midpoint of each age

---

<sup>2</sup>Solving for  $\tilde{\delta}$  first and then  $\tilde{\underline{H}}$  yields numerically similar but not identical results.

bin,  $t = \text{round}[(t_a^0 + t_a^1)/2]$ .<sup>3</sup> To reduce noise from the i.i.d. health shocks, we average over multiple daily ages near the center of each age bin. Specifically, we solve Equations (A.1) and (A.2) for 50 different days near the approximate midpoint of each age bin and take the average. For example, for  $a = 65$  (the 65–69 age group), we solve for  $\{\tilde{\delta}_{65,t}, \tilde{\mathbb{H}}_{65,t}\}$  using ages  $t = 68\text{y}1\text{d}, t = 68\text{y}2\text{d}, \dots, t = 68\text{y}50\text{d}$ .<sup>4</sup> Figure A.13 shows the model-implied cumulative mortality effects of acute (1-day) exposure across the 50 daily ages in the 65–69 age group, using the calibrated  $\{\tilde{\delta}_{65,t}, \tilde{\mathbb{H}}_{65,t}\}$  for each age  $t$ . By construction, the first-day effect matches the 1-day IV estimate for the 65–69 age group (see first row of Column (5) in Table A.6). The subsequent values report longer-run effects of exposure up to 90 days later. The “own-age prediction” in Figure 5 is the average of these 50 trajectories.

We compute the age-specific parameter solutions,  $\{\tilde{\mathbb{H}}_a, \tilde{\delta}_a\}$ , as the averages of these 50 solutions:

$$\begin{aligned}\tilde{\mathbb{H}}_a &= \frac{1}{50} \sum_t \tilde{\mathbb{H}}_{at} \\ \tilde{\delta}_a &= \frac{1}{50} \sum_t \tilde{\delta}_{at}\end{aligned}$$

Figure A.11 reports  $\{\tilde{\mathbb{H}}_a, \tilde{\delta}_a\}$  for the five oldest age groups, expressed as deviations from the baseline calibrated values (i.e.,  $\tilde{\mathbb{H}}_a - \mathbb{H}^* = \tilde{\mathbb{H}}_a$  and  $\tilde{\delta}_a - \delta^* = \tilde{\delta}_a$ ). The long-run survival projections shown in Figure 7 use the average across the five oldest age groups:

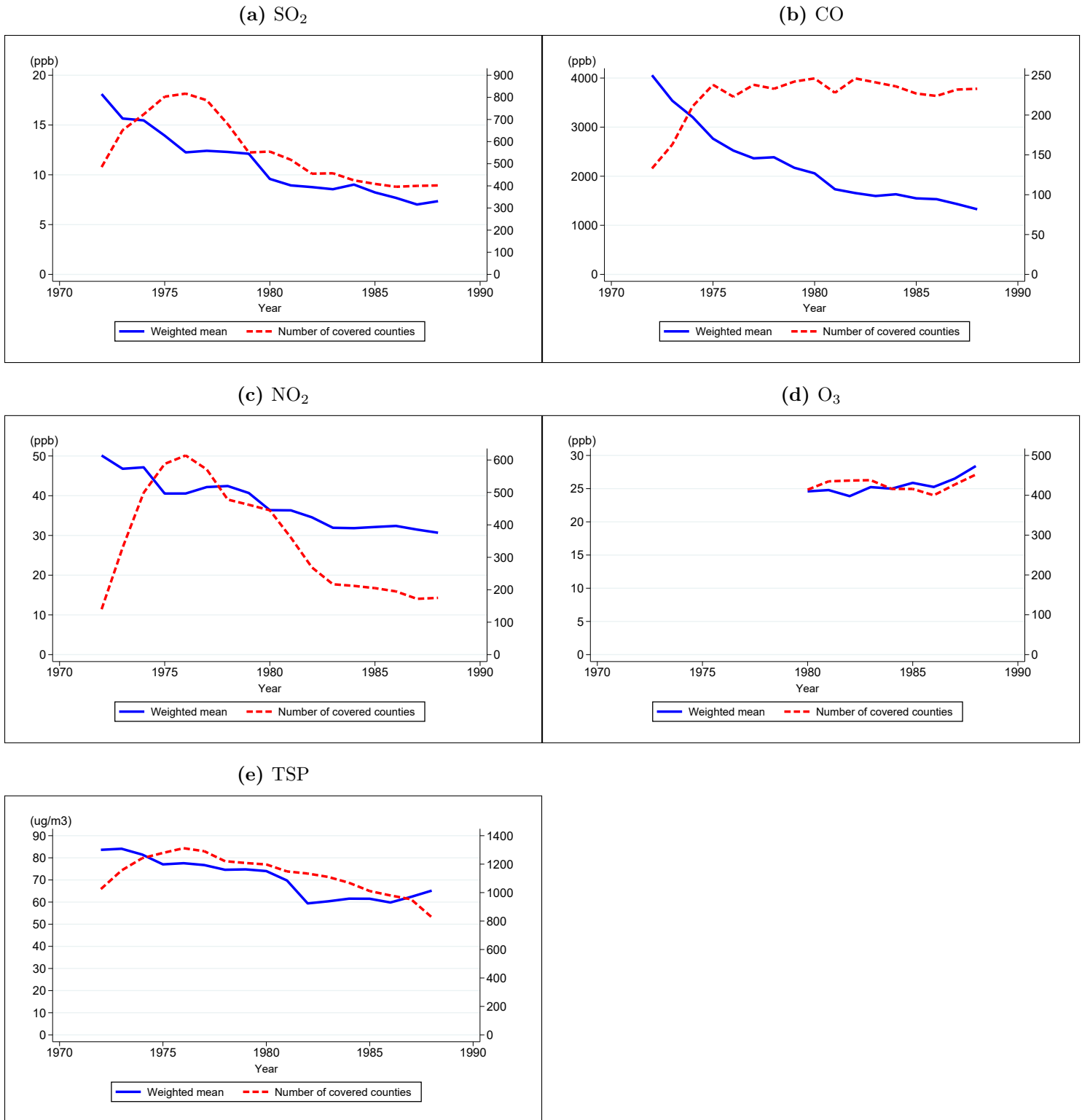
$$\begin{aligned}\tilde{\mathbb{H}} &= \frac{1}{5} \sum_{a \geq 65} \tilde{\mathbb{H}}_a \\ \tilde{\delta} &= \frac{1}{5} \sum_{a \geq 65} \tilde{\delta}_a\end{aligned}$$

---

<sup>3</sup>For the 85+ age group, we use a midpoint of 90, which is the average age of death in that group during our sample period.

<sup>4</sup>The optimal strategy would employ all  $365 \times 5 = 1825$  days in the 5-year age bin, giving more weight to the ages near the midpoint. However, this is computationally burdensome and offers limited additional precision.

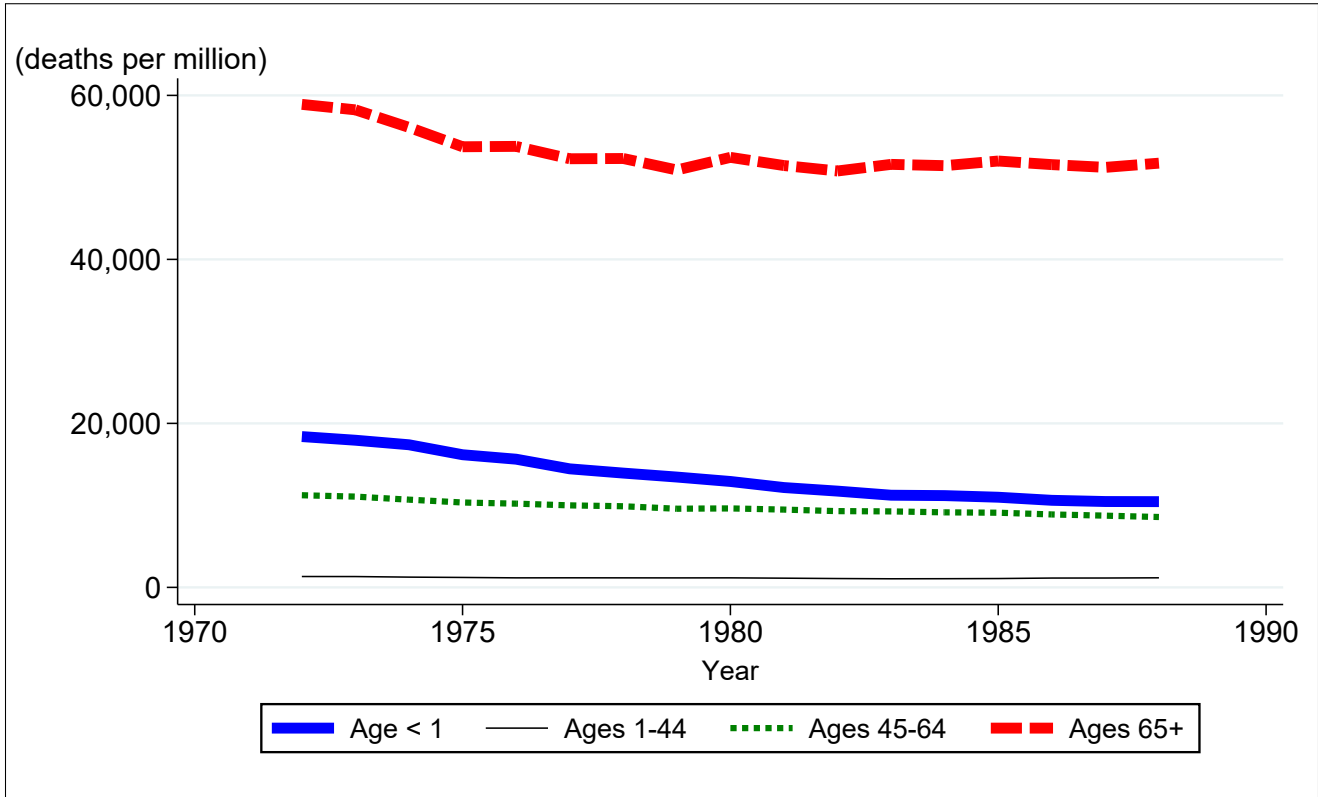
**Figure A.1: Air pollution means and population coverage levels, 1972–1988**



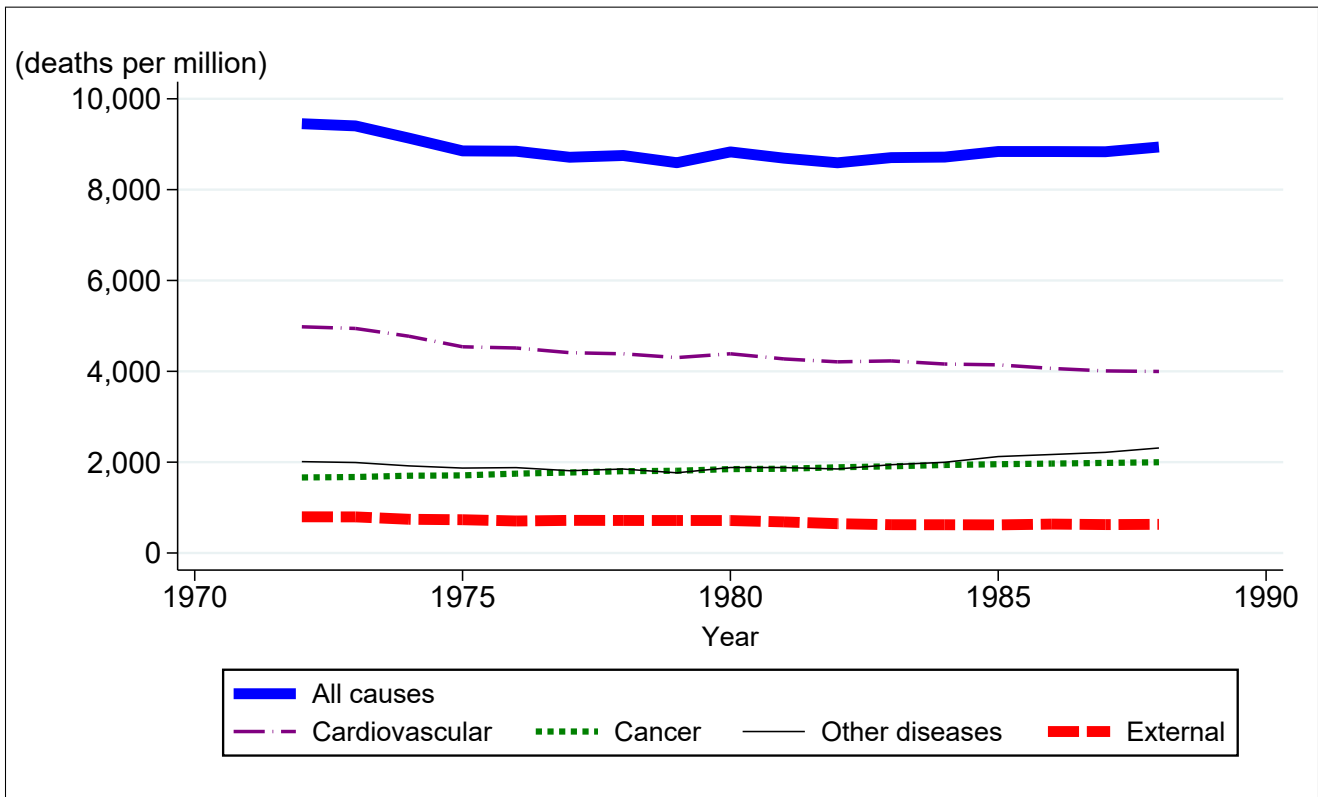
Notes: The solid blue lines report population-weighted pollution levels for all US counties with at least one daily reading for that pollutant. The dashed red line reports the number of counties with at least one operational monitor for the pollutant. Air pollution data are obtained from the EPA Air Quality database. SO<sub>2</sub>, CO, NO<sub>2</sub>, and O<sub>3</sub> are measured in parts per billion (ppb). Total suspended particulates (TSP) is measured in micrograms per cubic meter ( $\mu\text{g}/\text{m}^3$ ).

**Figure A.2:** Trends in US mortality rates, 1972–1988

(a) By age group

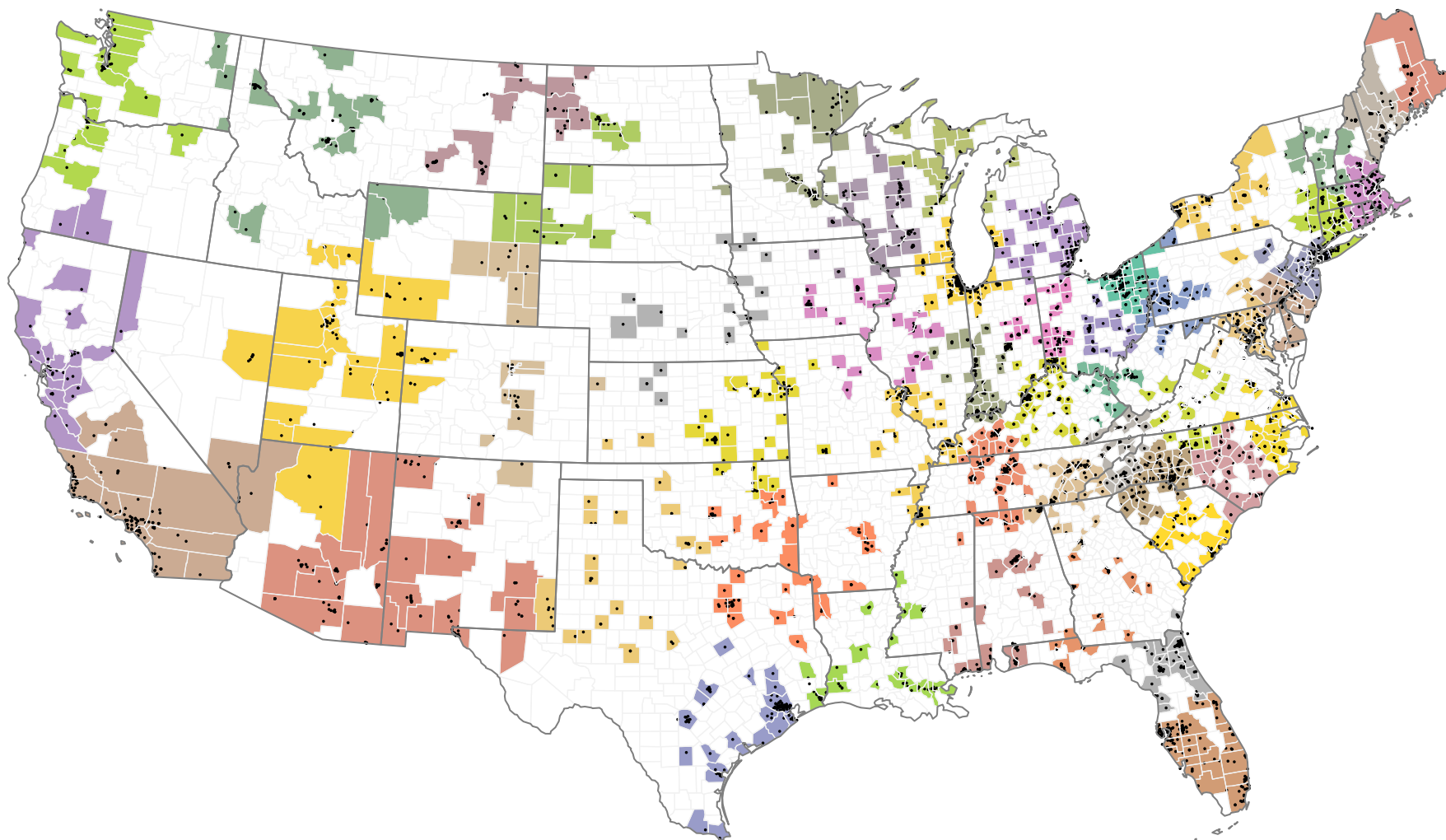


(b) By cause of death



Notes: These two figures report annual mortality rates for the US population. These rates are calculated using mortality data from the National Vital Statistics and population data from SEER. Annual mortality rates are approximately 365 times larger than the daily mortality rates used in the analysis.

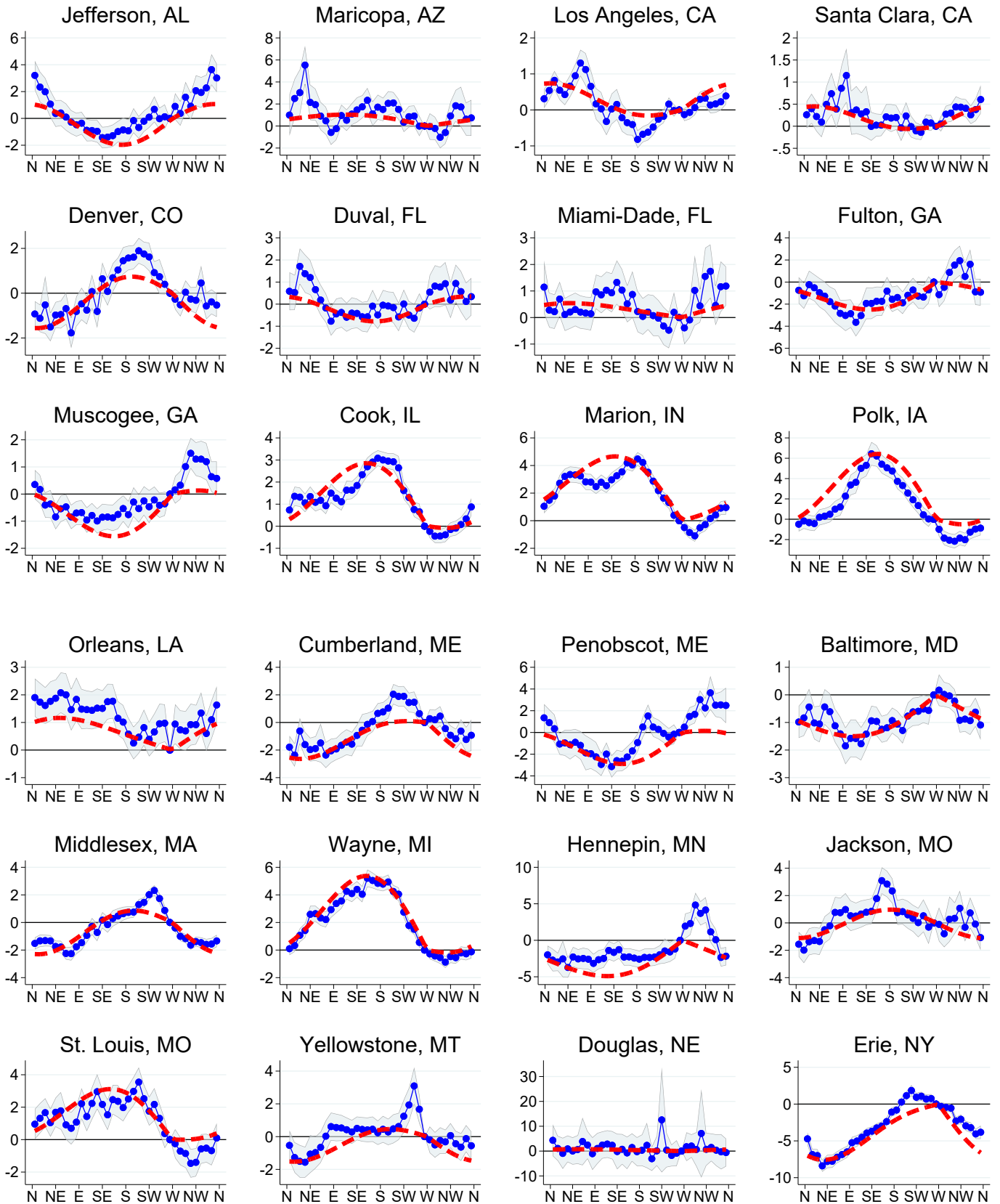
**Figure A.3:** SO<sub>2</sub> monitor locations and geographic group assignments

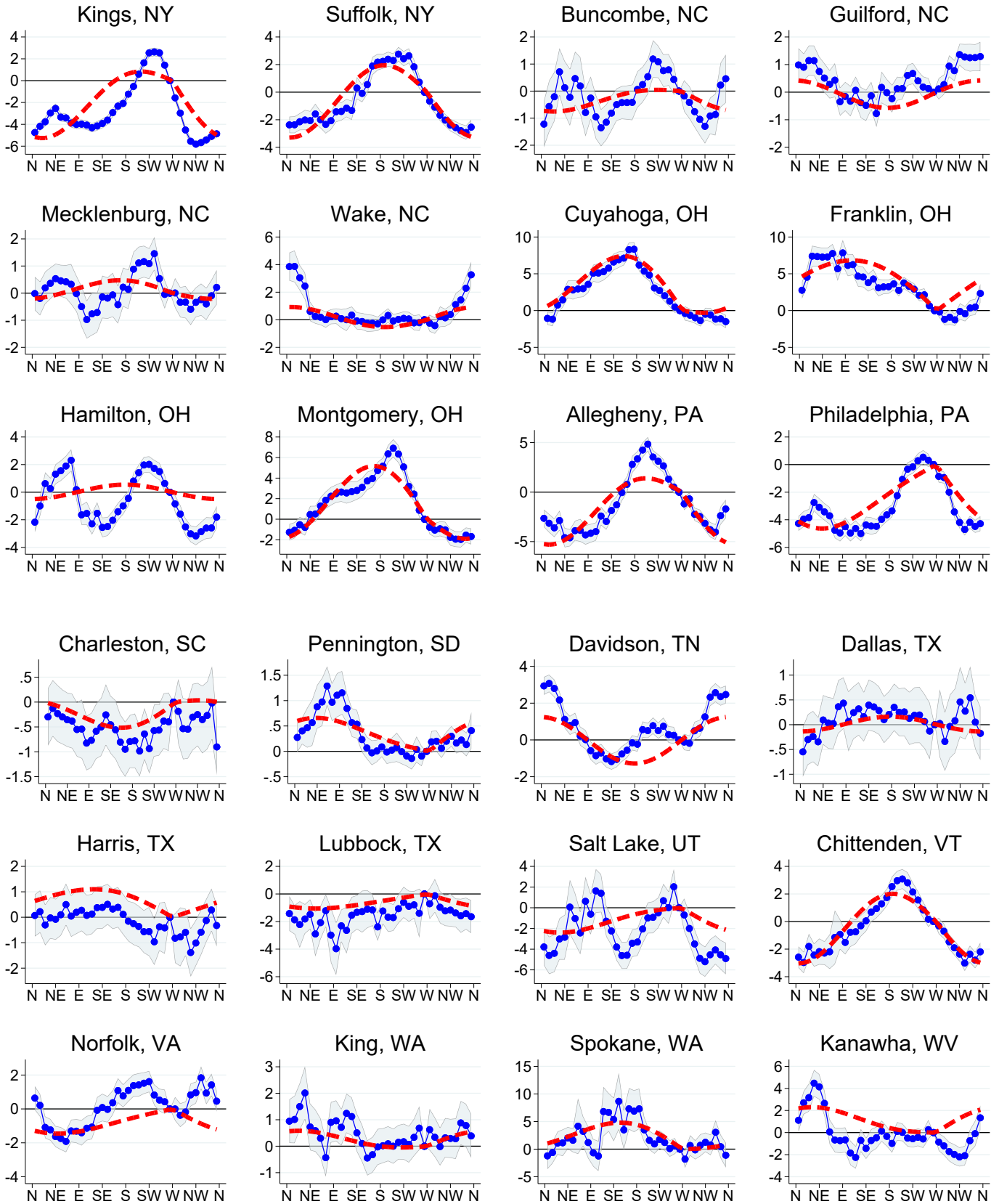


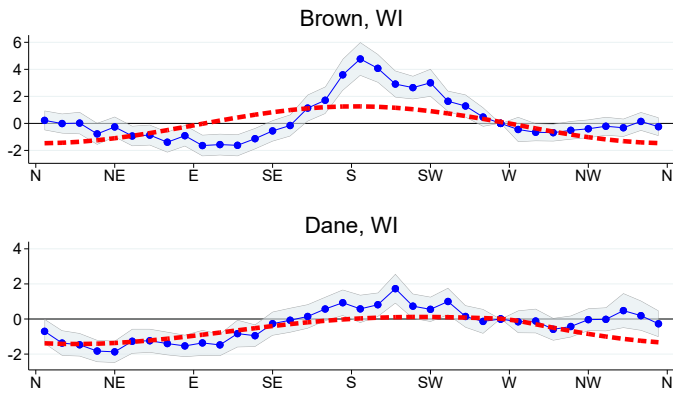
A-7

Notes: This map shows the 50 geographic groups included in our main estimation sample, each shaded in a different color. Black dots indicate the locations of SO<sub>2</sub> monitors. Unshaded (white) counties are excluded from the sample. The Southern California and Greater Philadelphia groups are shown in greater detail in Figure 1. As specified in Equation (2), the first-stage effect of wind direction on air pollution levels is allowed to vary across geographic groups.

**Figure A.4:** The relationship between wind direction and SO<sub>2</sub> levels, by geographic group

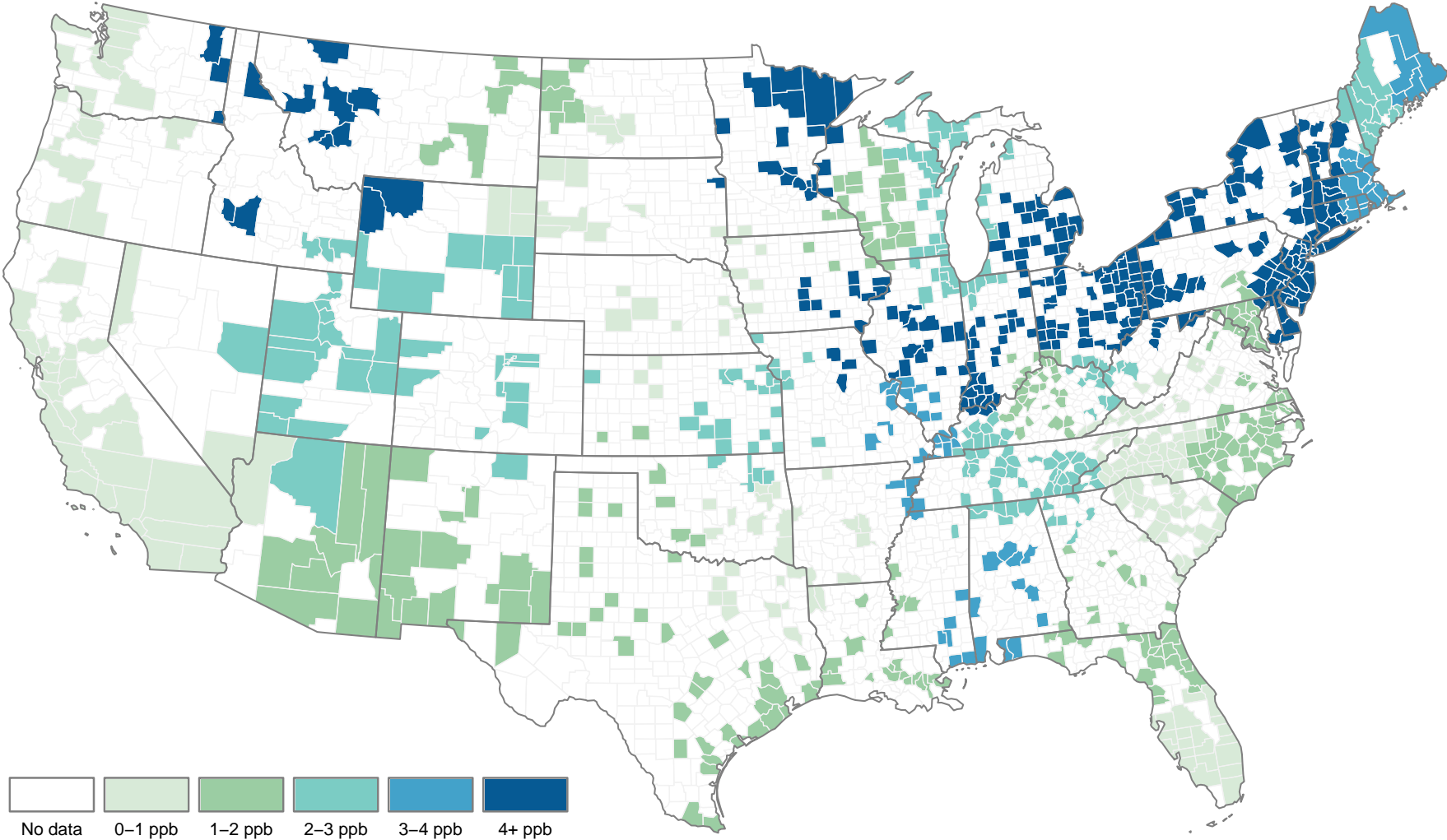






Notes: The graphs plot the relationship between  $\text{SO}_2$  levels and windward direction for each of the geographic groups shown in Figure A.3. Windward direction refers to the direction the wind is coming from (e.g., “N” for wind blowing from the North and “NE” for wind blowing from the Northeast). The 36 blue points report coefficient estimates from a non-parametric regression of  $\text{SO}_2$  levels on wind direction, grouped into 10-degree angle bins. The shaded areas denote 95% confidence intervals. Red dashed lines report fitted values from the parametric sine-based specification given by  $f^g(\theta)$  in Equation (2). All regressions include county-by-month and month-by-year fixed effects, as well as flexible controls for maximum temperature, precipitation, humidity, and wind speed; and two leads and two lags of the instruments. Standard errors are robust to heteroskedasticity. The plots for “Philadelphia, PA” and “Los Angeles, CA” are reproduced in Figure 1 with the labels “Greater Philadelphia area” and “Southern California area.”

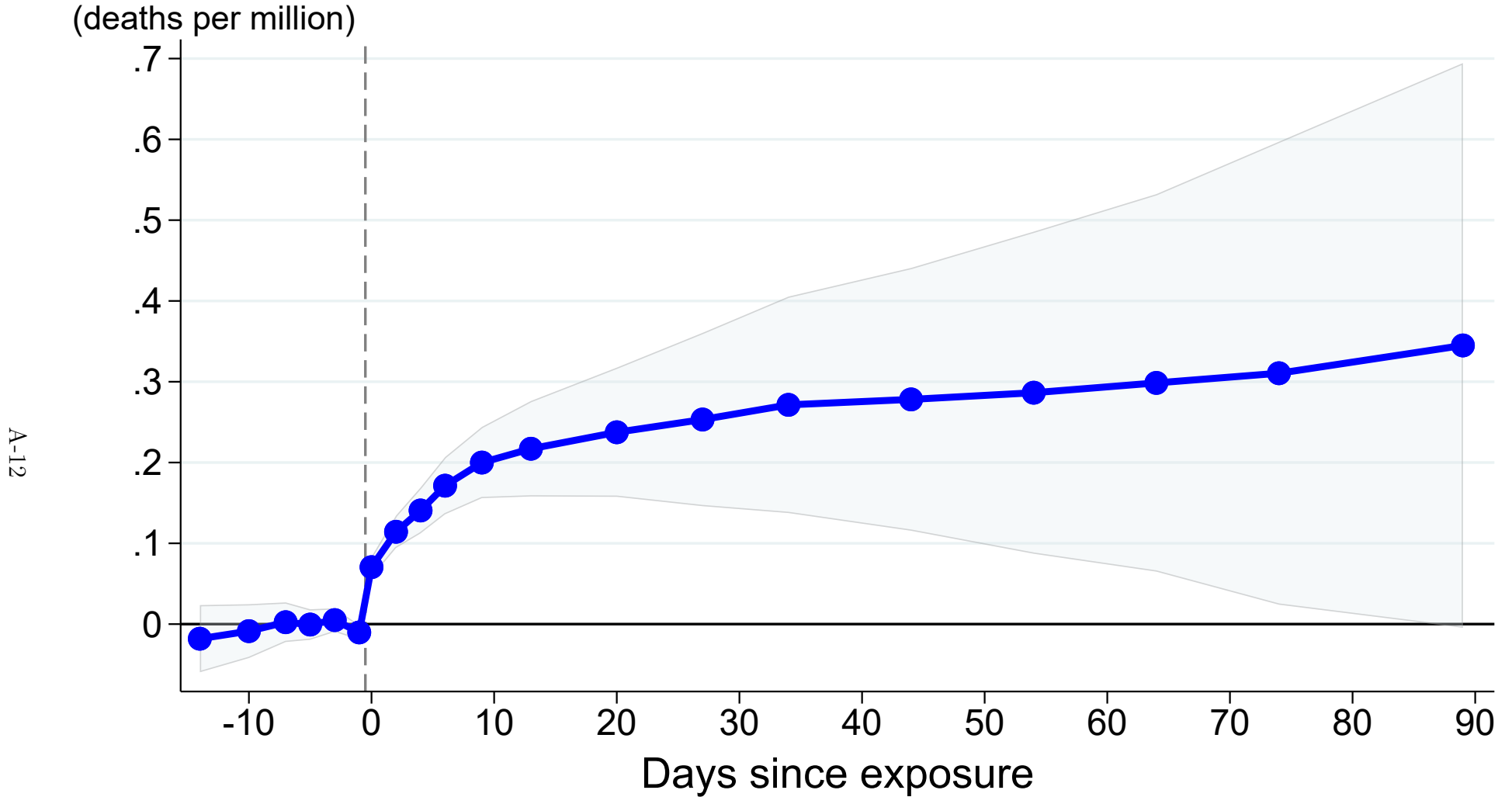
Figure A.5: Strength of the first stage, by geographic group



A-11

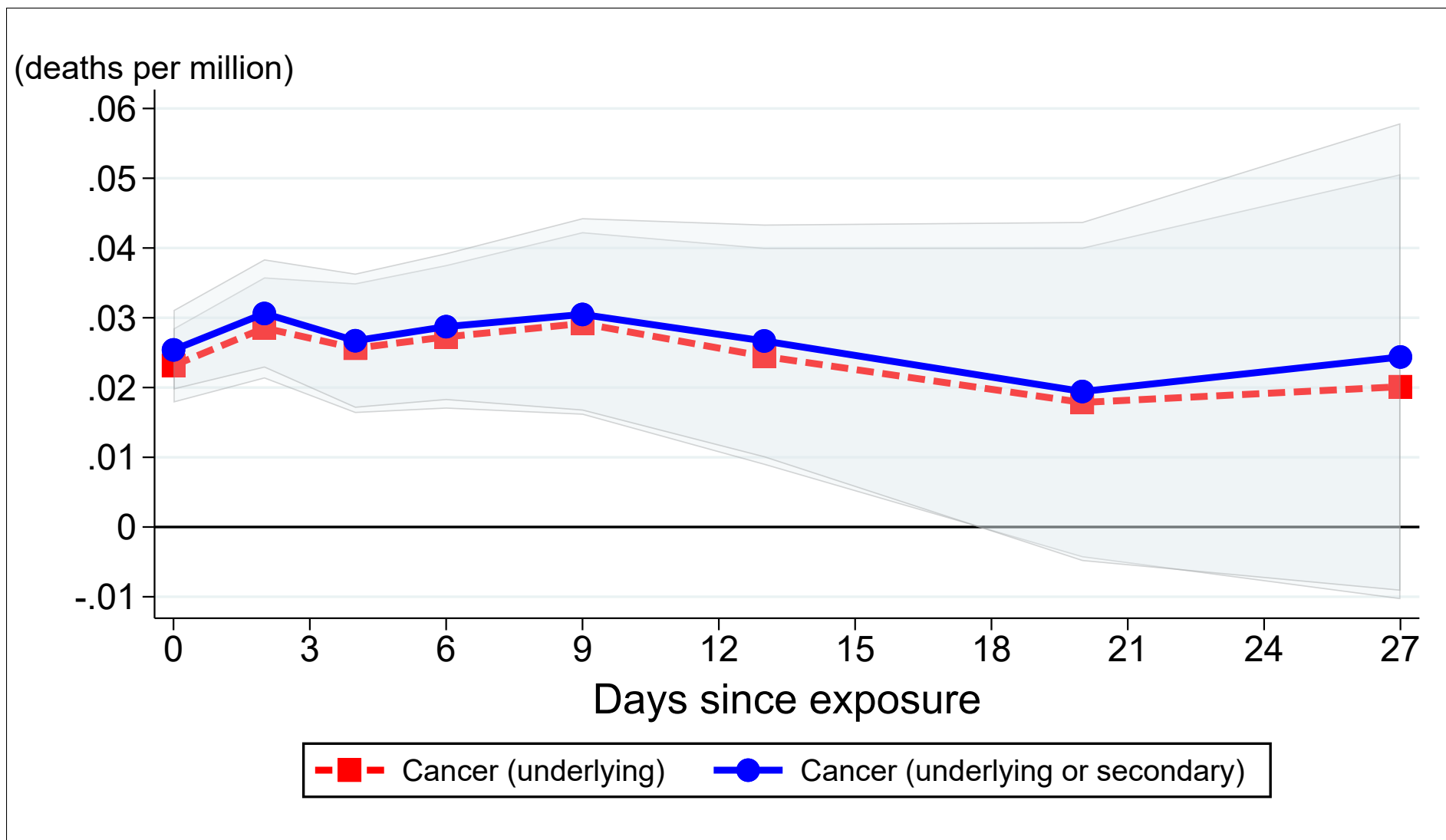
Notes: This map shows the strength of the first-stage relationship from Equation (2) for each of the 50 geographic groups included in our main estimation sample. Strength is measured as the difference in predicted  $\text{SO}_2$  levels (in parts per billion) between the most and least polluting wind directions. Predictions are based on the parametric sine specification  $\hat{f}^g(\theta) = \hat{\gamma}_g^1 \sin(\theta) + \hat{\gamma}_g^2 \sin(\theta/2)$ , for  $\theta \in [0, 2\pi)$ . Unshaded (white) counties are excluded from the sample.

Figure A.6: IV estimates for the effect of acute (1-day) SO<sub>2</sub> exposure on cumulative mortality up to 90 days following exposure



Notes: Each point reports an IV estimate from Equation (1) for the effect of a 1-day, 1 ppb increase in sulfur dioxide (SO<sub>2</sub>) exposure on mortality, measured as cumulative deaths per million over time windows ranging from 14 days before to 89 days after exposure (with 0 indicating the day of exposure). The shaded areas denote 95% confidence intervals. Corresponding point estimates for  $t = 0$  through  $t = 27$  are reported in Column (2) of Table A.4. All regressions include county-by-month and month-by-year fixed effects, as well as flexible controls for maximum temperature, precipitation, humidity, and wind speed; leads of these weather controls (up to 27 leads); and two leads and two lags of the instruments. Estimates are weighted by county population. Standard errors are clustered by county.

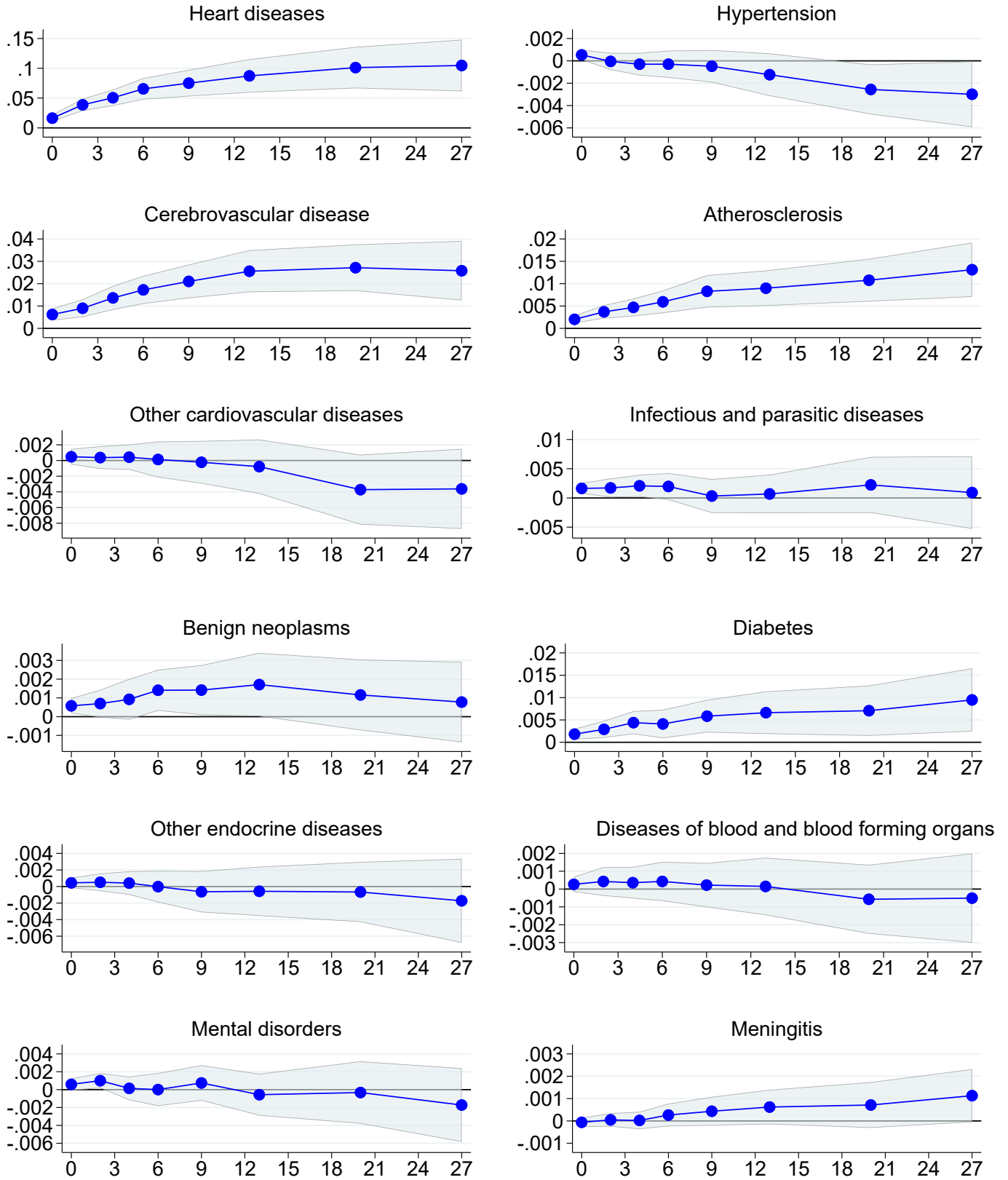
Figure A.7: IV estimates for the effect of acute (1-day) air pollution exposure on cancer-related mortality

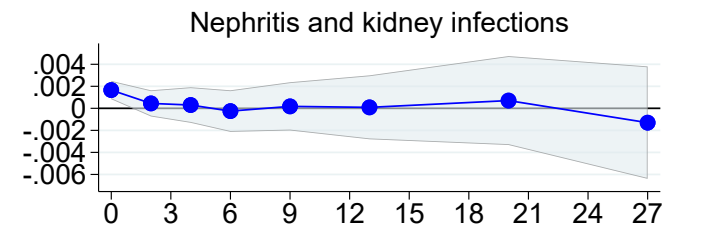
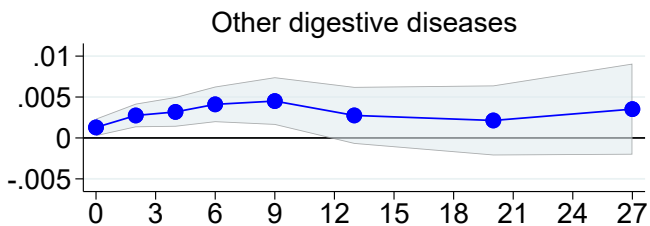
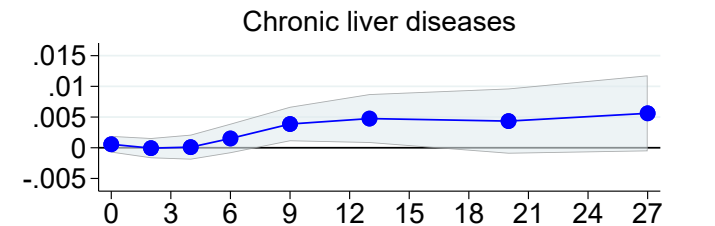
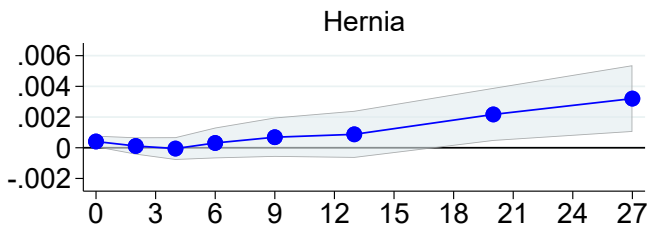
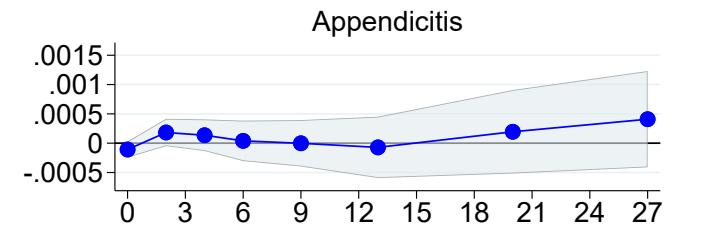
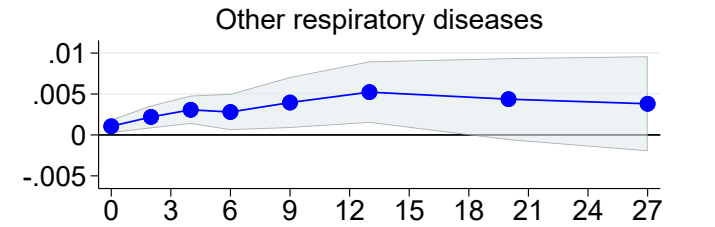
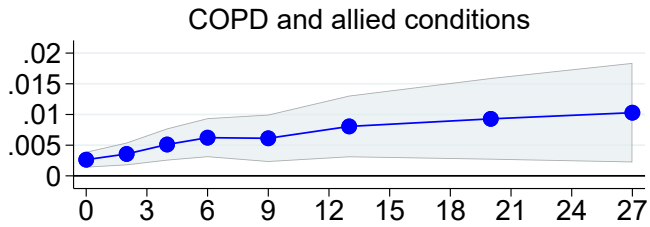
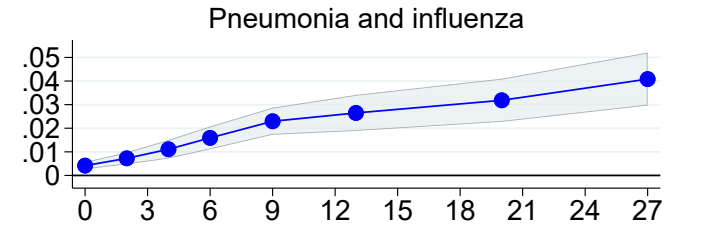
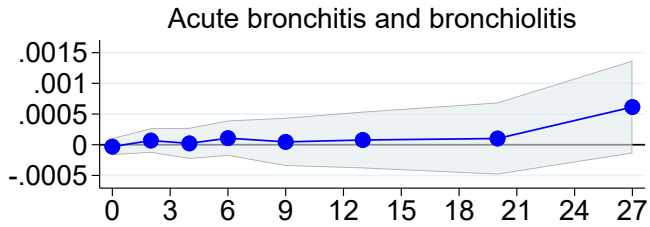
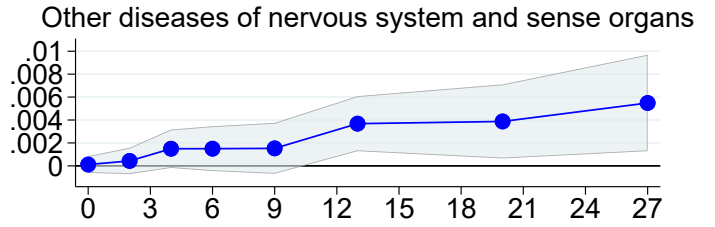
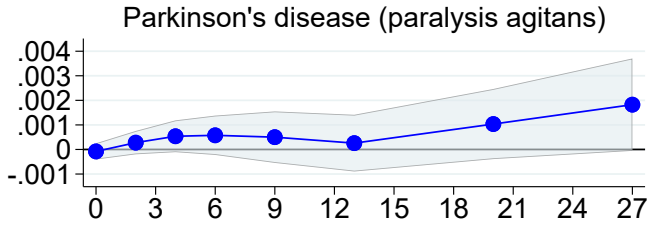


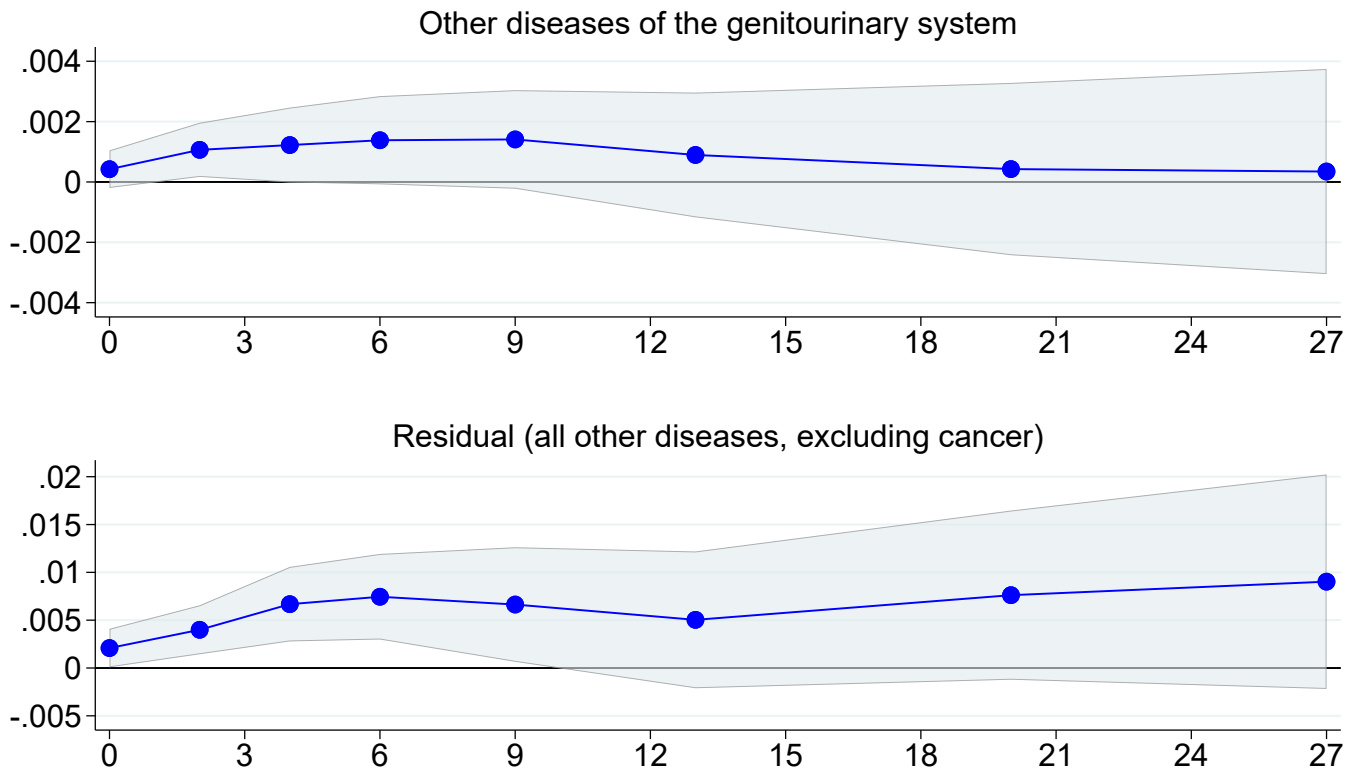
A-13

Notes: Each point reports an IV estimate from Equation (1) for the effect of acute (1-day) sulfur dioxide ( $\text{SO}_2$ ) exposure on cancer-related mortality (deaths per million). “Cancer (underlying)”, which replicates the cancer estimates shown in Figure 3, includes only deaths where cancer is listed as the underlying cause of death on the death certificate. “Cancer (underlying or secondary)” expands this definition to include deaths where cancer is listed either as the underlying cause or as a contributing secondary cause. Mortality is measured as cumulative deaths per million over time windows ranging from the day of exposure to 27 days after exposure (with 0 indicating the day of exposure). The shaded areas denote 95% confidence intervals. All regressions include county-by-month and month-by-year fixed effects, as well as flexible controls for maximum temperature, precipitation, humidity, and wind speed; leads of these weather controls; and two leads and two lags of the instruments. Estimates are weighted by county population. Standard errors are clustered by county.

**Figure A.8:** IV estimates for the effect of acute (1-day) air pollution exposure on mortality, by detailed cause of death



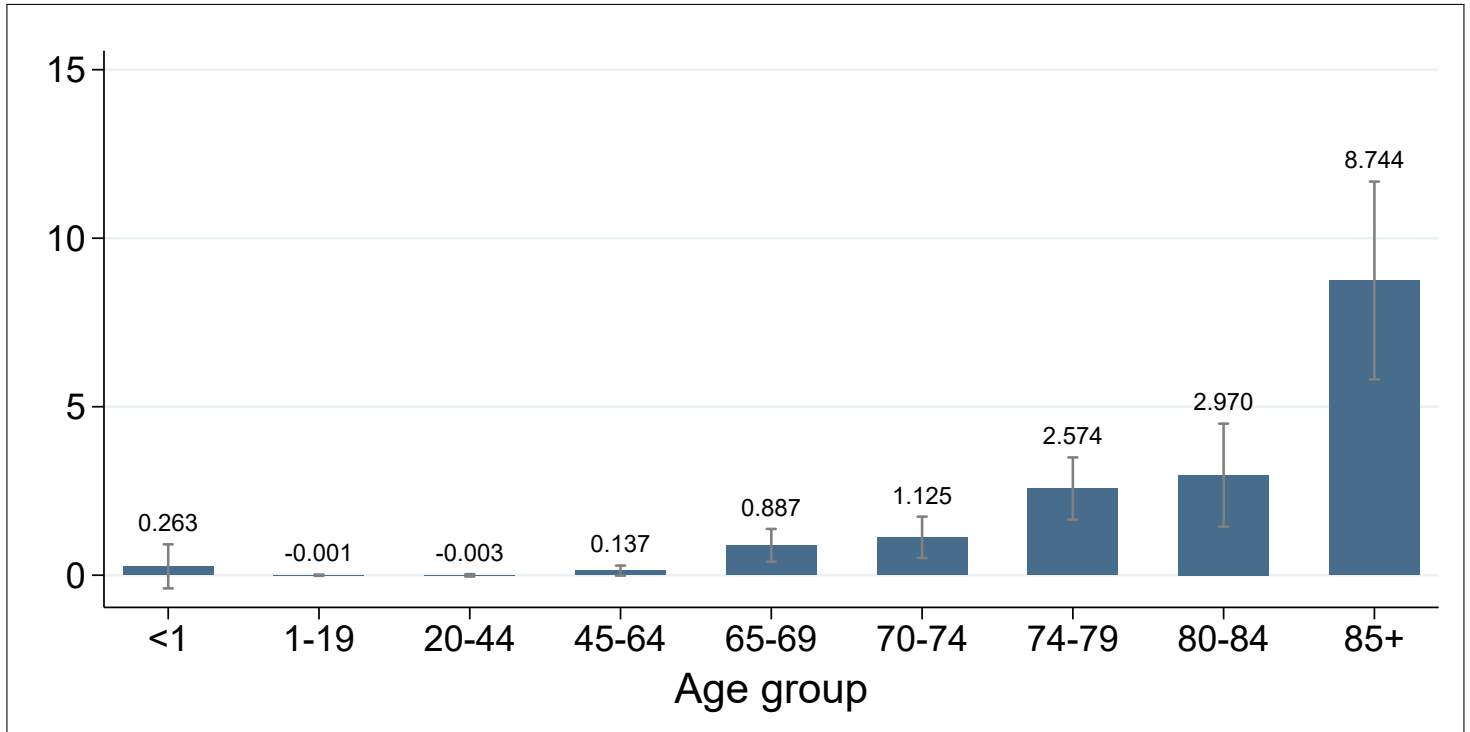




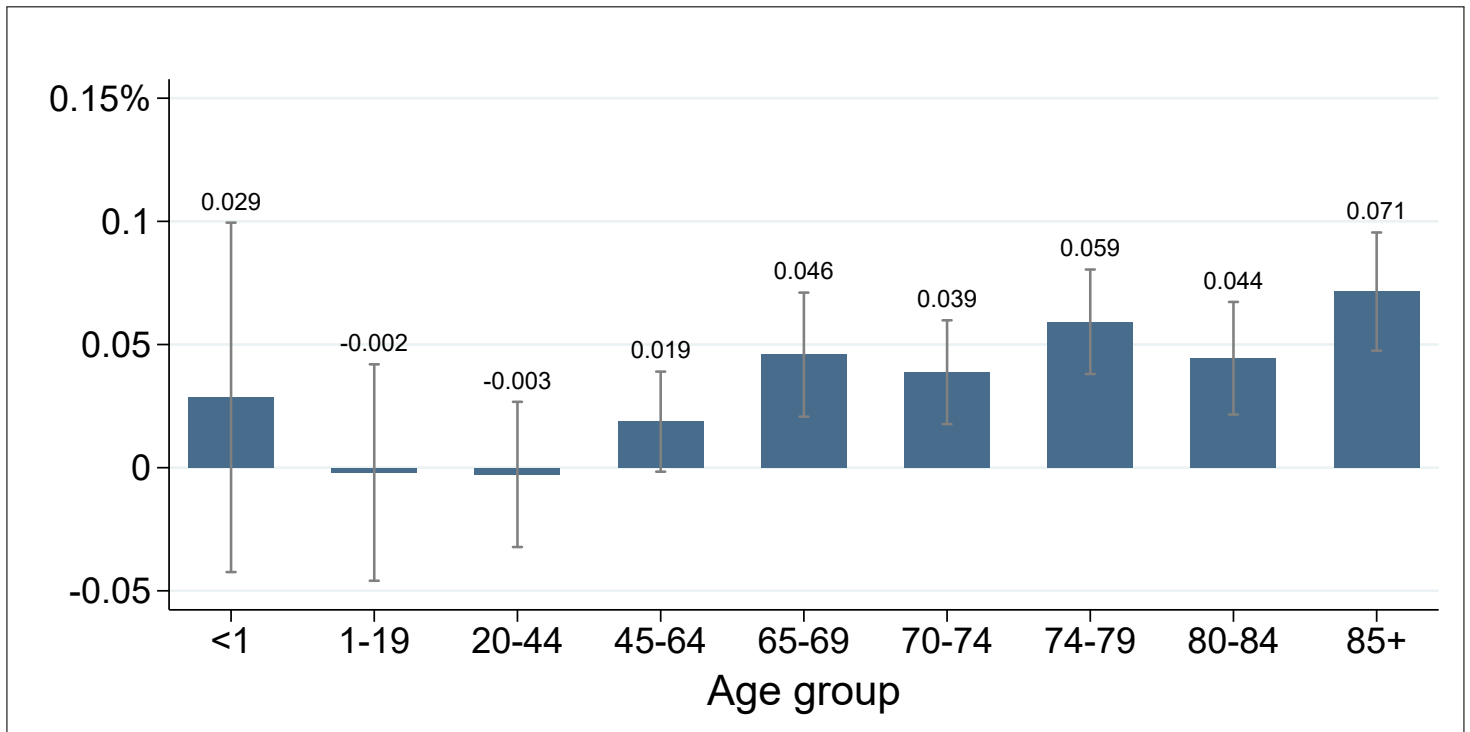
Notes: Each point reports an IV estimate from Equation (1) for the effect of a 1-day, 1 ppb increase in sulfur dioxide ( $\text{SO}_2$ ) exposure on mortality from twenty-six different causes of death. Cause-of-death definitions are available in Table A.14. Mortality is measured as cumulative deaths per million over time windows ranging from the day of exposure to 27 days after exposure. The shaded areas denote 95% confidence intervals. All regressions include county-by-month and month-by-year fixed effects, as well as flexible controls for maximum temperature, precipitation, humidity, and wind speed; leads of these weather controls; and two leads and two lags of the instruments. Estimates are weighted by county population. Standard errors are clustered by county.

**Figure A.9:** IV estimates for the effect of acute (1-day) air pollution exposure on 28-day mortality, by age group

(a) Absolute increase (deaths per million)

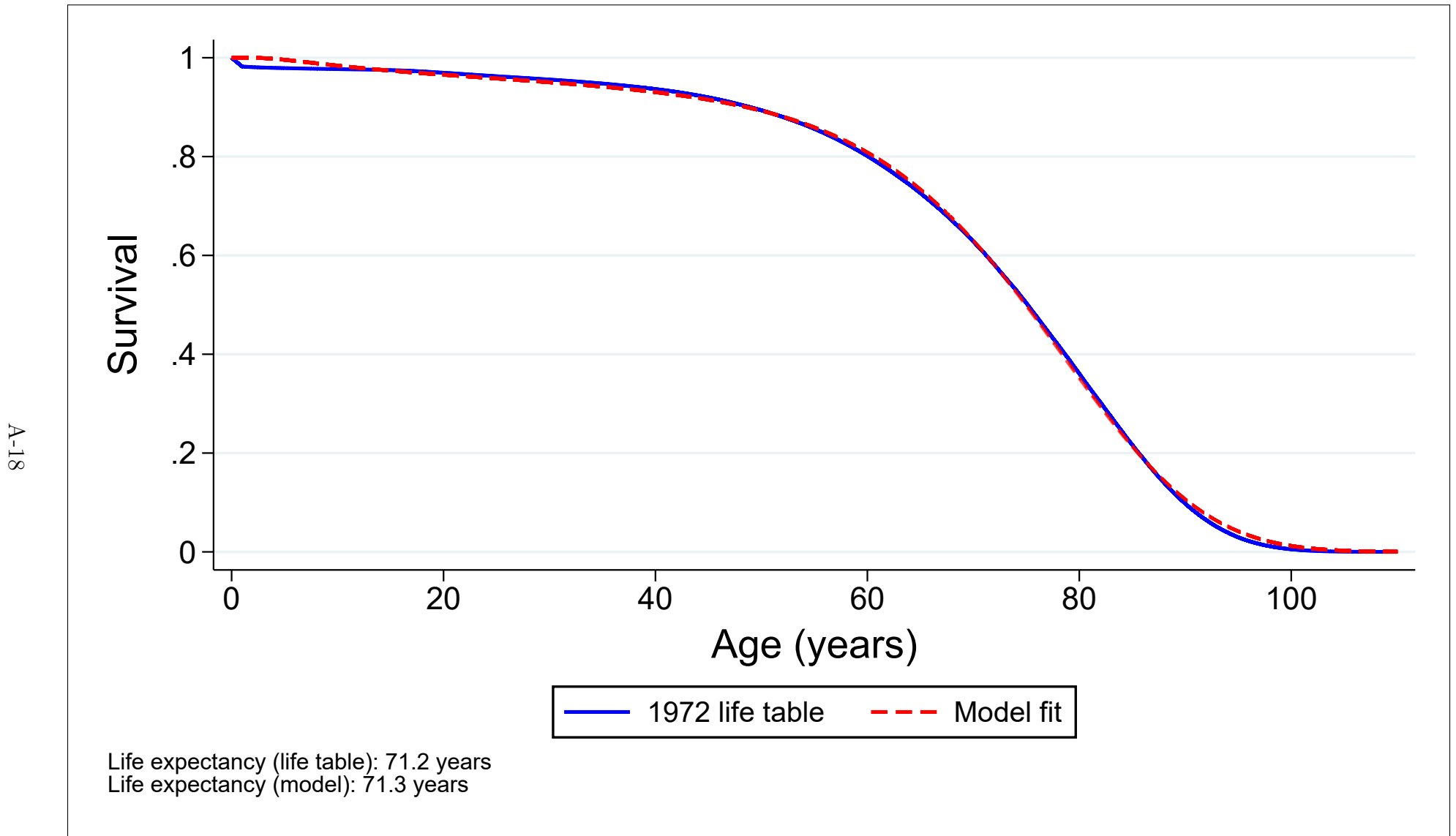


(b) Relative increase (percent of 28-day mortality)



Notes: Each bar represents an IV estimate from Equation (1) for the effect of a 1-day, 1 ppb increase in sulfur dioxide ( $\text{SO}_2$ ) exposure on 28-day mortality for a particular age group. Error bars represent 95% confidence intervals. Estimates are also reported in Table A.6. All regressions include county-by-month and month-by-year fixed effects, as well as flexible controls for maximum temperature, precipitation, humidity, and wind speed; leads of these weather controls; and two leads and two lags of the instruments. Estimates are weighted by county population. Standard errors are clustered by county.

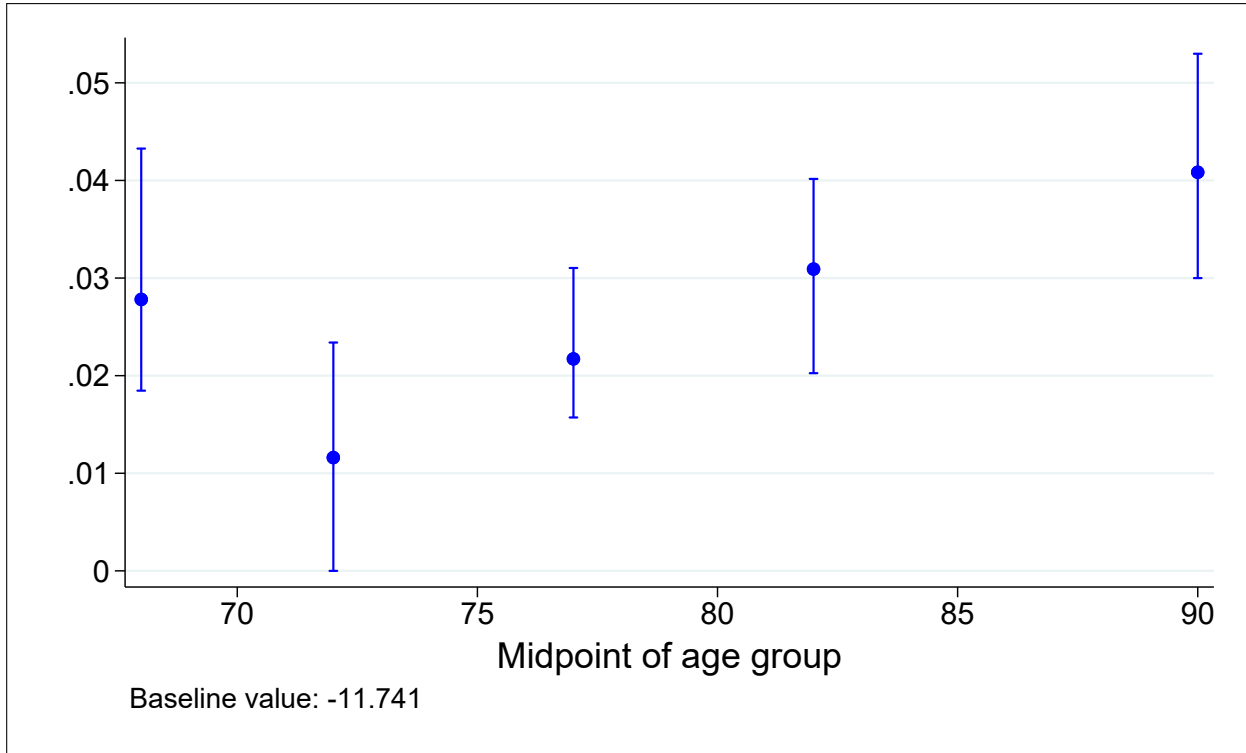
Figure A.10: Baseline calibration of the dynamic production model of health



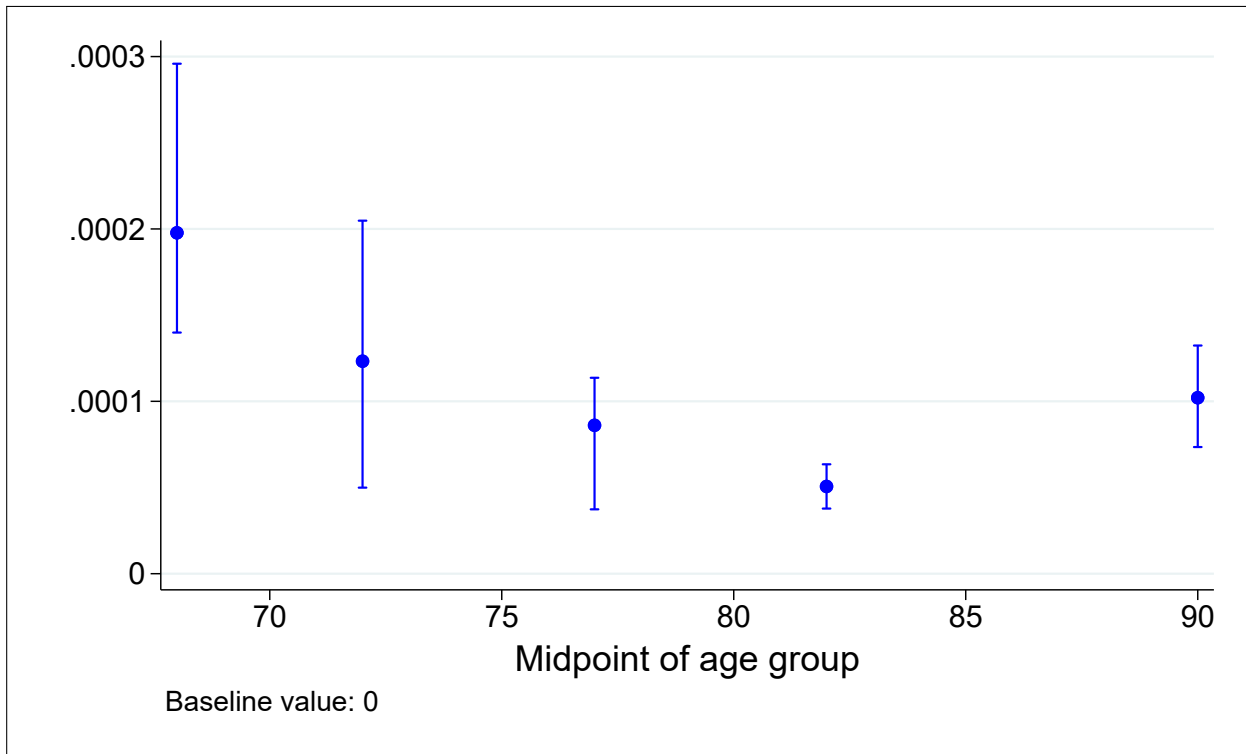
Notes: The solid blue line depicts the survival curve derived from the 1972 period life table for the United States. The dashed red line reports the predicted survival curve produced by our dynamic production model of health (3), which was calibrated using the 1972 life table data. The corresponding calibrated model parameters are reported in Column (2) of Table A.15.

**Figure A.11:** The effect of acute (1-day) air pollution exposure on model parameters

(a) Increase in  $\ln(\delta)$  ( $\ln(\tilde{\delta}_a) - \ln(\delta^*)$ )



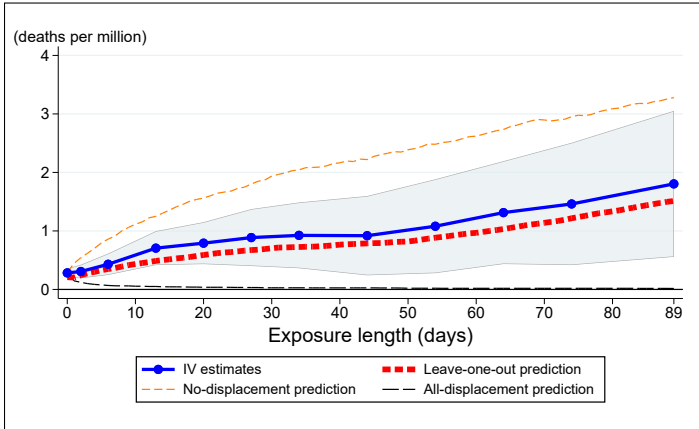
(b) Increase in  $\underline{H}$  ( $\tilde{H}_a - \underline{H}^*$ )



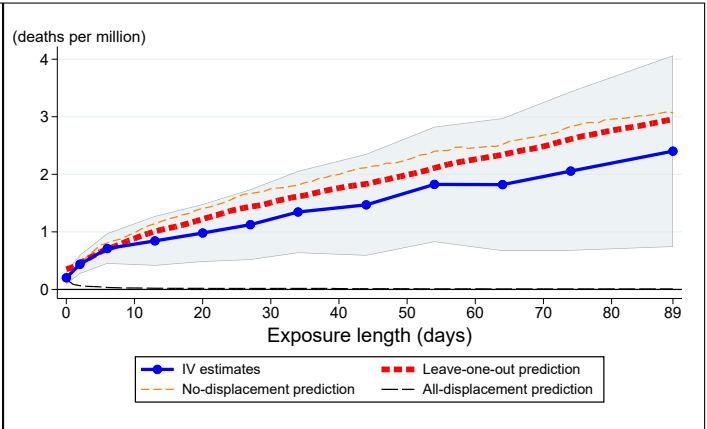
Notes: Panel (a) reports the effect of a 1-day, 1 ppb increase in  $\text{SO}_2$  exposure on the change in the parameter  $\delta$  from the health model (3), assuming all non-cancer deaths reflect changes in  $\delta$  while all cancer deaths reflect changes in  $\underline{H}$ . The baseline value is denoted by  $\delta^*$ , and the calibrated post-exposure value for age group  $a$  is denoted by  $\tilde{\delta}_a$ . Panel (b) reports the corresponding effect on the parameter  $\underline{H}$ , which governs mortality displacement and is calibrated using cancer-related deaths. The error bars report the 5th and 95th percentiles from 100 bootstrap replications. Baseline parameter values are reported in Column (2) of Table A.15.

**Figure A.12:** Comparison of model predictions to IV estimates, by age group

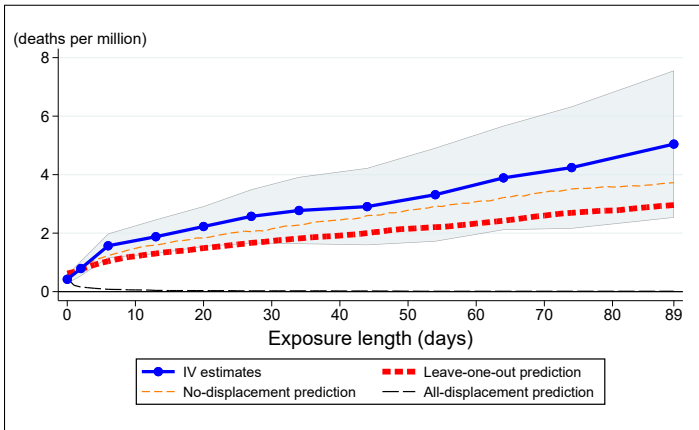
(a) Ages 65–69



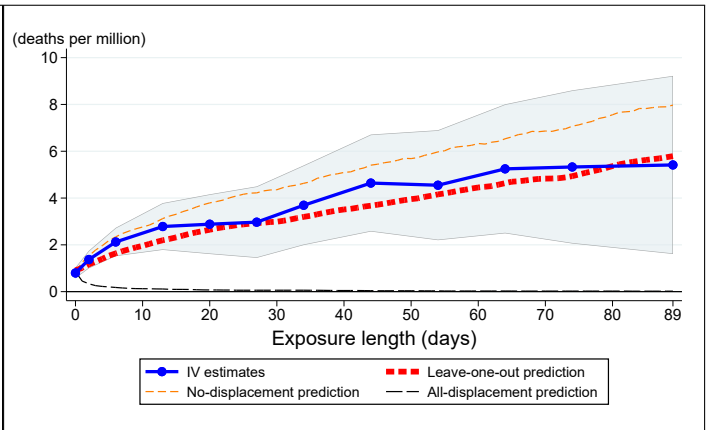
(b) Ages 70–74



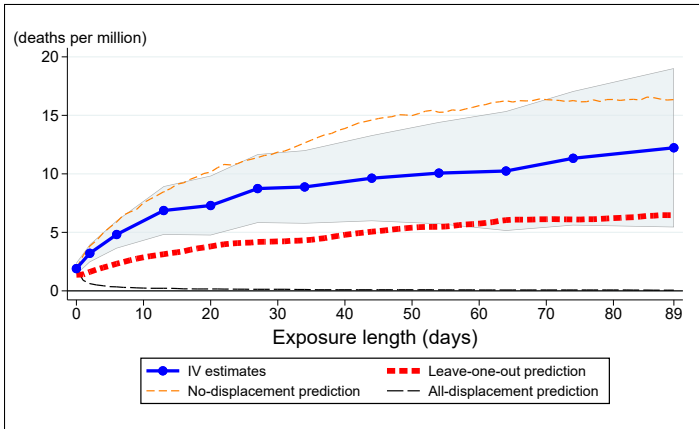
(c) Ages 75–79



(d) Ages 80–84

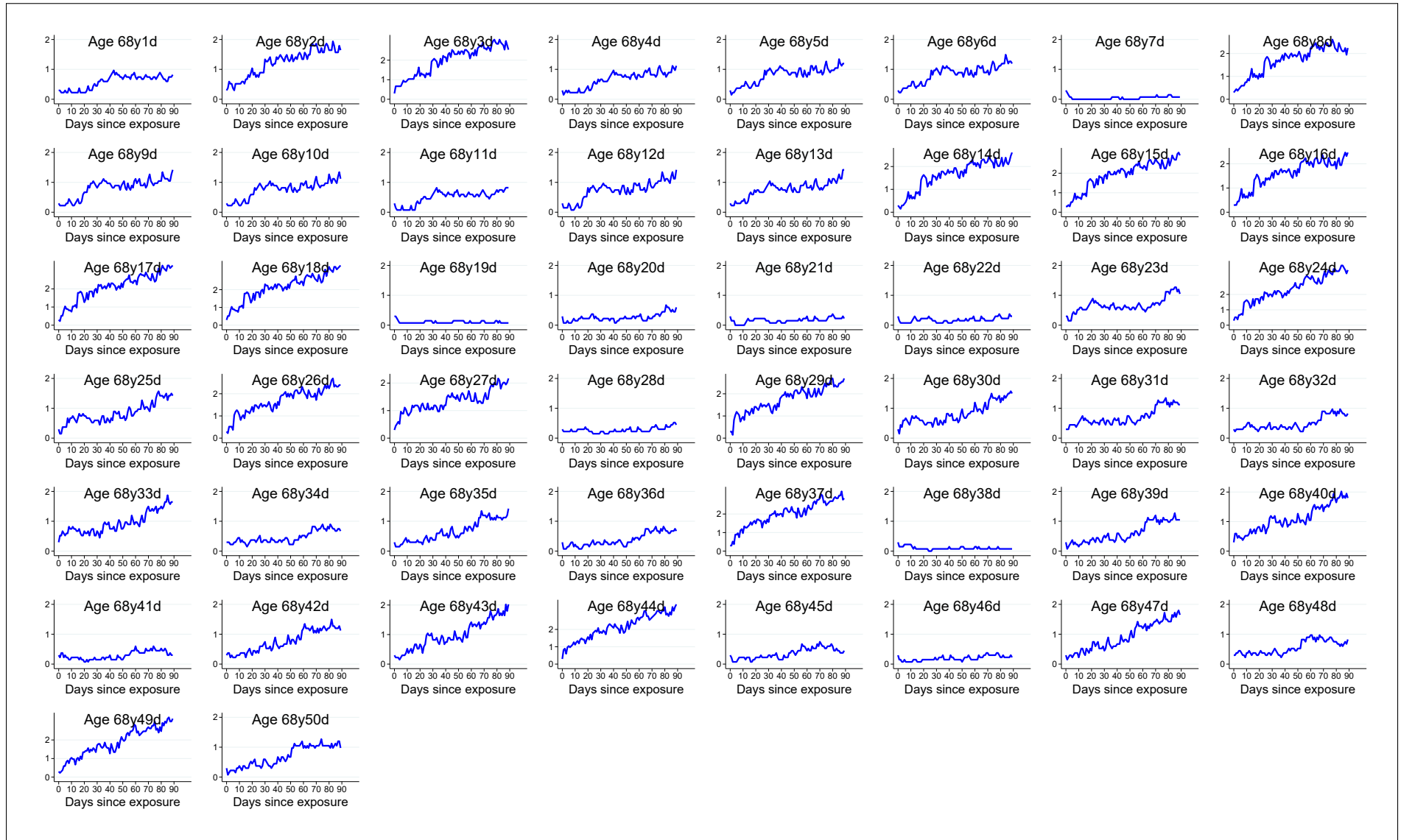


(e) Ages 85+



Notes: The solid blue line reports IV estimates from Equation (1) for the effect of a 1-day, 1 ppb increase in  $\text{SO}_2$  exposure on cumulative mortality, with 95% confidence intervals given by the blue shaded area. The thick red dashed line (“leave-one-out”) reports model predictions using the average of the calibrated values from other older age groups (70–74, 75–79, 80–84, and 85+). The orange dashed line (“no-displacement”) at the top of the plot reports model predictions under the assumption that none of the 1-day mortality effect reflects mortality displacement, while the black dashed line (“all-displacement”) at the bottom of the plot assumes that the entire 1-day effect reflects mortality displacement.

**Figure A.13:** Predicted effects of acute (1-day) air pollution exposure on cumulative mortality, for selected ages

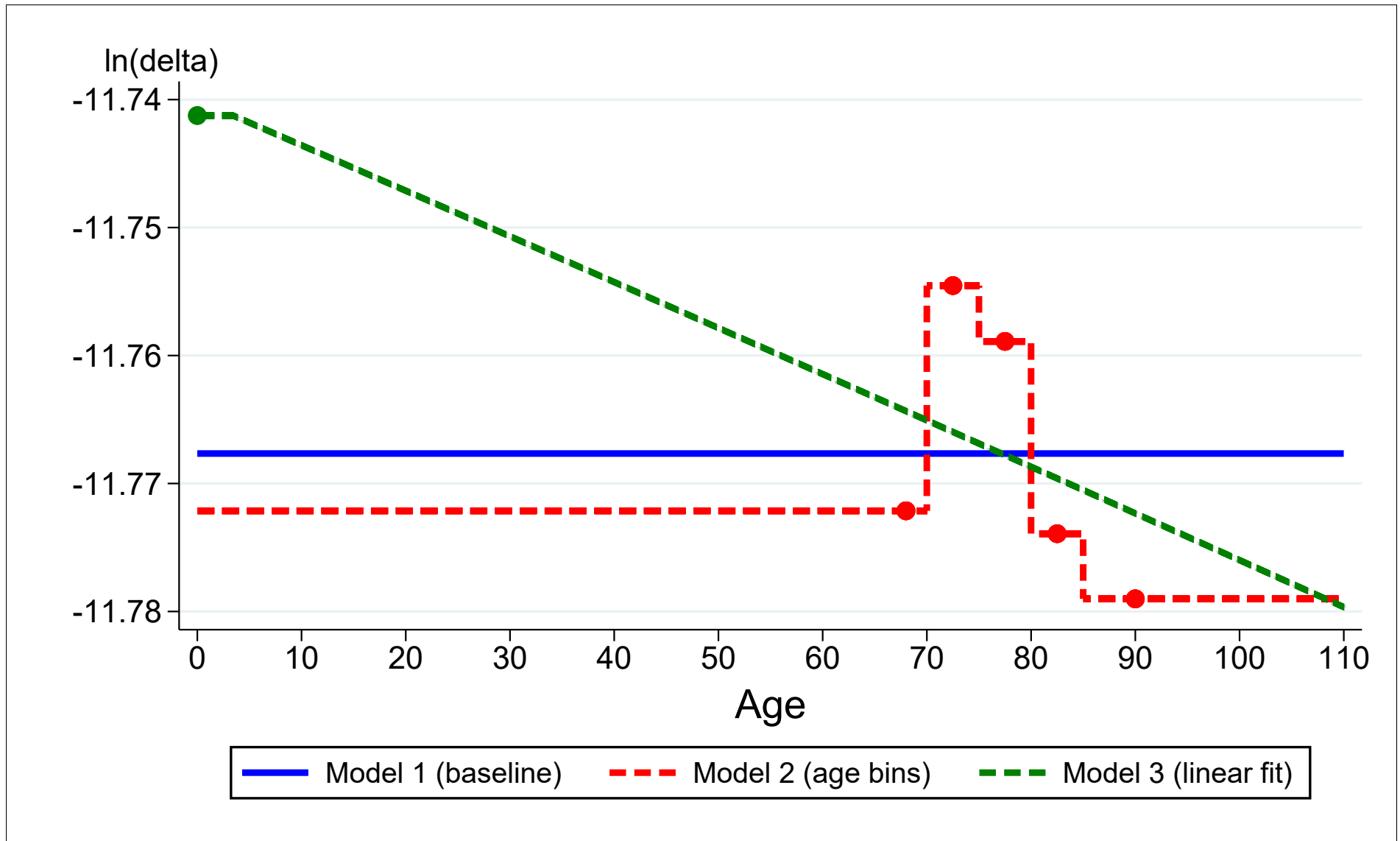


A-21

Notes: Each plot corresponds to a different age (68 years and 1 day, 68 years and 2 days, etc.) from the dynamic production model of health (3). The plots show the predicted effect of a 1-day, 1 ppb increase in  $\text{SO}_2$  exposure on mortality, measured as cumulative deaths per million over time windows ranging up to 90 days after exposure (with 0 indicating the day of exposure). The average across these 50 plots corresponds to the green dot-dashed line (“own-age prediction”) in Figure 5.

Figure A.14: Values of  $\tilde{\delta}$  used across models for long-run survival projections

A-22



Notes: This figure shows the counterfactual values  $\tilde{\delta}$  assumed by the different models producing the long-run survival projections shown in Figure 7. The five red markers report the log of  $\tilde{\delta}_a$  from the age-specific calibrations. The “baseline” specification uses the average of these five values,  $\{\frac{1}{5} \sum_{a \geq 65} \tilde{\delta}_a\}$ , represented by the solid blue line. The “age bins” model uses separate parameter values for each older age group (65–69, 70–74, 75–79, 80–84, and 85+) and assigns the 65–69 values to younger ages. The “linear fit” model assumes the effect is zero at birth (age 0) and fits a line through the five calibrated values and the age-zero point, subject to the constraint that exposure cannot improve health. The same approach is used to assign counterfactual values for  $\tilde{H}$ .

**Table A.1:** Complier county characteristics for the wind direction instruments

	Population	Percent 65+	Percent Black	Per- capita income (dollars)	Per- capita transfers (dollars)	Employment rate	Mean SO <sub>2</sub> (ppb)
	(1)	(2)	(3)	(4)	(5)	(6)	(7)
First-stage strength, ppb	-144,700 (137,372)	0.19* (0.086)	-0.24 (0.33)	62 (74)	55** (11)	-0.66 (0.76)	1.5** (0.15)
Mean outcome	1,303,561	11	13	10,987	1,290	52	9.5
Sample size	9,497	9,497	9,365	9,356	9,356	9,356	9,497
R-squared	0.040	0.075	0.0056	0.79	0.74	0.042	0.42

Notes: Complier characteristics are estimated by regressing the county-level variable reported at the top of each column on the strength of the first stage. First-stage strength is measured as the difference in predicted SO<sub>2</sub> levels between the most and least polluting wind directions. All regressions include year fixed effects and are weighted by county population. County characteristics are obtained from the Regional Economic Information System dataset published by the Bureau of Economic Analysis. Standard errors, clustered by county, are reported in parentheses. A \*/\*\* indicates significance at the 5%/1% level.

**Table A.2:** Autocorrelation in wind-driven SO<sub>2</sub> exposure, for different numbers of instrument leads and lags

	(1)	(2)	(3)	(4)	(5)
SO <sub>2</sub> , ppb	0.26** (0.022)	0.028 (0.016)	0.010 (0.014)	0.0095 (0.013)	0.012 (0.013)
Number of instrument leads	0	1	1	2	3
Number of instrument lags	0	0	1	2	3
First-stage <i>F</i> -statistic	765	667	616	576	577
Sample size	1,864,366	1,864,366	1,864,366	1,864,366	1,863,479

Notes: The dependent variable is tomorrow's SO<sub>2</sub> levels. We instrument for today's SO<sub>2</sub> levels using today's wind direction instruments. All regressions include county-by-month and month-by-year fixed effects, along with flexible controls for both today's and tomorrow's maximum temperature, precipitation, humidity, and wind speed. Columns (2)–(5) also include varying numbers of leads and lags of the instruments. All regressions are weighted by county population. Standard errors, clustered by county, are reported in parentheses. A \*/\*\* indicates significance at the 5%/1% level.

**Table A.3:** IV estimates for the effect of acute SO<sub>2</sub> exposure on 1-day mortality, using different numbers of instrument leads and lags

	(1)	(2)	(3)	(4)	(5)	(6)
SO <sub>2</sub> , ppb	0.070** (0.0065)	0.076** (0.0070)	0.076** (0.0065)	0.071** (0.0065)	0.070** (0.0065)	0.070** (0.0064)
# of instrument leads	2	0	1	3	4	6
# of instrument lags	2	0	1	3	4	6
First-stage <i>F</i> -statistic	636	866	681	637	633	633
Mean outcome	24	24	24	24	24	24
Sample size	2,042,258	2,042,258	2,042,258	2,041,316	2,040,383	2,038,559

Notes: The dependent variable is number of deaths per million people on the day of exposure. All regressions include county-by-month and month-by-year fixed effects, along with flexible controls for maximum temperature, precipitation, humidity, and wind speed; and two leads and two lags of the instruments. All regressions are weighted by county population. Standard errors, clustered by county, are reported in parentheses. A \*/\*\* indicates significance at the 5%/1% level.

**Table A.4:** OLS and IV estimates for the effect of acute SO<sub>2</sub> exposure on cumulative mortality, for different outcome windows

	(1)	(2)
Outcome window	OLS	IV
1 day	0.0083** (0.0028)	0.070** (0.0065)
3 days	0.022** (0.0084)	0.11** (0.010)
5 days	0.031* (0.014)	0.14** (0.014)
7 days	0.034 (0.019)	0.17** (0.018)
10 days	0.039 (0.026)	0.20** (0.022)
14 days	0.045 (0.036)	0.22** (0.030)
21 days	0.051 (0.051)	0.24** (0.041)
28 days	0.048 (0.065)	0.25** (0.055)

Notes: The dependent variable is cumulative number of deaths per million people in the days following acute (1-day) exposure. Each estimate comes from a separate regression. IV estimates in Column (2) correspond to those shown in Figure 2. All regressions include county-by-month and month-by-year fixed effects, along with flexible controls for maximum temperature, precipitation, humidity, and wind speed; leads of these weather controls; and two leads and two lags of the instruments. All regressions are weighted by county population. Standard errors, clustered by county, are reported in parentheses. A \*/\*\* indicates significance at the 5%/1% level.

**Table A.5:** IV estimates for the effect of acute SO<sub>2</sub> exposure on 1-day mortality, for different age groups

Age group	(1) Absolute effect, deaths per million	(2) Relative effect, percent
0–1	–0.0055 (0.044)	–0.017 (0.13)
1–19	0.00029 (0.0016)	0.019 (0.10)
20–44	0.0087** (0.0033)	0.20** (0.076)
45–64	0.050** (0.0099)	0.19** (0.038)
65–69	0.28** (0.038)	0.41** (0.055)
70–74	0.20** (0.060)	0.20** (0.058)
75–79	0.42** (0.078)	0.27** (0.050)
80–84	0.80** (0.12)	0.33** (0.050)
85+	1.9** (0.26)	0.44** (0.060)

Notes: The dependent variable is number of deaths per million people on the day of exposure. Each estimate comes from a separate regression. The relative effect is expressed as a percentage of the age group’s mean one-day mortality rate. Estimates are also shown in panels (a) and (b) of Figure 4. All regressions include county-by-month and month-by-year fixed effects, along with flexible controls for maximum temperature, precipitation, humidity, and wind speed; and two leads and two lags of the instruments. All regressions are weighted by county population. Standard errors, clustered by county, are reported in parentheses. A \*/\*\* indicates significance at the 5%/1% level.

**Table A.6:** IV estimates for the effect of acute SO<sub>2</sub> exposure on cumulative mortality, for different age groups and outcome windows

	(1)	(2)	(3)	(4)	(5)	(6)	(7)	(8)	(9)
Outcome window	0–1	1–19	20–44	45–64	65–69	70–74	75–79	80–84	85+
1 day	–0.0055 (0.044)	0.00029 (0.0016)	0.0087** (0.0033)	0.050** (0.0099)	0.28** (0.038)	0.20** (0.060)	0.42** (0.078)	0.80** (0.12)	1.9** (0.26)
3 days	0.15* (0.060)	–0.00038 (0.0031)	0.012* (0.0046)	0.076** (0.016)	0.31** (0.059)	0.44** (0.084)	0.79** (0.13)	1.4** (0.19)	3.2** (0.39)
7 days	0.17 (0.12)	–0.0021 (0.0052)	0.023** (0.0077)	0.076** (0.024)	0.43** (0.093)	0.71** (0.13)	1.6** (0.21)	2.1** (0.31)	4.8** (0.61)
14 days	0.098 (0.20)	–0.0074 (0.0063)	0.014 (0.010)	0.11* (0.043)	0.71** (0.15)	0.84** (0.22)	1.9** (0.30)	2.8** (0.51)	6.9** (1.1)
28 days	0.26 (0.33)	–0.00083 (0.0094)	–0.0033 (0.018)	0.14 (0.076)	0.89** (0.25)	1.1** (0.31)	2.6** (0.47)	3.0** (0.78)	8.7** (1.5)

Notes: The dependent variable is cumulative number of deaths per million people in the days following acute (1-day) exposure. Each estimate comes from a separate regression. Age groups are indicated at the top of each column. All regressions include county-by-month and month-by-year fixed effects, along with flexible controls for maximum temperature, precipitation, humidity, and wind speed; leads of these weather controls; and two leads and two lags of the instruments. All regressions are weighted by county population. Standard errors, clustered by county, are reported in parentheses. A \*/\*\* indicates significance at the 5%/1% level.

**Table A.7:** IV estimates for the effect of acute SO<sub>2</sub> exposure on cumulative mortality, for different causes of death and outcome windows

	(1)	(2)	(3)	(4)
Outcome window	Cardiovascular	Cancer	Other	External
1 day	0.026** (0.0032)	0.023** (0.0027)	0.020** (0.0026)	0.0020 (0.0011)
3 days	0.052** (0.0057)	0.029** (0.0037)	0.030** (0.0035)	0.0041* (0.0018)
5 days	0.069** (0.0078)	0.026** (0.0047)	0.042** (0.0056)	0.0044 (0.0026)
7 days	0.088** (0.011)	0.027** (0.0052)	0.050** (0.0067)	0.0053 (0.0029)
10 days	0.10** (0.013)	0.029** (0.0067)	0.062** (0.0084)	0.0053 (0.0034)
14 days	0.12** (0.017)	0.024** (0.0079)	0.068** (0.011)	0.0050 (0.0041)
21 days	0.13** (0.021)	0.018 (0.011)	0.079** (0.015)	0.0081 (0.0058)
28 days	0.14** (0.027)	0.020 (0.016)	0.093** (0.020)	0.0033 (0.0074)

Notes: The dependent variable is cumulative number of deaths per million people in the days following acute (1-day) exposure. Each estimate comes from a separate regression. The underlying cause of death is indicated at the top of each column. Estimates are also shown in Figure 3. All regressions include county-by-month and month-by-year fixed effects, along with flexible controls for maximum temperature, precipitation, humidity, and wind speed; leads of these weather controls; and two leads and two lags of the instruments. All regressions are weighted by county population. Standard errors, clustered by county, are reported in parentheses. A \*/\*\* indicates significance at the 5%/1% level.

**Table A.8:** IV estimates for the effect of acute SO<sub>2</sub> exposure on 1-day mortality, controlling for all pollutants except TSP

	(1)	(2)	(3)	(4)	(5)	(6)	(7)
SO <sub>2</sub> , ppb	0.085** (0.0092)	0.063** (0.013)	0.090** (0.011)	0.078** (0.0098)	0.063** (0.013)	0.082** (0.011)	0.067** (0.014)
NO <sub>2</sub> , ppb		0.028* (0.012)			0.027 (0.014)		0.028 (0.014)
O <sub>3</sub> , ppb			-0.021 (0.018)			-0.016 (0.017)	-0.019 (0.018)
CO, ppm				0.25 (0.15)	0.023 (0.19)	0.23 (0.15)	-0.021 (0.21)
First-stage <i>F</i> -statistic	256	64	39	93	42	38	38
Mean outcome	26	26	26	26	26	26	26
Sample size	277,600	277,600	277,600	277,600	277,600	277,600	277,600

Notes: The dependent variable is number of deaths per million people on the day of exposure. All regressions include county-by-month and month-by-year fixed effects, along with flexible controls for maximum temperature, precipitation, humidity, and wind speed; and two leads and two lags of the instruments. All regressions are weighted by county population. Standard errors, clustered by county, are reported in parentheses. A \*/\*\* indicates significance at the 5%/1% level. National means for all air pollutants are available in Table 1.

**Table A.9:** IV estimates for the effect of acute SO<sub>2</sub> exposure on 1-day mortality, using different fixed effects

	(1)	(2)	(3)	(4)	(5)	(6)
SO <sub>2</sub> , ppb	0.070** (0.0065)	0.066** (0.0065)	0.071** (0.0066)	0.072** (0.0067)	0.072** (0.0068)	0.071** (0.0068)
Fixed effects	county- month, month-year	county, year, month	county, state- year-month	county-year, state-month	county, year, state-month	county, month-year, state-month
First-stage <i>F</i> -statistic	636	613	681	723	612	613
Mean outcome	24	24	24	24	24	24
Sample size	2,042,258	2,042,258	2,042,236	2,042,243	2,042,258	2,042,258

Notes: The dependent variable is number of deaths per million people on the day of exposure. All regressions include flexible controls for maximum temperature, precipitation, humidity, and wind speed; and two leads and two lags of the instruments. All regressions are weighted by county population. Standard errors, clustered by county, are reported in parentheses. A \*/\*\* indicates significance at the 5%/1% level.

**Table A.10:** IV estimates for the effect of acute SO<sub>2</sub> exposure on 1-day mortality, clustering standard errors at different levels

	(1)	(2)	(3)	(4)
SO <sub>2</sub> , ppb	0.070** (0.0065)	0.070** (0.0065)	0.070** (0.0064)	0.070** (0.0061)
Clustering level(s)	County	County, geographic group by year	Geographic group	State
First-stage $F$ -statistic	636	636	636	636
Mean outcome	24	24	24	24
Sample size	2,042,258	2,042,258	2,042,258	2,042,258

Notes: The dependent variable is number of deaths per million people on the day of exposure. All regressions include county-by-month and month-by-year fixed effects, along with flexible controls for maximum temperature, precipitation, humidity, and wind speed; and two leads and two lags of the instruments. All regressions are weighted by county population. Standard errors, clustered at the level(s) indicated in each column, are reported in parentheses. Geographic groups are shown in Figure A.3. A \*/\*\* indicates significance at the 5%/1% level.

**Table A.11:** IV estimates for the effect of acute SO<sub>2</sub> exposure on 1-day mortality, using different first-stage specifications

	(1)	(2)	(3)	(4)	(5)	(6)
SO <sub>2</sub> , ppb	0.070** (0.0065)	0.082** (0.0075)	0.061** (0.0054)	0.060** (0.0051)	0.063** (0.0056)	0.066** (0.0061)
Number of geographic groups	50	25	100	50	50	50
Wind angle parameterization	Sines	Sines	Sines	40-degree bins	60-degree bins	90-degree bins
Number of instruments	100	50	200	400	250	150
First-stage $F$ -statistic	636	1,116	371	181	251	340
Mean outcome	24	24	24	24	24	24
Sample size	2,042,258	2,042,258	2,042,258	2,042,258	2,042,258	2,042,258

Notes: The dependent variable is number of deaths per million people on the day of exposure. Column (1) reports our main specification, which allows the effect of wind direction to vary across 50 geographic groups and assumes that its effect on pollution,  $f^g(\cdot)$ , follows the sine parameterization in Equation (2). Columns (2)–(3) vary the number of geographic groups employed in the first stage. Columns (4)–(6) use alternative non-parametric parameterizations for  $f^g(\cdot)$ . All regressions include county-by-month and month-by-year fixed effects, along with flexible controls for maximum temperature, precipitation, humidity, and wind speed; and two leads and two lags of the instruments. All regressions are weighted by county population. Standard errors, clustered by county, are reported in parentheses. A \*/\*\* indicates significance at the 5%/1% level.

**Table A.12:** 2SLS and LIML estimates for the effect of acute SO<sub>2</sub> exposure on cumulative mortality, for different outcome windows

	(1)	(2)	(3)	(4)	(5)	(6)
SO <sub>2</sub> , ppb	0.070** (0.0065)	0.070** (0.0063)	0.17** (0.018)	0.16** (0.015)	0.25** (0.055)	0.24** (0.023)
IV method	2SLS	LIML	2SLS	LIML	2SLS	LIML
Outcome window (days)	1	1	7	7	28	28
First-stage <i>F</i> -statistic	636	895	567	799	472	665
Mean outcome	24	24	170	170	681	681
Sample size	2,042,258	2,040,800	2,042,258	2,040,794	2,042,258	2,040,781

Notes: The dependent variable is cumulative number of deaths per million people in the days following acute (1-day) exposure. All regressions include county-by-month and month-by-year fixed effects, along with flexible controls for maximum temperature, precipitation, humidity, and wind speed; leads of these weather controls; and two leads and two lags of the instruments. All regressions are weighted by county population. Standard errors, clustered by county, are reported in parentheses. A \*/\*\* indicates significance at the 5%/1% level.

**Table A.13:** Placebo tests for the effect of acute SO<sub>2</sub> exposure on mortality

	(1)	(2)	(3)
SO <sub>2</sub> , ppb	0.027 (0.060)	-0.32 (0.22)	-0.51 (0.50)
Outcome window, days	1	7	28
First-stage <i>F</i> -statistic	3.3	3.5	3.7
Mean outcome	24	170	681
Sample size	2,042,258	2,042,258	2,042,258

Notes: This table reports the results of placebo regressions where the instruments are based on wind direction that is a randomly generated variable. The dependent variable is cumulative number of deaths per million people in the days following acute (1-day) exposure. All regressions include county-by-month and month-by-year fixed effects, along with flexible controls for maximum temperature, precipitation, humidity, and wind speed; leads of these weather controls; and two leads and two lags of the instruments. All regressions are weighted by county population. Standard errors, clustered by county, are reported in parentheses. A \*/\*\* indicates significance at the 5%/1% level.

**Table A.14:** ICD-8 and ICD-9 codes for subcategories of cardiovascular and other diseases

ID	Disease	ICD-8 codes (1968–1978)	ICD-9 codes (1979–1998)	Prevalence (%)
<b>Cardiovascular diseases</b>				
1	Heart diseases	390–398.9, 402–402.9, 404–429.9, 410–429.9	390–398.9, 402–402.9, 404–429.9	37.58
2	Hypertension	400–400.9, 401–401.9, 403–403.9	401–401.9, 403–403.9	0.37
3	Cerebrovascular disease	Same as ICD-9	430–438.9	8.69
4	Atherosclerosis	Same as ICD-9	440–440.9	1.38
5	Other cardiovascular diseases	Same as ICD-9	441–448.9	1.17
<b>Other diseases</b>				
6	Infectious and parasitic diseases	Same as ICD-9	001–139.9	1.13
7	Benign neoplasms	Same as ICD-9	210–239.9	0.29
<b>Endocrine, nutritional and metabolic diseases, and immunity disorders</b>				
8	Diabetes	Same as ICD-9	250–250.9	1.81
9	Other endocrine, nutritional and metabolic diseases, and immunity disorders	Same as ICD-9	240–249.0, 260–279.9	0.57
10	Diseases of blood and blood forming organs	Same as ICD-9	280–289.9	0.32
11	Mental disorders	Same as ICD-9	290–319	0.71
<b>Diseases of the nervous system and sense organs</b>				
12	Meningitis	Same as ICD-9	320–322.9	0.08
13	Parkinson’s disease (paralysis agitans)	342	332–332.1	0.21
14	Other diseases of nervous system and sense organs	320–341.9, 343–389.9	323–331.9, 332.2–389.9	0.89
<b>Diseases of the respiratory system</b>				
15	Acute bronchitis and bronchiolitis	Same as ICD-9	466–466.9	0.03
16	Pneumonia and influenza	470–474.9, 480–486.9	480–487.9	2.97
17	COPD and allied conditions	490–493.9	490–496.9	2.52
18	Other respiratory diseases	460–469.9, 475–479.9, 487–489.9, 494–519.9	460–465.9, 467–479.9, 488–489.9, 497–519.9	1.25
<b>Diseases of the digestive system</b>				
19	Ulcer of stomach and duodenum	Same as ICD-9	531–533.9	0.33
20	Appendicitis	Same as ICD-9	540–543.9	0.03
21	Hernia	Same as ICD-9	550–553.9, 560–560.9	0.29
22	Chronic liver diseases	Same as ICD-9	571–571.9	1.48
23	Other digestive diseases	Same as ICD-9	520–530.9, 534–539.9, 544–549.9, 554–559.9, 561–570.9, 572–579.9	1.54
<b>Diseases of the genitourinary system</b>				
24	Nephritis and kidney infections	Same as ICD-9	580–590.9	0.91
25	Other diseases of the genitourinary system	Same as ICD-9	591–629.9	0.64
26	Residual: Complications of pregnancy, childbirth, and the puerperium; diseases of veins and lymphatics, and other diseases of circulatory system; diseases of the skin and subcutaneous tissue; diseases of the musculoskeletal system and connective tissue; congenital anomalies; certain conditions originating in the perinatal period; and ill-defined conditions	Same as ICD-9	450–459.9, 630–799.9	4.28

Notes: This table lists the ICD-8 and ICD-9 codes used to define the causes of death shown in Figure A.8. Death certificates used ICD-8 codes during the years 1968–1978 and ICD-9 codes during the years 1979–1998. ICD-8 codes are shown only when they differ from the corresponding ICD-9 codes. Prevalence reports the number of deaths from each cause during 1972–1988 as a percentage of total deaths.

**Table A.15:** Baseline parameter values for the dynamic production model of health

	(1)	(2)
Parameter	Annual data	Daily data
$I$	0.74773	0.0020521
$\alpha$	1.53762	1.537619
$\ln \delta$	-5.83878	-11.74124
$\mu_H$	10.39737	11.43803
$\sigma_e$	2.25247	0.1178985
$N$	1,000,000	100,000
SSE	57.80479	20880.82

Notes: This table reports baseline parameter values for the dynamic production model of health given by Equation (3). Column (1) presents values calibrated to annual survival data from a 1972 period life table, while Column (2) reports corresponding values based on daily data. The parameters  $\underline{H}$  and  $\sigma_H$  (not shown) are normalized to 0 and 1, respectively.  $N$  denotes the number of individuals in the simulation, and SSE is the sum of squared errors. The model fit corresponding to Column (2) is shown in Figure A.10.

**Table A.16:** IV estimates for the effect of acute SO<sub>2</sub> exposure on all-cause and cancer-related 1-day mortality, ages 65 and over

	(1)	(2)
Age group	All causes	Cancer-related causes
65–69	0.28** (0.038)	0.13** (0.021)
70–74	0.20** (0.060)	0.12** (0.025)
75–79	0.42** (0.078)	0.14** (0.034)
80–84	0.80** (0.12)	0.12* (0.053)
85+	1.9** (0.26)	0.16** (0.060)

Notes: These estimates are used to calibrate the effect of air pollution exposure on mortality in the dynamic production model of health given by Equation (3). The dependent variable is number of deaths per million people on the day of exposure. Each estimate comes from a separate regression. All regressions include county-by-month and month-by-year fixed effects, along with flexible controls for maximum temperature, precipitation, humidity, and wind speed; and two leads and two lags of the instruments. All regressions are weighted by county population. Standard errors, clustered by county, are reported in parentheses. A \*/\*\* indicates significance at the 5%/1% level.

**Table A.17:** Projected effect of permanent change in SO<sub>2</sub> on survival gains (years)

	(1)	(2)	(3)	(4)
	IV extrapolation	Model 1 (baseline)	Model 2 (age bins)	Model 3 (linear fit)
1-ppb decrease	0.15 [0.06, 0.29]	1.13 [0.40, 1.99]	1.24 [0.70, 1.98]	0.77 [0.04, 1.63]
2-ppb decrease	0.29 [0.11, 0.58]	2.32 [0.70, 4.10]	2.28 [1.55, 3.03]	1.58 [-0.04, 3.35]
3-ppb decrease	0.44 [0.17, 0.88]	3.45 [0.99, 6.26]	3.40 [2.35, 4.77]	2.36 [-0.09, 5.17]
1-ppb increase	-0.14 [-0.28, -0.06]	-1.03 [-1.96, -0.39]	-1.04 [-1.71, -0.71]	-0.68 [-1.61, -0.04]
2-ppb increase	-0.28 [-0.56, -0.11]	-2.20 [-3.77, -0.59]	-2.23 [-2.95, -1.38]	-1.45 [-3.04, 0.16]
3-ppb increase	-0.42 [-0.83, -0.17]	-3.10 [-4.98, -0.92]	-3.24 [-3.95, -2.39]	-2.06 [-3.97, 0.14]

Notes: Each value in this table reports the projected change in life expectancy (in years) resulting from a permanent change in SO<sub>2</sub> exposure of up to 3 part per billion (ppb) for the cohort of US individuals born in 1972. In the absence of any change in exposure, predicted life expectancy is 71.32 years. 90% bootstrap confidence intervals, based on the 5th to 95th percentiles of the bootstrapped distribution, are reported in brackets. Values in Column (1) are calculated by extrapolating our age-specific 28-day IV estimates to the whole life-cycle. Values in Column (2) come from the dynamic production model of health described by Equation (3), under the assumption that the effect of pollution exposure on model parameters is constant across ages. Values in Column (3) allow these effects to vary across age groups. Values in Column (4) also incorporate age variation but assume a linear age trend. Figure 7 shows how the survival gains reported in the first row are distributed across the life cycle.